RESERVOIR HISTORY MATCHING USING CONSTRAINED ENSEMBLE KALMAN FILTER AND PARTICLE FILTER METHODS

by

Abhinandhan Raghu

A thesis submitted in partial fulfillment of the requirements for the degree of

Master of Science

in

Process Control

Department of Chemical and Materials Engineering
University of Alberta

Abstract

The high heterogeneity of petroleum reservoirs, represented by their spatially varying rock properties (porosity and permeability), greatly dictates the quantity of recoverable oil. In this work, the estimation of these rock properties, which is crucial for the future performance prediction of a reservoir, is carried out through a history matching technique using constrained ensemble Kalman filtering (EnKF) and particle filtering (PF) methods. The first part of the thesis addresses some of the main limitations of the conventional EnKF. The EnKF, formulated on the grounds of Monte Carlo sampling and the Kalman filter (KF), arrives at estimates of parameters based on statistical analysis and hence could potentially yield reservoir parameter estimates that are not geologically realistic and consistent. In order to overcome this limitation, hard and soft data constraints in the recursive EnKF estimation methodology are incorporated. Hard data refers to the actual values of the reservoir parameters at discrete locations obtained by core sampling and well logging. On the other hand, the soft data considered here is obtained from the variogram, which characterize the spatial correlation of the rock properties in a reservoir. In this algorithm, the correlation matrix obtained after the unconstrained EnKF update is transformed to honour the true correlation structure from the variogram by applying a scaling and projection method. This thesis also deals with the problem of spurious correlation induced by the Kalman gain computations in the EnKF update step, potentially leading to erroneous update of parameters. In order to solve this issue, a covariance localization-based EnKF coupled with geostatistics is implemented in reservoir history matching. These algorithms are implemented on two synthetic reservoir models and their efficacy in yielding estimates consistent with the geostatistics is observed. It is found that the computational time involved in the localization-based EnKF framework for reservoir history matching is considerably reduced owing to the reduction in the size of the parameter space in the EnKF update

step. Also, the geostatistics-based covariance localization performs better in capturing the spatial heterogeneity and variability of the reservoir permeability than the traditional methods. In the second part of the thesis, we extend the history matching implementation using the particle filtering. Reservoir models, being nonlinear, the distributions of the noise and parameters are generally non-Gaussian in nature. Since the EnKF may fail to obtain accurate estimates when the distributions involved in the model are non-Gaussian, we attempt to use a completely Bayesian filter, the particle filter, to estimate reservoir parameters. In addition, the geostatistics-based covariance localization is also coupled with the particle filter and is found to perform better than the filter without any localization.

Preface

The results of Chapter 2 and Chapter 3 of this thesis have been submitted as Abhinandhan Raghu, Xiongtan Yang, Swanand Khare, Prakash Jagadeesan, Biao Huang and Vinay Prasad, "Reservoir History Matching Using Constrained Ensemble Kalman Filtering" to Chemical Engineering Science, Dec 2014. The algorithms were developed by Vinay Prasad, Biao Huang and myself. Xiongtan Yang and I were responsible for the implementation of the algorithm. Swanand Khare and Prakash Jagadeesan suggested ideas regarding the implementation. I wrote the first draft of the journal submission. Dr. Prasad and Dr. Huang were the supervisory authors and were involved with composition and editing of the manuscript.

Acknowledgements

I would like to express my sincere gratitude to my supervisors Dr. Biao Huang and Dr. Vinay Prasad for being a constant source of motivation and guiding me with great patience and understanding throughout my thesis. I would like to thank Dr. Prasad for his valuable discussions and insight. Dr. Huang's critical reviews and suggestions have been very helpful in developing my analytical skills. I acknowledge them for providing me financial support throughout my graduate studies.

I would take the opportunity to mention special thanks to Xiongtan Yang for his guidance in the implementation of soft sensor algorithms. His constant inputs were instrumental in developing my statistical skills. Sincere appreciation is due to Swanand Khare for the discussions on Linear algebra and error analysis. I would like to thank Rouxia Li for helping me in particle filtering during the last few months of my masters. I owe a special thanks to Dr. Japan Trivedi for helping me to get access to the commercial reservoir simulator CMG. Siavash Nejadi was of terrific help and was always ready to help me with geostatistical simulations. I would like to thank Dr. Saneej Chitralekha for providing data for the reservoir models.

Special thanks to my close friends and roommates – Pramod Sripada, Deepesh Kumar, Khushaal Popli, Shivam Shahi, Manjeet Chowdhry and Rohan Gaikwad for always being there for support and for making my stay here in Edmonton very comfortable. I would like to thank my dearest friends in my hometown in Chennai – Ashok, Hemnath, Swarup, Varun, Kaushik and Aprajith for always staying in touch with me through Skype and supporting me.

I would like to express my deepest gratitude to my parents for their considerable understanding, love and support.

Table of Contents

List of Tables

List of Figures

Chapter 1

Introduction

1.1 Motivation and objective

In the modern day, there is a significant demand on competitive operating performance and high oil productivity of petroleum reservoirs. Industries invest millions of dollars in petroleum reservoir characterization to study the economic feasibility of reservoirs. Petroleum reservoir characterization is required to analyze and perform optimization studies on a reservoir to improve its productivity under different operating conditions and make long term predictions of its future performance. However, this is not an easy task in practice due to the high heterogeneity of petroleum reservoirs, represented by their spatially varying rock properties – porosity and permeability, which greatly dictate the quantity of recoverable oil. This uncertainty in reservoir characterization poses challenging problems for reservoir engineers in today's oil industry.

The problem of reservoir characterization is an inverse problem where a set of dynamic reservoir production data is used to compute the reservoir states and parameters that have caused that behavior. This inverse reservoir problem is commonly known as history matching. Over the last few decades, the field of history matching has grown at a brisk pace and several techniques have been proposed.

In spite of the rapid progress and advancement being made in the field of reservoir process monitoring and control, the inability to place multiple online sensors over the entire reservoir volume has led to poor observability and identifiability of reservoir states and parameters. Moreover, information obtained from the reservoir seismic images, geological surveys, well logging, dynamic production data and bottom hole pressure measurement is very limited and is available only at certain discrete locations in a reservoir.

This thesis focuses on the estimation of these rock properties (porosity and permeability) to forecast a reservoir's future performance, and is carried out through two history matching techniques: constrained ensemble Kalman filtering (EnKF) and particle filtering (PF).

1.2 Why is reservoir characterization difficult?

The characteristic feature of most reservoirs is that they are extremely heterogeneous. This heterogeneity is a measure of extent of variation in the reservoir rock properties as a function of location in the reservoir. The scale of variation of these properties may vary from one reservoir to another with some reservoirs exhibiting pore scale variation in properties such as porosity. Hence, a thorough knowledge about reservoir heterogeneity and properties is necessary to make accurate long term performance predictions and optimize its oil productivity, making reservoir characterization indispensable.

To perform reservoir characterization, vital information about the reservoir has to be gleaned from 3D and 4D-seismic studies, well logging and core measurements (these constitute prior information). However, the data obtained from these techniques is very limited. In order to get the complete picture of a reservoir, hundreds of wells need to be drilled and completed, which will turn into a very expensive venture for industries. Also, the data obtained through above-mentioned methods are generally corrupted by noise, making it not very reliable. This adds to uncertainty in reservoir characterization.

The process of integrating the prior information about a reservoir in the form of hard and soft data and dynamic production data into the existing reservoir models, also called as history matching, leads to many challenges. One of the main challenges associated with history matching applied to reservoir characterization is that this is an ill-posed problem. This is due to the fact that several possible combinations of model parameters can lead to the same set of observed reservoir behavior; hence, there is no unique solution [1].

1.3 Reservoir simulation and geostatistics

Reservoir simulation models are a set of complex and coupled non-linear partial differential equations describing the fluid flow (water, oil and gas) in a reservoir, represented by their porous rock structure. Any reservoir model can be characterized by a set of static and dynamic properties. Static properties are time-invariant in nature, e.g., porosity and permeability. On the other hand, the dynamic data are time variant and includes measurements from wells such as the bottom hole pressure, the oil production rate and water cut.

There are a number of commercial reservoir simulators available to optimize and predict reservoir performance. The most commonly used ones are CMG and ECLIPSE. Reservoir simulation consists of four stages – physical model development, mathematical model development, numerical model development and finally the design of computer algorithms [2]. In the first stage, the physical model describing the physics behind the reservoir simulation i.e., flow through porous media, is constructed. In the second stage, mathematical differential equations describing energy conservation and mass conservation are developed. The third stage is associated with the derivation of a numerical model by discretizing the differential equations. In the final stage, an algorithm is developed to solve the algebraic difference equations obtained through the discretization [2].

These equations are built upon the conservation of mass, fluid dynamics equations and Darcy's law, which explains the flow of fluids through porous media and and is given below:

$$v = \frac{k}{\mu}\frac{dp}{dx}$$

where

v = fluid flow rate through the medium (m/s),

k = permeability of the medium (mD),

μ = dynamic viscosity of the medium (Pa.s),

$\frac{dp}{dx}$= applied pressure difference per unit thickness of the medium (Pa/m).

In processes where thermal methodologies are used to aid in oil recovery such as the steam assisted gravity drainage (SAGD) process or the cyclic steam stimulation (CSS), energy conservation is also taken into account while developing the reservoir models. These equations are explained in appendix A.

The reservoir data obtained through the well core measurements, well logging and seismic studies are commonly classified into hard data and soft data. Hard data refers to the core measurements of the reservoirs obtained from well logging at discrete locations, and these include the values of porosity, permeability, water saturation and oil saturation. In other words, hard data gives the

absolute true values of the reservoir properties at some locations. Soft data, on the other hand, is obtained from seismic surveys and these reveal crucial information regarding the connectivity of a reservoir, its anisotropy and the distance based correlation structure of the rock properties such as porosity and permeability. In petroleum geology, this correlation structure is represented by a variogram.

A variogram gives a measure of the spatial dependence of a spatial random field or a stochastic process and is inversely related to correlation as shown in equation 1.1:

$$\Upsilon(\Delta x,\Delta y) = \frac{1}{2}\varepsilon\left[\{Z(x+\Delta x, y+\Delta y) - Z(x, y)\}^{2}\right] \quad (1.1)$$

where Z(x, y) is the value of variable of interest at the location (x , y). Mathematically, the variogram at a distance h can be defined as the average or the expectations of squared differences between pairs of data separated by h units.

Geostatistics deals with the estimation of rock properties at unknown locations given conditions of hard and soft data. Several algorithms have been developed to address this problem of interpolation and extrapolation, making geostatistics a highly mature field. Details of these geostatistical algorithms are provided in Appendix B. Geologists and reservoir engineers utilize these techniques to generate several plausible distributions of porosity and permeability, each honouring the hard and the soft data. These distributions serve as inputs to reservoir models for commercial reservoir simulators to make predictions of oil productivity. SGeMS and GSLIB are the most commonly used software packages for geostatistics.

1.4 A brief literature review

State and parameter estimation has grown at a rapid pace ever since the ground-breaking research of Kalman [3], leading to his proposal of a minimum variance state estimator for a linear system characterized by a Gaussian process and measurement noise, commonly called the Kalman Filter. The Kalman filter has been used successfully in the past for estimation in different applications in aerospace engineering, radar tracking, object tracking in computer vision, seismology and satellite navigation systems [4]. Many variants of the Kalman filter were introduced over the years to extend the estimation technique to different applications. For instance, the extended Kalman filter

(EKF) is used to estimate states in nonlinear systems. The other common variants of Kalman filter are the unscented Kalman filter (UKF) and the ensemble Kalman filter (EnKF).

In reservoir engineering, many history matching algorithms have been proposed for estimating the reservoir states and parameters and implemented successfully in the past few decades. Oliver et al [1] present a detailed timeline for the progress of history matching since its inception. Research in this field has grown rapidly, especially in the last decade, due to increased computational power and the popularity of geostatistical modeling and Monte Carlo methods to quantify uncertainty in reservoir performance prediction.

During the early stages of the history matching implementation, traditional methods were used. These include manual history matching procedures, in which model parameters such as porosity and permeability were tuned iteratively until the mismatch or error between the estimates and historical data is reduced. However, this process is not rigorous and extremely time consuming and is computationally expensive [5]. Over the years, history matching has been performed successfully using different methods including genetic algorithms [6], the gradual deformation method [7], neighborhood algorithms [8], gradient downhill methods [9], Markov chain Monte Carlo methods, randomized maximum likelihood and the ensemble Kalman filter (EnKF) [10].

The ensemble Kalman Filter (EnKF) is a Monte Carlo variant of the Kalman filter, and was proposed by Evensen [10] to perform state and parameter estimation for highly nonlinear ocean models. Following its success, the methodology was implemented for reservoir characterization by Lorentzen et al [11]. The reservoir engineering literature is now filled with hundreds of papers detailing different approaches used in history matching for efficient reservoir characterization. The main reason behind the widespread adoption of the EnKF in reservoir applications is because of its ease in handling nonlinearities and the fact that one does not need to know the explicit structure of the nonlinear reservoir model. Moreover, the computational complexity scales approximately linearly with the number of variables.

Despite the enormous success of the EnKF in reservoir applications, it suffers from a few limitations. The main drawback is its inability to yield geologically realistic estimates of reservoir properties such as porosity and permeability in some instances. Like other recursive estimators, its estimates do not honour hard and soft data constraints. As pointed out by Gosselin et al [12],

conditioning reservoir models to the seismic soft data is a very challenging task. Skjervheim et al [13] incorporated 4D seismic data using the EnKF with reasonable success. Moreover, calibrating large scale reservoir models using the EnKF may potentially yield erroneous estimates of the reservoir properties. This is because a typical reservoir simulation model is discretized into thousands of grid blocks; on the other hand, there are few well measurements available, leading to poor identifiability of the reservoir parameters. Now, the EnKF uses these limited measurements to update all the grid blocks of a reservoir irrespective of their distance from these wells. This leads to spurious updates of reservoir states and parameters. To counter this, studies have focused on determining a region of influence within a reservoir which has the greatest impact on the oil and gas production. In the update step, only the region of influence is updated sequentially by the EnKF, leading to great reduction in the dimension of the estimation problem. This procedure is also called as parameterization or covariance localization. Many metrics have been employed to perform covariance localization-based estimation; these include sensitivity analysis [9], wavelet transformations [14], discrete cosine transform (DCT) [15] and the sub space methods [16].

The particle filter (PF), has also been used in reservoir history matching. A set of particles and their associated weights, representing the reservoir states and parameters, are propagated through the simulator to obtain predictions. After the prediction step, these weights are used to sample the particles to obtain the posterior representation of these particles. There are several sampling techniques such as the sequential importance sampling (SIS) and the sequential importance resampling (SIR). These sampling techniques differ in the manner in which particles are selected for the importance distribution to obtain a posterior distribution. Generally, the particles with higher weights have more chances of being propagated into the simulator for the next prediction step and vice versa. Heimhuber et al [17] present history matching results using the polynomial chaos expansion-based bootstrap particle filters. Luo et al [18] compare the EnKF and PF for reservoir history matching applications.

1.5 Objective

The main objective of this work is to address the shortcomings of the conventional EnKF implementation for the challenging reservoir history matching problem. In this work, we have proposed a novel method by integrating the EnKF with geostatistics by using the hard and the soft data constraints in order to obtain geologically consistent estimates of the reservoir parameters. Another goal of this work is to couple the covariance localization-based EnKF with geostatistical

algorithms such as the sequential Gaussian simulation so that geological continuity information obtained from the soft data is honoured. Finally, a completely Bayesian-based stochastic estimation method, the particle filter, is also used for yielding estimates of reservoir parameters such as permeability.

1.6 Contributions of this thesis

The main contributions of this thesis are listed below:

A) Implementation of the hard data constrained ensemble Kalman filter (EnKF)
B) Variogram-constrained reservoir history matching using the EnKF using a novel projection method
C) Unconstrained and the variogram-constrained covariance localization-based history matching using the EnKF
D) Reservoir characterization and history matching using the particle filtering method.

1.7 Thesis Outline

This thesis is written in a paper format and the reminder of the thesis is organized as follows:

Chapter 2 focuses on the hard and soft data-constrained EnKF using a scaling and projection method. Here, the correlation matrix obtained after the unconstrained EnKF update is transformed to honour the true correlation structure from the variogram. The constraint algorithm results in better history matching compared to the unconstrained EnKF update method. The history matching is performed for a two-dimensional water flooding case and a three-dimensional SAGD process.

Chapter 3 presents the soft constrained covariance localization algorithm. The method of selecting the region of influence for performing localization is introduced. A novel approach to implement soft constraints in a localized EnKF model is described. The results of this constrained localization are compared with the unconstrained covariance localization. Again, a two-dimensional water flooding and a three dimensional SAGD reservoir processes are considered.

In chapter 4, the reservoir parameter estimation problem is studied using the particle filtering technique. The implementation of constraints using the above-mentioned methods is carried out for the particle filtering also and compared with results for unconstrained particle filtering.

Chapter 5 presents the conclusions and future work relating to this reservoir parameter estimation problem.

Appendices A and B describe the governing equations behind the reservoir simulator CMG and a brief summary of algorithms commonly used in geostatistics, respectively.

Chapter 2

Hard Data and Soft Data Constrained Reservoir Parameter Estimation with Ensemble Kalman Filter

The challenging problem of reservoir parameter estimation and history matching is studied in this chapter by applying a constrained Ensemble Kalman filter (EnKF) methodology. Ensemble Kalman filtering is a Monte Carlo-based method for data assimilation widely used in highly non-linear ocean, weather and reservoir models. It employs the reservoir model along with an ensemble of initial states and parameters to make a prediction for a time interval, at the end of which, in the update step, the model predictions are reconciled with data to provide updated state and parameter estimates. The main advantage of this method is the integration of most recent available measurements with the model predictions. However, the main drawback of the EnKF is that the states and parameters are updated based on the Kalman update equation, potentially making their estimates physically and geologically inconsistent. In this chapter, we present a novel approach to counter this limitation by implementing constraints in the algorithm so that estimates are geologically consistent and honour the prior reservoir information available in the form of hard and soft data. We then show that the constrained estimation leads to better history matching than its unconstrained counterpart by demonstrating the proposed methodology on two synthetic reservoir models.

2.1 Introduction

Hydrocarbon reservoir modeling and characterization are crucial to make forecasts on reservoir performance, optimize its productivity, make reservoir management decisions and conduct risk analysis. The rapid advancement of sensor technology has led to the development of numerous data acquisition techniques [19]. These tools have been applied successfully in reservoir management to extract crucial information about the underlying reservoir geometry, stratigraphy, anisotropy, faults and fractures. However, economic and practical factors limit the total number of such sensors that can be sampled in a real reservoir field. To obtain reliable predictions, it is of

paramount importance to integrate the prior geological data (hard and soft data) and dynamic reservoir information into the modeling process. Hard data generally refers to direct reservoir measurements like formation tops, thickness, obtained through well core sampling, while the soft data reveals fine details regarding the spatial variability, reservoir connectivity and distribution of rock properties in the reservoir volume obtained through seismic surveys, well logging and geologic insight. Dynamic data includes reservoir production measurements such as the cumulative oil production, the bottom hole pressure, water cut and the steam-oil ratio, and these are obtained during the stage of production. With the rapid development of seismic imaging, the petroleum industry is also incorporating 4-D seismic studies as a part of dynamic data to assist in the characterization process [20].

The calibration of reservoir models to match the dynamic production data is known as history matching. It is currently the most widely used technique employed by reservoir engineers to construct reasonably sound predictive reservoir models. In history matching, the model parameters and states such as porosity, permeability, facies indicators and pressure are adjusted and tuned so that the simulated results match historical observations from real petroleum reservoirs [21]. Mathematically, it can be framed as an inverse problem, aimed at arriving at the best possible solution space firmly grounded on the dynamics of fluid flow through porous media and production data. As is the case with any physical modeling process, history matching contains many assumptions and errors, leading to uncertainty in reservoir characterization.

Fig 2.1 gives a schematic representation of the generic reservoir history matching problem [22]. During the nascent stage of its implementation, history matching was performed by means of a trial and error approach, in which the model parameters were manually tuned until a good match with the production data was obtained [19]. However, this is a very time consuming process and is not ideal for large scale reservoir applications [5]. Due to its time consuming nature, optimization techniques such as a Gauss-Newton search, simulated annealing and genetic algorithms were applied to this inverse problem. In all of these methods, an objective function representing a mismatch between simulated data and history data is minimized to arrive at the model estimates. Gradient-based optimization algorithms were introduced in the history matching literature by Vasco et al [23], where sensitivity coefficients were used to arrive at a locally

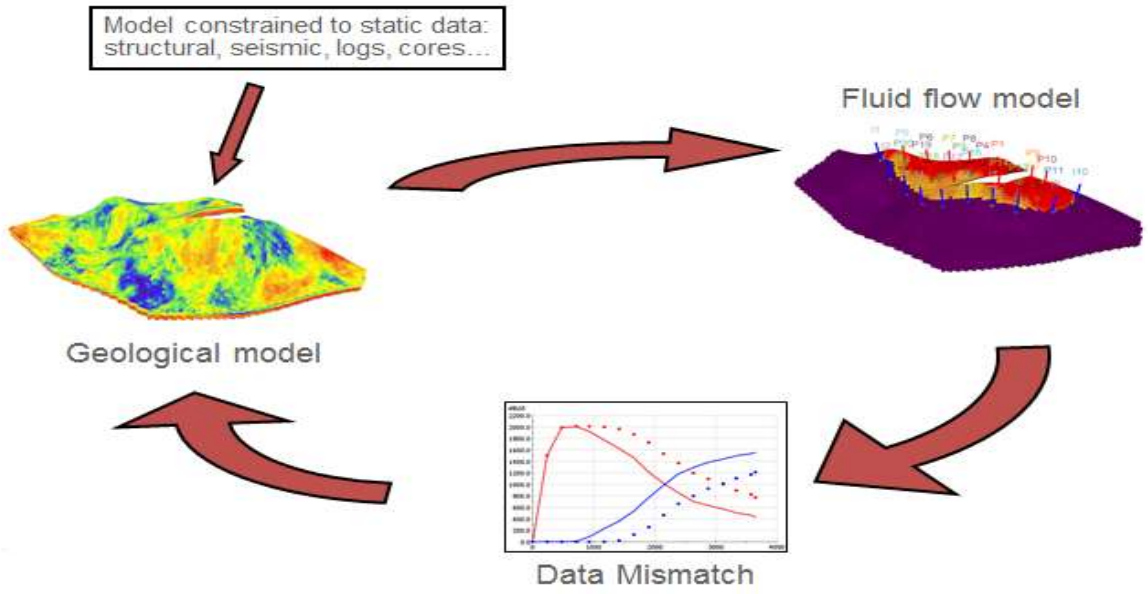

Fig 2.1 Reservoir history matching workflow [22]

minimum solution of the objective function for the parameter estimation problem. Details on some of these optimization methods for history matching can be found in Schulze-Riegert et al [24]. The most popular technique that is widely used for history matching is the ensemble Kalman Filter (EnKF). The implementation of the EnKF for history matching has led to promising results in the past. Apart from reservoir engineering, it has been extensively used in oceanography, hydrology and weather forecasting [25-28]. It is a Monte Carlo-based variant of the commonly used Kalman filters and was devised by Evensen [29] for the determination of ocean models using data assimilation.

The EnKF, like other Kalman filters, is a sequential recursive estimation and is characterized by the integration of the measurement data (dynamic data) into the reservoir model as and when it is available. In reservoir models, this data includes measurement data from the wells. Implementation of the EnKF consists of three stages: a prediction/ forecast step, an analysis step and an update step. In the prediction step, an ensemble of realizations is propagated through the reservoir model to generate the prior ensemble. In the analysis step, the Kalman gain is computed based on the ensemble covariance matrix. Finally, in the update step, measurement observations are used to arrive at an updated posterior ensemble. Details of each of these steps are provided in section 2.3.

The main advantage of the EnKF compared to other Kalman filters is that EnKF can handle nonlinearity in the model with great ease. In addition, this technique is non-iterative and requires only a limited number of Monte Carlo simulations using an ensemble of realizations [19]. Moreover, since the EnKF uses an ensemble of stochastic realizations to describe the model parameters, a measure of the uncertainty in the estimation of model parameters is obtained along with the model forecast. However, the EnKF suffers from certain drawbacks for use in reservoir simulation. The main limitation is that the EnKF may generate spurious correlations in the regions distant from the observation wells [30]. Secondly, the EnKF assumes a Gaussian distribution for the model parameters, which is not exactly in reality. To counter the problem of spurious correlation, covariance localization is performed, where the impact of observations is reduced up to a certain finite distance from the observation point as opposed to the entire system. Covariance localization [31-33] is a highly researched topic in petroleum engineering history matching problem, because the number of observable variables in a reservoir system is not very high and it could lead to spurious correlation in regions far from the wells. The topic of covariance localization and its implementation will be covered in Chapter 3. As mentioned in the beginning of this chapter, we have proposed a novel method to arrive at geologically and physical consistent estimates. Before discussing this in detail, it is necessary to have a sound basic knowledge on geostatistics and the methodology of the EnKF, which are respectively dealt with in the following two sections.

2.2 Geostatistics

This section explains the basic terminology associated with geostatistics. Geostatistics is a highly mature field concerned with the modeling of spatially correlated data. It was first introduced into the applied statistics literature by Matheron [34], when he tries to quantify the ore properties of a mine. Since a petroleum reservoir is also characterized by spatially varying geological layers and rock structures, it is currently being widely adapted for reservoir engineering applications [35]. Geostatistics aids in accurate forecasting of reservoir performance by quantitatively combining the different types of available hard and soft data [36], and many details are available [37-40].

The most common measures of the spatial continuity widely used in earth sciences are the variogram, the covariogram and the correlogram. A variogram is defined as the variance of the difference between the values of the spatial properties at two locations in a spatial study area. Its expression is given below:

$$\gamma(h) = \frac{1}{2\,N(h)} \sum_{\propto=1}^{N(h)} [z(u_\propto + h) - z(u_\propto)]2 \tag{2.1}$$

where $z(u)$ is the value of variable of interest at the location u, 'h' is the separation lag, representing the spatial distance between two points under consideration and $N(h)$ is the number of pairs of grid blocks whose separation distance is 'h'. On a similar note, the covariance and the correlogram, which provide the covariance function and average correlation coefficient as a function of the spatial separation distance 'h', can be written as:

$$C(h) = \frac{1}{N(h)} \sum_{\propto=1}^{N(h)} [z(u_\propto + h)z(u_\propto)] - \; m_0.m_{+h} \tag{2.2}$$

$$\rho(h) = \frac{C(h)}{(\sigma_0.\sigma_{+h})^{1/2}} \tag{2.3}$$

where $C(h)$ and $\rho(h)$ denote the covariance function and the correlogram respectively, m_0 and m_{+h} represent the mean head and tail values and σ_0 and σ_{+h} are the corresponding standard deviations. These are explained below:

$$m_0 = \frac{1}{N(h)} \sum_{\propto=1}^{N(h)} z(u_\propto) \tag{2.4}$$

$$m_{+h} = \frac{1}{N(h)} \sum_{\propto=1}^{N(h)} z(u_\propto + h) \tag{2.5}$$

$$\sigma_0 = \frac{1}{N(h)} \sum_{\propto=1}^{N(h)} [z(u_\propto) - m_0]^{\,2} \tag{2.6}$$

$$\sigma_{+h} = \frac{1}{N(h)} \sum_{\propto=1}^{N(h)} [z(u_\propto + h) - m_{+h}]^{\,2} \tag{2.7}$$

The variogram of a property is associated with unique parameters, namely the sill, the range and the nugget (see **Fig 2.2**).

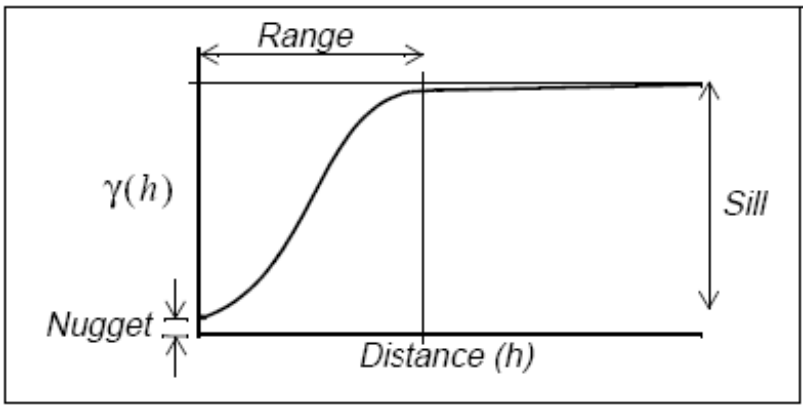

Fig 2.2 A typical variogram for a reservoir

Theoretically, the ideal value of variogram at the origin should be zero. However, in real cases, small values of the variogram, called the nugget are observed at zero lag, possibly due to measurement errors. The nugget in a variogram model represents this error. With increasing lag distance, the autocorrelation between properties separated by h units decreases. The lag distance at which this autocorrelation value reduces to zero is called the range of the variogram. The variogram value at the lag distance corresponding to its range is called the sill.

Geostatistics involve many assumptions regarding the variogram calculations. The most important one is the stationary assumption. All geostatistical estimation is characterized by some sort of stationarity – strict stationarity, second order stationarity or intrinsic hypothesis. Usually, either second order or intrinsic stationarity is assumed. For a second order stationary process, the covariance function is assumed to be independent of spatial location and is constant for a given separation distance 'h'. For such processes, the correlogram and the variogram are related by the following equation:

$$\rho(h) = 1 - \left(\frac{c(h)}{C(0)}\right) \tag{2.8}$$

where, $C(0)$ is the covariance function at zero lag.

There are many geostatistical estimation and simulation algorithms, details of which can be found in Appendix B.

2.3 Ensemble Kalman Filter (EnKF) Methodology

The EnKF uses a Bayesian approach, where an initial ensemble is obtained by generating permeability and porosity fields using *a priori* geostatistical assumptions. The production data is incorporated sequentially in time, and the permeability and porosity fields are updated as new production data is introduced. Moreover, the dynamic states of a reservoir, i.e., reservoir pressure and saturations, are also updated along with the rock properties such as porosity and permeability.

For the case of history matching of a reservoir, a stochastic model represented by the following set of equations is considered [1].

$$X_k = f(X_{k-1}, \theta) \tag{2.9}$$

$$Y_k = g(X_k) + V_k \tag{2.10}$$

$$V_k \sim N(0, R) \tag{2.11}$$

where

X_k : State variables of the reservoir at a given time instant *k*. This may include either the dynamic variable such as the pressure, oil saturation and the water saturation, which change with time or the static variables such as porosity and permeability, which do not change with time.

f : Reservoir simulator function which relates the state variables at a given instant to the state variables at the previous instant.

Y_k : Represents the dynamic production data obtained at the wells such as the oil production rate, the steam oil ratio, the gas production rate, the monthly oil production, the bottom-hole pressure, water cuts, oil cuts and the cumulative liquid production rate.

V_k : Represents the measurement noise associated with the process. It is assumed to follow a normal distribution with zero mean and covariance matrix R.

The main advantage of the EnKF is that we do not need to know the structure of functions f and g explicitly, but only need their values, which is consistent for use with commercial reservoir simulators. These functions are reservoir simulator functions and are extremely nonlinear and implicit.

The model parameters such as porosity and permeability are taken as a random walk model [13] as given below:

$$\theta_k = \theta_{k-1} + w_{k-1} \tag{2.12}$$

where w_{k-1} follows a Gaussian distribution with zero mean and low variance Q [1]. This is a typical way to transfer a parameter estimation problem to a state estimation problem. It is important to note that while the true value of θ is a constant, its estimates obtained by using the EnKF varies with each assimilation step.

The EnKF consists of three steps – a prediction step, analysis step and an update step. In the prediction step, an ensemble of realizations is propagated through the reservoir model to generate the prior ensemble. In the analysis step, Kalman gain is computed based on the ensemble covariance matrix. Finally, in the update step, the measurement dynamic data are used to make an update to prior ensemble to get the updated posterior ensemble.

This process is schematically represented in **Fig 2.3** and **Fig 2.4**.

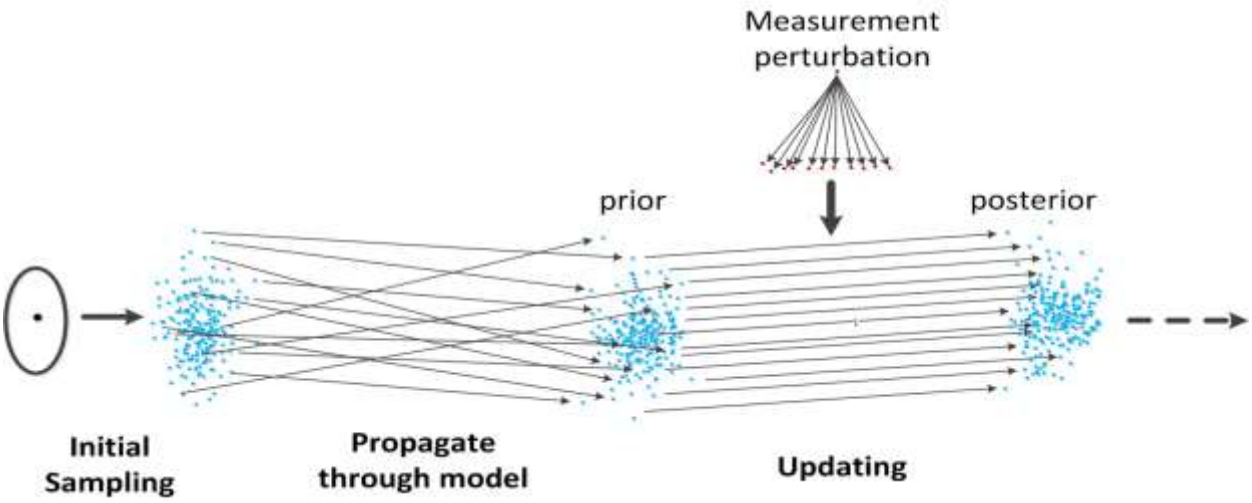

Fig 2.3 Schematic of the ensemble Kalman filter

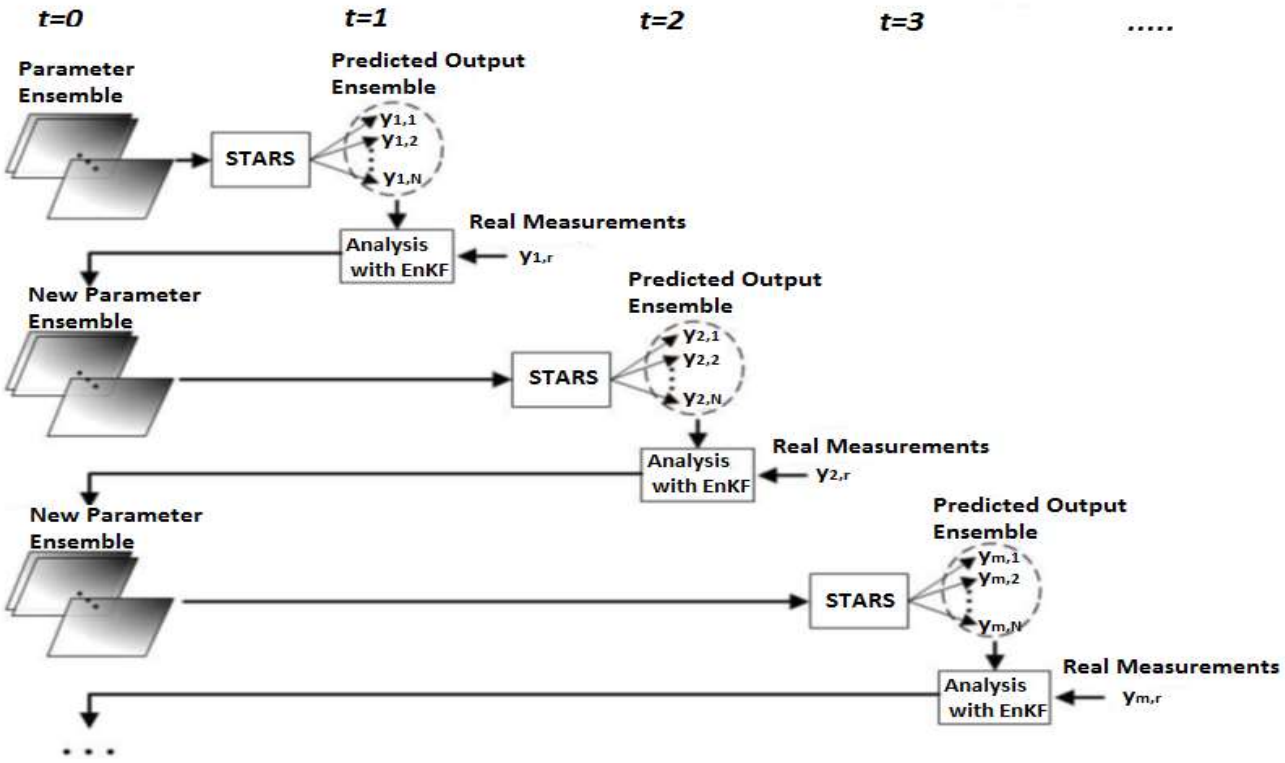

Fig 2.4 Schematic representation of EnKF for history matching a reservoir. STARS is one of the toolboxes that comes along with the commercial reservoir simulation package CMG

2.3.1 PREDICTION STEP:

The first stage in the prediction step is the generation of N realizations from the prior probability distribution to represent an ensemble of model parameters.

For the generation of the initial ensemble of the permeability field, the geostatistical simulation package SGeMS was used in this work and the spatial distribution was generated using sequential Gaussian simulation.

Each of these generated realizations was then propagated in time using the reservoir simulator (CMG), resulting in the prior ensembles for $x^{i}_{k|k-1}$ and $\theta^{i}_{k|k-1}$.

$$x^{i}_{k|k-1} = f\left(x^{i}_{k-1|k-1}, \theta^{i}_{k-1|k-1}\right) \tag{2.13}$$

$$\theta^{i}_{k|k-1} = \theta^{i}_{k-1|k-1} + w^{i}_{k-1} \tag{2.14}$$

Being a joint state and parameter estimation problem, the equations 2.13 and 2.14 can be represented by means of an augmented state vector $z^{i}_{k|k-1}$ (see equation 2.15).

$$z^{i}_{k|k-1} = \begin{bmatrix} x^{i}_{k|k-1} \\ \theta^{i}_{k|k-1} \end{bmatrix} = z^{i}_{k|k-1} = \begin{bmatrix} f\,(x^{i}_{k-1|k-1}\,, \theta^{i}_{k-1|k-1}) \\ \theta^{i}_{k-1|k-1} + w^{i}_{k-1} \end{bmatrix} \tag{2.15}$$

Now, the mean of the predicted state ensemble with respect to this augmented state vector at time instant k given their values until time instant k-1 for any realization i can be written as:

$$\mu^{z}_{k|k-1} = \frac{1}{N} \sum_{i=1}^{N} z^{i}_{k|k-1} \tag{2.16}$$

It is important to calculate the error or the uncertainty in the predicted states and parameters in the prediction step with respect to the overall ensemble. This error (say $e^{i}_{k|k-1}$) can be calculated using the mean of the predicted ensemble $\mu^{i}_{k|k-1}$ as shown in equation 2.17.

$$e^{i}_{k|k-1} = z^{i}_{k|k-1} - \mu^{z}_{k|k-1} \tag{2.17}$$

Along similar lines, the mean of the predicted measurement ensemble ($\mu^{i}_{k|k-1}$)and the error in the predicted measurement with respect to the overall ensemble ($\varepsilon^{i}_{k|k-1}$) can be calculated by using equations 2.18 and 2.19.

$$\mu^{y}_{k|k-1} = \frac{1}{N} \sum_{i=1}^{N} y^{i}_{k|k-1} \tag{2.18}$$

$$\varepsilon^{i}_{k|k-1} = y^{i}_{k|k-1} - \mu^{y}_{k|k-1} \tag{2.19}$$

Now the sample covariance matrixes of the ensemble can be estimated using equations 2.20 and 2.21.

$$\hat{P}^{\varepsilon,\varepsilon}_{k|k-1} = \frac{1}{N-1} \sum_{i=1}^{N} (\varepsilon^{i}_{k|k-1})\,(\varepsilon^{i}_{k|k-1})^{T} \tag{2.20}$$

$$\hat{P}^{e,\varepsilon}_{k|k-1} = \frac{1}{N-1} \sum_{i=1}^{N} (e^{i}_{k|k-1})\,(\varepsilon^{i}_{k|k-1})^{T} \tag{2.21}$$

where

$\widehat{P}^{e,\varepsilon}_{k|k-1}$: Cross-covariance matrix between the predicted state ensemble and the predicted measurement ensemble.

$\widehat{P}^{\varepsilon,\varepsilon}_{k|k-1}$: Sample auto-covariance matrix between the predicted state ensemble.

2.3.2 ANALYSIS STEP:

In the analysis step, the Kalman gain is computed based on the covariance matrices of the error ensemble as given below:

$$K_{gain} = \widehat{P}^{\varepsilon,\varepsilon}_{k|k-1}(\widehat{P}^{e,\varepsilon}_{k|k-1} + R)^{-1} \tag{2.22}$$

where R is the measurement noise covariance matrix defined in equation 2.11.

2.3.3 CORRECTION / UPDATE STEP:

In the correction / update step, the actual measurements from the reservoir are used to update the model parameters obtained from forward simulations of the ensemble realizations. Since the actual measurements are contaminated with noise in real process, N perturbed measurements are generated using samples drawn from the process noise v_k (see equation 2.11), which follows a normal distribution with zero mean and covariance matrix R.

$$y^{i,obs}_k = y^{obs}_k + v^i_k \tag{2.23}$$

After the generation of N perturbed measurements, the reservoir parameters and states are updated using the well-known Kalman update equation given by:

$$z^i_{k|k} = z^i_{k-1|k-1} + K_{gain}(y^{i,obs}_k - y^i_{k|k-1}) \tag{2.24}$$

Jointly estimating both the states and parameters by means of the augmented state vector $z^i_{k|k}$ using equation 2.24 implies that the dynamic states of the reservoir such as the pressure, oil saturation and temperature are updated without solving any flow equations. On the other hand, they are updated based on the linear Kalman update equation (2.24). As pointed out by Wen et al [24], this could potentially lead to physically meaningless estimates of the reservoir states and may not be consistent with respect to the updated static parameters such as porosity and permeability. In order to overcome this problem, they proposed a confirming option-based EnKF update. In this method, only the static parameters are updated during each correction step as shown in equation 2.25

$$\theta^{i}_{k|k} = \theta^{i}_{k-1|k-1} + K_{gain}(y^{i,obs}_{k} - y^{i}_{k|k-1}) \quad (2.25)$$

The dynamic states are then updated by running the simulator again using the most recently updated static parameters from the previous time instant to the current time instant so that the updated static parameters are at all times physically consistent with the updated dynamic reservoir states [24]. In this work, we have used this confirming option-based joint reservoir state and parameter estimation. Fig 2.5 illustrates the schematics of this method.

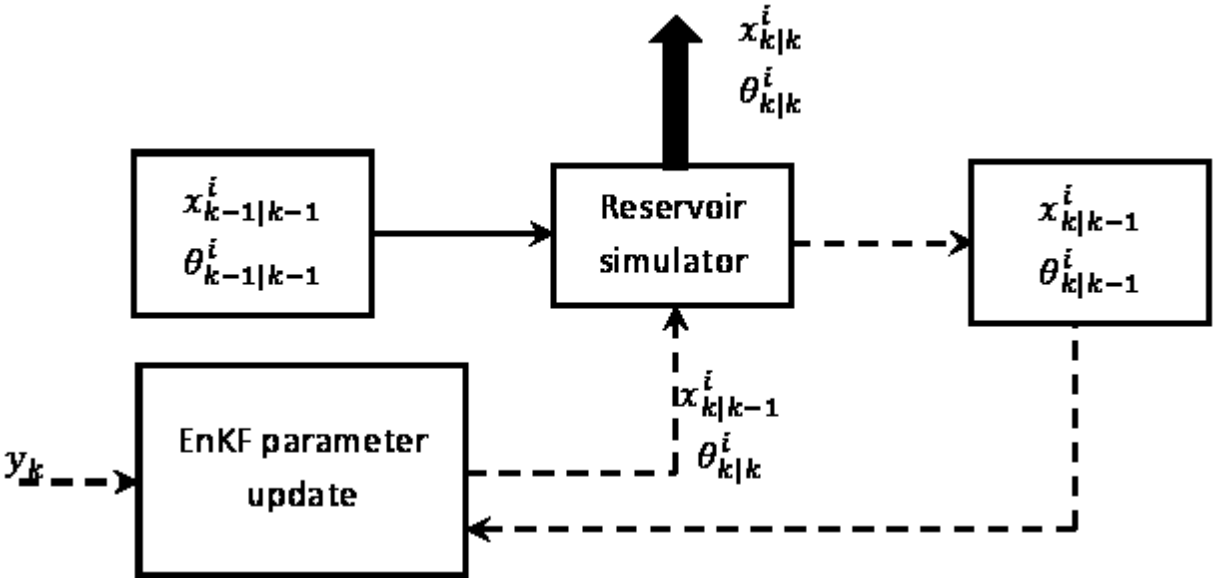

Fig 2.5 Schematic representation of the confirming option-based EnKF joint state and parameter update. The dashed lines represent the pre-confirming confirming stage and the solid block arrow represents the post-confirming stage.

2.4 Proposed methodology of soft constraint implementation:

To get reliable forecasts on reservoir productivity, it is important to obtain multi-probable realizations of model parameters that not only lead to a good match with historical production data but are also geologically realistic. The geological realism, as mentioned earlier corresponds to the spatial connectivity, anisotropy and variability of the facies and the rock structure.

In this work, we have chosen correlograms of permeability to represent the soft data information obtained from seismic studies. A correlogram gives a measure of the degree of spatial variation through a plot of average correlation coefficients ($\widehat{\boldsymbol{\rho}_{\boldsymbol{h}}}$) as a function of lag distance h. h represents

the distance between any two grid blocks, i.e., h=n represents all pairs of grid blocks whose separation distance is n.

In the first stage of the constraint implementation, the variograms are first calculated in the vertical and horizontal directions to find the major and minor directions of continuity. Correlograms corresponding to these directions are also generated. After this stage, a correlation matrix (CR) and a correlogram corresponding to the major direction of spatial correlation is obtained.

Since the EnKF update does not necessarily match the known spatial correlation defined by the correlogram, it is very important to apply a transformation or a projection on the updated parameters so that the transformed parameters honor this spatial correlation. In the method proposed, we have used a set of matrix transformation operations (see equations 2.26 – 2.36) to honour the soft data information. This technique is described below:

It is well known that the correlation matrix (CR) is related to covariance matrix (CV) through equation 2.26.

$$CV = (\sigma)^{\frac{1}{2}}(CR)(\sigma)^{\frac{1}{2}} \tag{2.26}$$

Extending equation 2.26 to the true spatial correlation matrix of the reservoir *($(CR)_{true}$)*, we have:

$$(CV)_{true} = (\sigma_{true})^{1/2}(CR)_{true}(\sigma_{true})^{1/2} \tag{2.27}$$

where σ_{true} is the diagonal matrix whose elements represent the variance of the parameter (permeability and porosity) in every grid block of the true model.

After the EnKF update, we have

$$(CV)_{EnKF} = (\sigma_{EnKF})^{1/2}(CR)_{EnKF}(\sigma_{EnKF})^{1/2} \tag{2.28}$$

To transform $(CR)_{EnKF}$ to $(CR)_{true}$, we have

$$(CR)_{EnKF}(T) = (CR)_{true} \tag{2.29}$$

where T is the transformation/projection matrix and is calculated as:

$$T = ((CR)_{EnKF})^{-1}\,(CR)_{true} \tag{2.30}$$

$$(CR)_{EnKF} = (CR)_{true}\,(T)^{-1} \tag{2.31}$$

Substituting $(CR)_{EnKF}$ from equation 2.31 in equation 2.28, we have:

$$(CV)_{EnKF} = (\sigma_{EnKF})^{1/2}(CR)_{true}\,(T)^{-1}(\sigma_{EnKF})^{1/2} \tag{2.32}$$

$$= (\sigma_{EnKF})^{1/2}(CR)_{true}\,((\sigma_{EnKF})^{-\frac{1}{2}}(T))^{-1} \tag{2.33}$$

Now, post multiplying both sides of equation 2.33 by $(\sigma_{EnKF})^{-\frac{1}{2}}(T)$, we get:

$$(CV)_{EnKF}(\sigma_{EnKF})^{-\frac{1}{2}}(T) = (\sigma_{EnKF})^{1/2}(CR)_{true} \tag{2.34}$$

$$(CV)_{EnKF}(\sigma_{EnKF})^{-\frac{1}{2}}(T)(\sigma_{EnKF})^{1/2} = (\sigma_{EnKF})^{1/2}(CR)_{true}(\sigma_{EnKF})^{1/2} \tag{2.35}$$

Equation 2.35 is obtained by post multiplying both sides of equation 2.34 by $(\sigma_{EnKF})^{1/2}$.

$$(CV)_{EnKF,modified} = (\sigma_{EnKF})^{1/2}(CR)_{true}(\sigma_{EnKF})^{1/2} \tag{2.36}$$

where $(CV)_{EnKF,modified} = (CV)_{EnKF}(\sigma_{EnKF})^{-\frac{1}{2}}(T)(\sigma_{EnKF})^{1/2}$

It can be easily inferred from equation 2.36 that the modified EnKF covariance matrix has the same correlation matrix as that of the true model. Hence, after every update step, the covariance matrix is transformed in the above manner. Once the transformed covariance matrix is obtained, realizations of the ensemble to be used for the next prediction stage are generated by resampling with this covariance matrix and the mean values given by the update step of the EnKF.

Thus, in this manner, the ensemble statistics derived from the EnKF update operation as well as the spatial correlation statistics derived from the soft data are both used in generating the new realizations for every prediction step. In this way, the prior ensemble members honour geostatistics at all times during the parameter estimation process.

2.5 Results

2.5.1 Heterogeneous 2D reservoir model:

A two-dimensional reservoir model of dimension 100 x 1 x 20 is created using the commercial simulator CMG IMEX. **Fig 2.6** represents the permeability map of the reservoir. The model consists of one injector well placed at the center of the well and two producer wells located at

either side of the injector. The data set for this model was taken from 2000 SPE Project [41]. Initially, it is assumed that the reservoir is fully saturated with oil, i.e., the oil saturation $S_o = 1.0$ and values of the gas saturation S_g and water saturation S_w being equal to zero. The permeabilities at all the grid block locations were taken from the above mentioned model. There are totally 2000 permeability values and permeabilities in all the directions were set to be equal. Since this is a highly heterogeneous model, the value of permeability is different in different grid blocks. The values of permeability range from 0 to 1000 mD in this model. It is assumed that certain information is available in the form of hard data obtained, for example, from well core measurements. The values of permeability is assumed to be known at 100 grid block locations at i=1, 25, 50, 75 and 100 and the corresponding grid blocks along the vertical direction. The porosity was assumed to be homogeneous in the reservoir was assigned the value of 0.25.

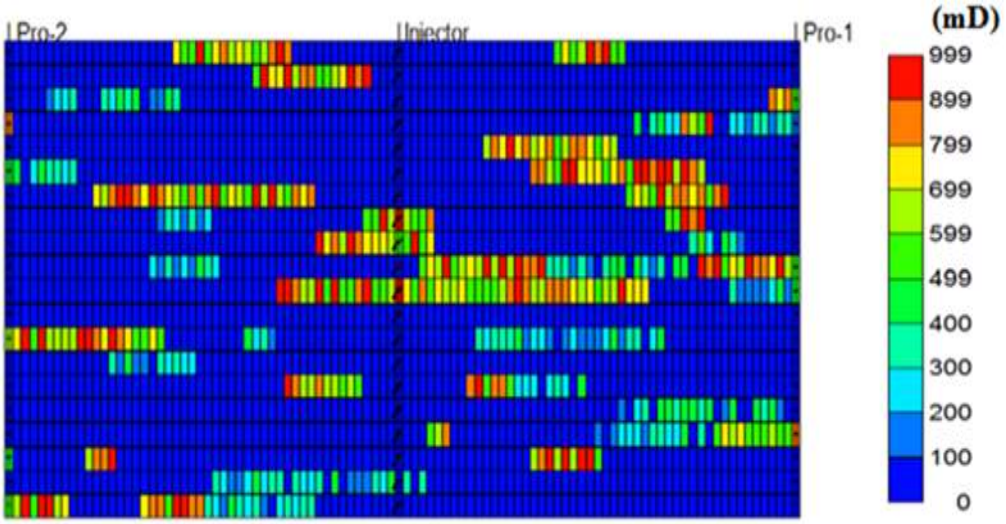

Fig 2.6 Two dimensional reservoir model

In this case, oil was produced by a waterflooding process. In a waterflooding process, water is injected in order to increase the reservoir pressure leading to increased oil production from the reservoir. Water displaces oil from the pore spaces. In this exercise, we have used the permeability information from the reference data set [41] and simulated the reservoir for 4500 days to obtain historical data. After obtaining this data, the permeability values at all grid blocks except those corresponding to the hard data locations are frozen and hidden from the model. The objective was to estimate these permeability values using prior geological information and the historical data. The inputs used in the process were the water injection rate and its mole fraction in the injection

phase. The parameter to be estimated is permeability. The parameter vector is comprised of the permeability values at 2000 grid blocks. The state vector consisted of three dynamic reservoir properties, namely, the oil saturation, pressure and the water saturation. Since there are 2000 grid blocks in total with each block having a particular set of values of these states, there are 6000 states in total. The production data vector consisted of four components, namely the gas production at well 1, the gas production at well 2, the oil production at well 1 and the oil production at well 2. The variance of permeability is set to 10^{-4} md^2 at all grid block locations and the variance in the gas and oil productions were set to be 5 cubic feet and 10 cubic feet respectively.

It is well known that the EnKF performs best when the distributions of the states and parameters follow a Gaussian distribution. In petroleum engineering, ln(permeability) is usually assumed to honour Gaussian distribution. Taking this into consideration, 50 realizations of ln(permeability) fields were generated to construct the initial ensemble for the EnKF. For the generation of this initial ensemble, the geostatistical simulation package SGeMS was used, where the spatially distributed permeability fields were generated using sequential Gaussian simulation (SGS). The initial ensemble was constructed to honour both the hard data and the correlogram. The history matching of the production data was carried out using both the conventional and the projection method-based EnKF algorithms. The update step of the EnKF was performed at 14 time instances. To be precise, it was carried out after 250, 400, 500, 600, 700, 800, 1000, 1200, 1400, 1500, 1750, 2500, 3500 and 4500 days.

Fig 2.7 shows the history matched mean permeability map of the estimated models and the initial models. It can be observed that the history matched mean permeability fields are in better agreement to the reference field compared to the initial mean permeability field. Moreover, the projection method-based history matched mean permeability map more closely resembles the reference permeability map compared to the conventional EnKF-based estimated field. This is because, in the projection method, the EnKF-based estimates are modified through the algorithm described in section 2.4 to honour the prior geostatistical information. This operation makes the permeability estimates more consistent with the reservoir geology compared to the estimates derived from the traditional EnKF method. Moreover, the projection method-based EnKF was able to capture the spatial variation and heterogeneity of permeability better than the traditional method

and resulted in estimates with very similar distribution of low, medium and high permeability values to that of the reference reservoir model. This is shown in the form of a histogram in **Fig 2.8**.

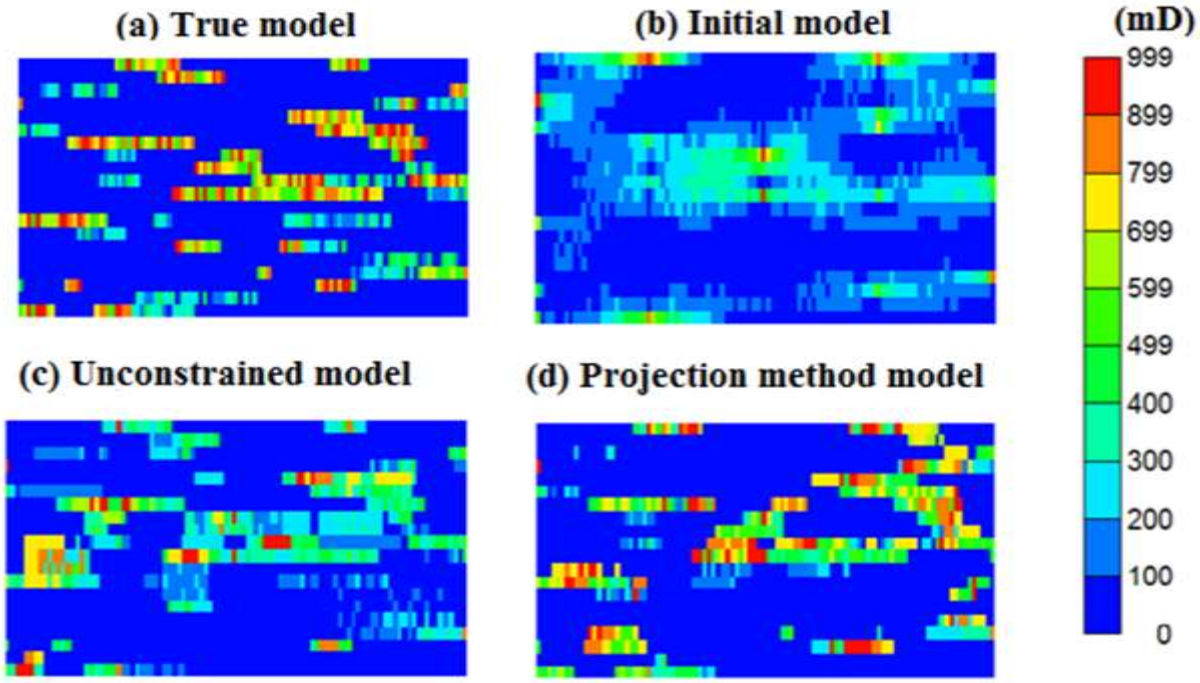

Fig 2.7 Comparison of constrained vs. unconstrained estimation. Clockwise from top left: Reference permeability field from true model, estimated permeability field using projection method-based EnKF and initial permeability field

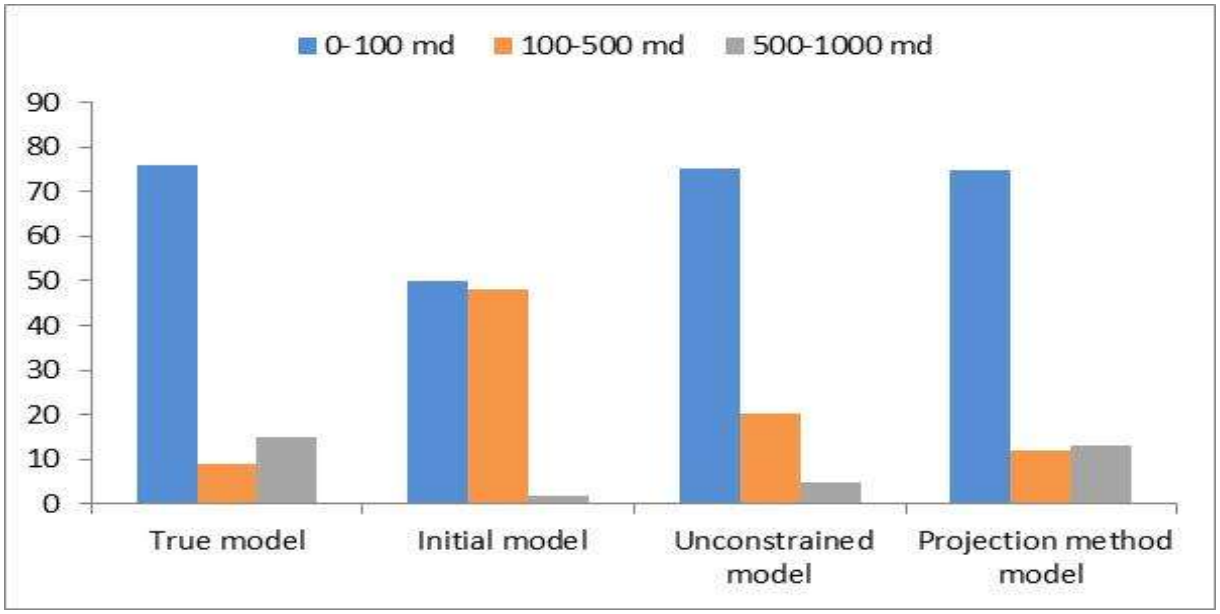

Fig 2.8 Comparison of the histograms of the permeability distribution for true, initial, unconstrained and projection method models.

To validate the history matching performance using unconstrained and soft data-constrained EnKF algorithms, we carried out simulations of the reservoir for 20 years - from the first time instant (t=0 day) to the last instant (t = 7300 days) using the reference and the estimated models and the production data obtained for these cases were compared. **Fig 2.14** and **Fig 2.15** compare the ensemble predictions for the monthly oil production obtained using the mean permeability fields of the initial and the estimated models with the actual historical oil production data for the production wells Pro-1 and Pro-2 respectively. **Fig 2.16** and **Fig 2.17** provide a comparison of the ensemble predictions for the monthly gas production obtained using the mean permeability field of the initial and the estimated models with the actual historical gas production data for the production wells Pro-1 and Pro-2 respectively. It can clearly be observed that a very good match between the historical data and the production data corresponding to the estimated models using both conventional and the projection method-based EnKF methods is obtained, demonstrating the efficacy of the EnKF algorithm. This successful performance can be attributed to the correction step of the EnKF algorithm, where the available online measurements from the production wells reduce the uncertainty in the reservoir parameters with each data assimilation step. **Fig 2.9** and **Fig 2.11** give a comparison of the profiles of average oil and gas saturations at the last time instant corresponding to the true model, the initial predicted model and the final estimation models

respectively. The evolution of the mean oil saturation and gas saturation in the entire reservoir field is shown in **Fig 2.10** and **Fig 2.12** respectively for the reference model, means of the initial and the estimated models. The reduction in the mean oil saturation in the reservoir is indicative of the recovery process, resulting in lesser oil concentration in the reservoir with the progress of time. It can be noted from these figures that the projection method-based EnKF performs better than the traditional EnKF. **Fig 2.13** gives a comparison of the profiles of the pressure distribution in the reservoir at the last time instant corresponding to true model, the initial predicted model and the final estimation models.

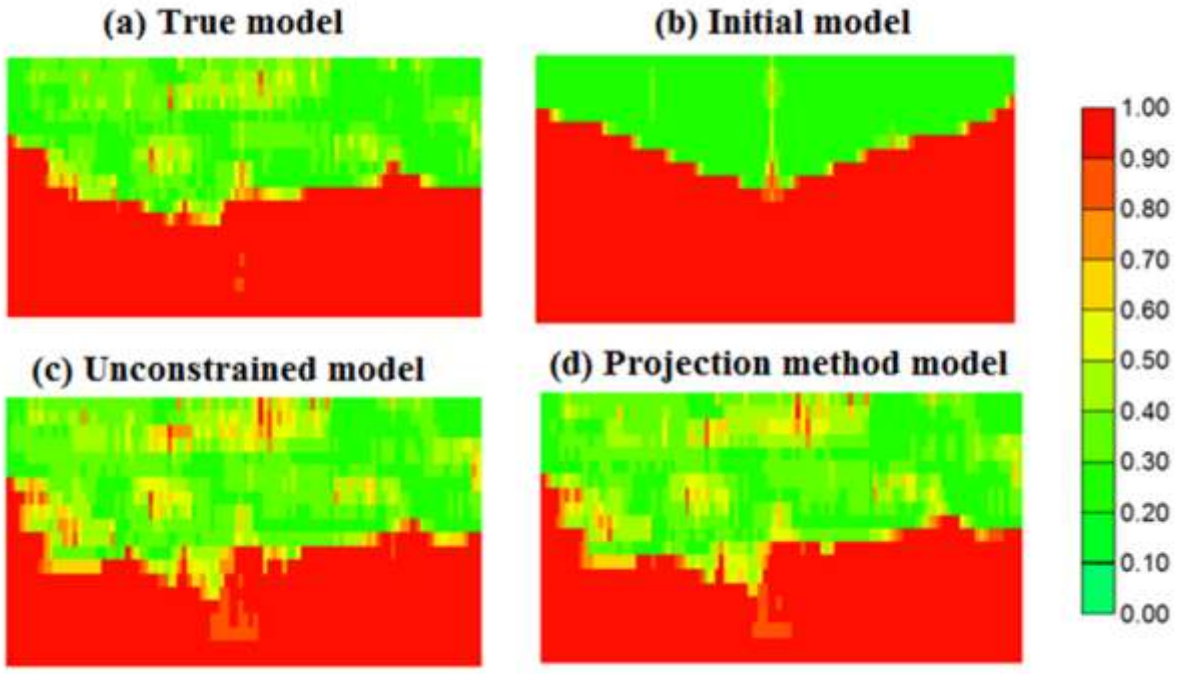

Fig 2.9 Comparison of constrained vs. unconstrained estimation with respect to oil saturation at the last time instant (t=7300 days). Clockwise from top left corner: Oil saturation field corresponding to the true model, mean oil saturation fields corresponding to the initial model, projection method-based EnKF model and the unconstrained EnKF model.

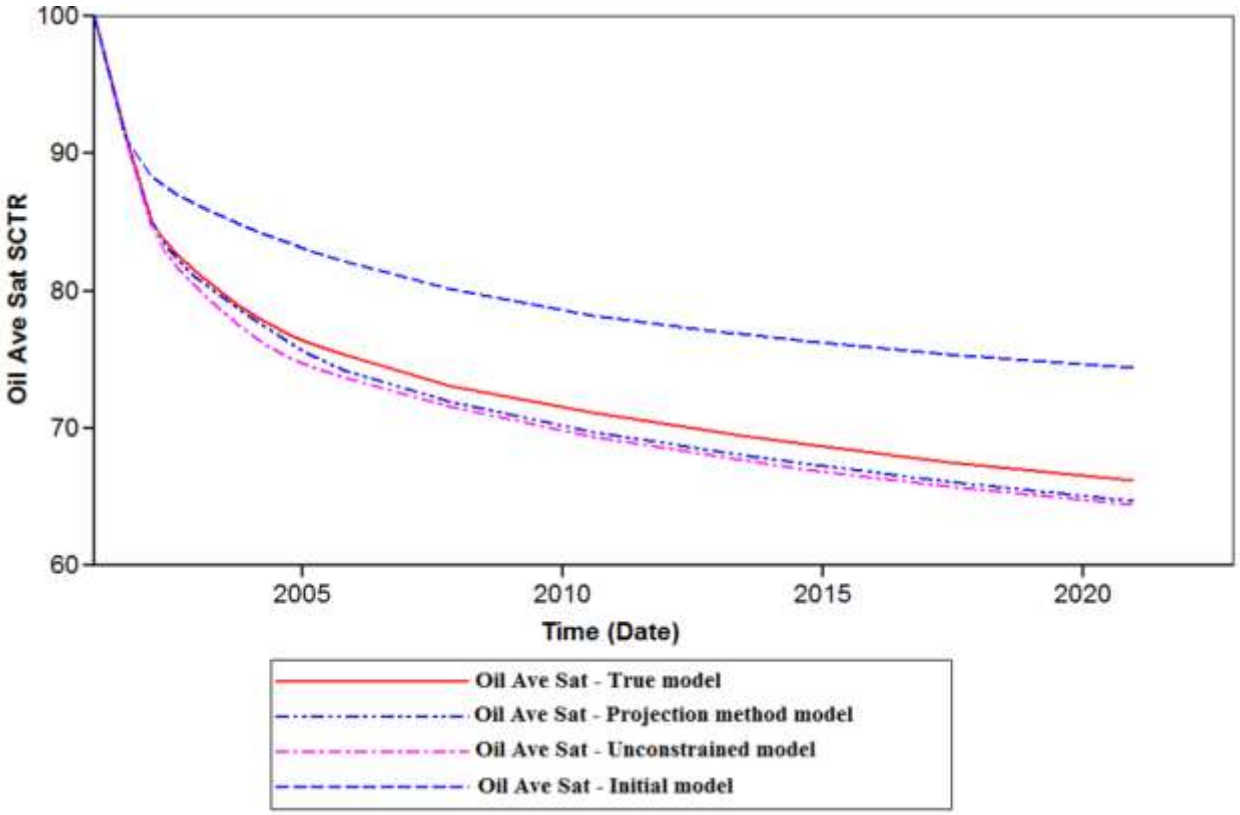

Fig 2.10 Comparison of the average oil saturation in the entire reservoir with the progress of the waterflooding process for true model, initial model, projection method-based EnKF and unconstrained EnKF model.

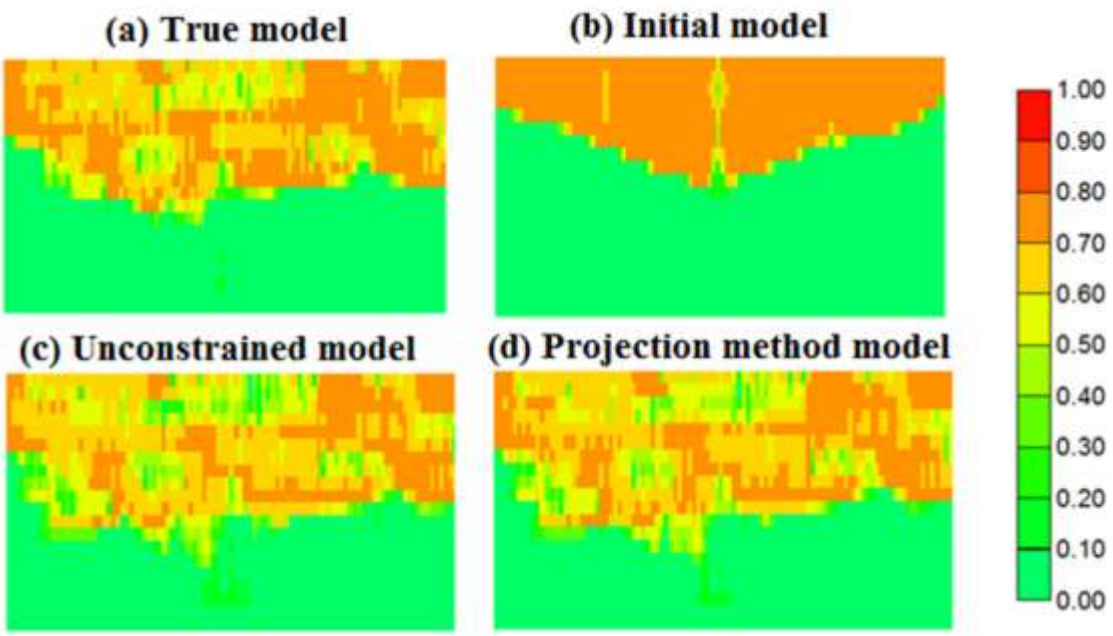

Fig 2.11 Comparison of constrained vs. unconstrained estimation with respect to gas saturation at the last time instant (t=7300 days). Clockwise from top left corner: Gas saturation corresponding to true model, average gas saturation fields obtained from the initial model, projection method-based EnKF model and the unconstrained EnKF model.

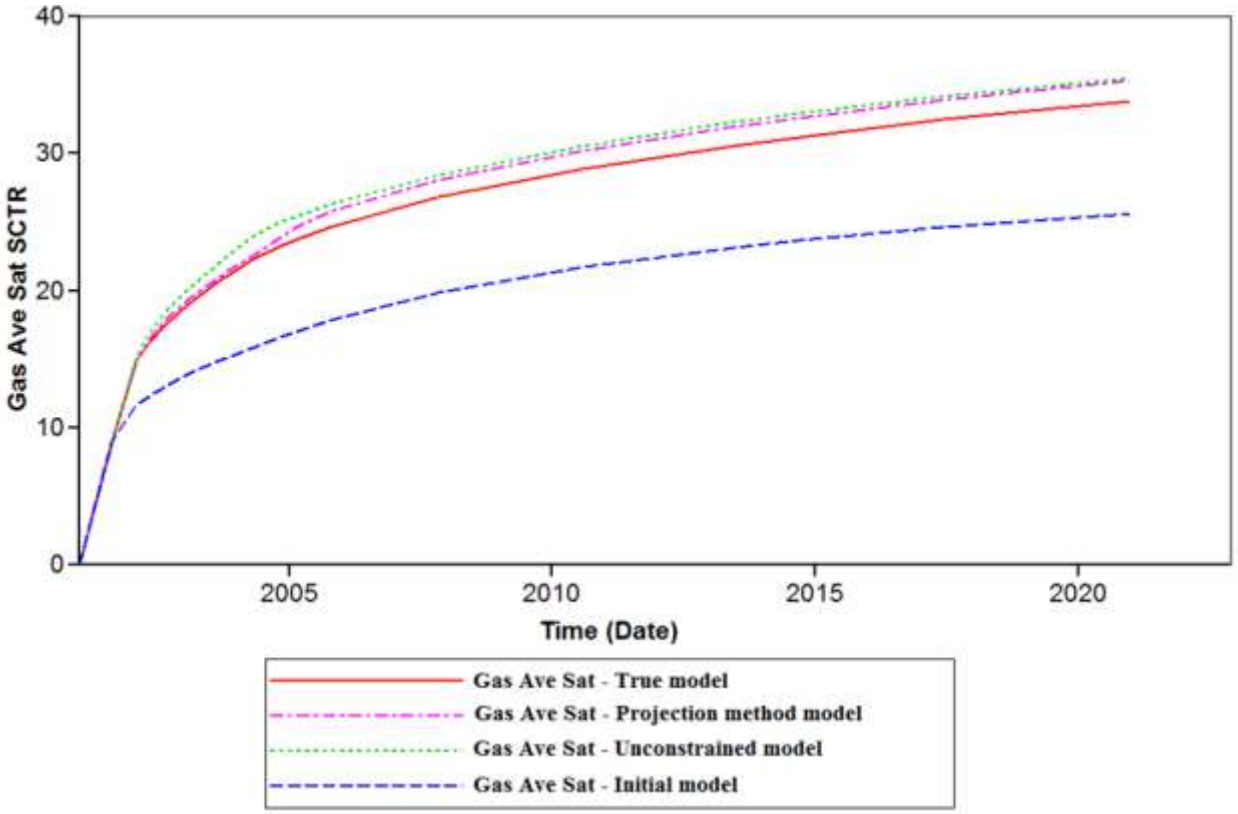

Fig 2.12 Comparison of the average gas saturation in the entire reservoir with the progress of the waterflooding process for true model, initial model, projection method-based EnKF and unconstrained EnKF model.

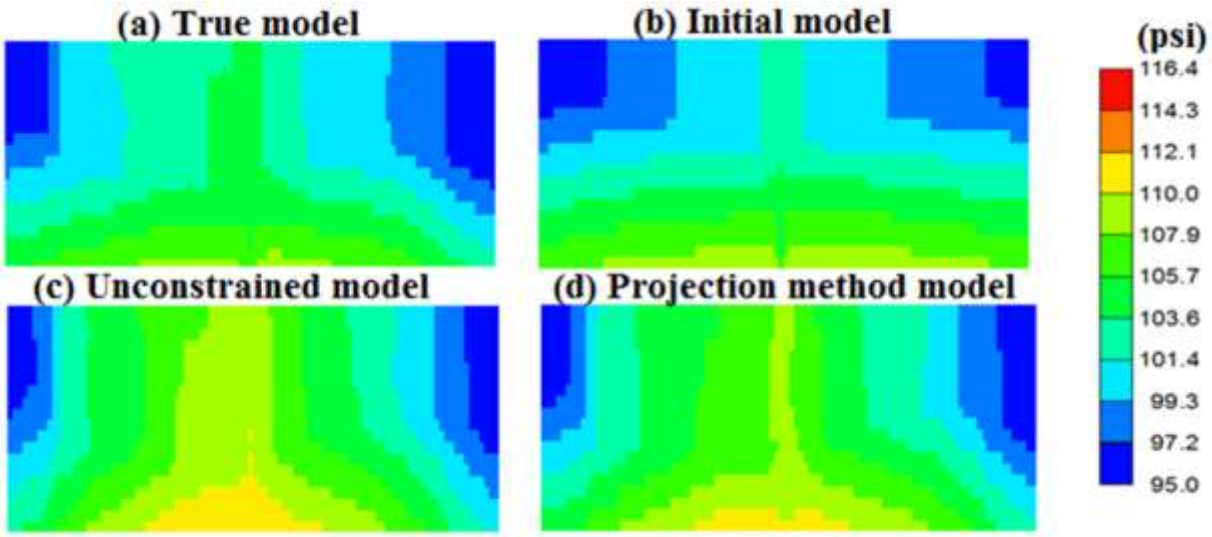

Fig 2.13 Comparison of constrained vs. unconstrained estimation with respect to pressure distribution at the last time instant (t=7300 days). Clockwise from top left corner: Pressure corresponding to true model, average pressure field obtained from mean permeability field corresponding to the initial model, projection method-based EnKF model and the unconstrained EnKF model.

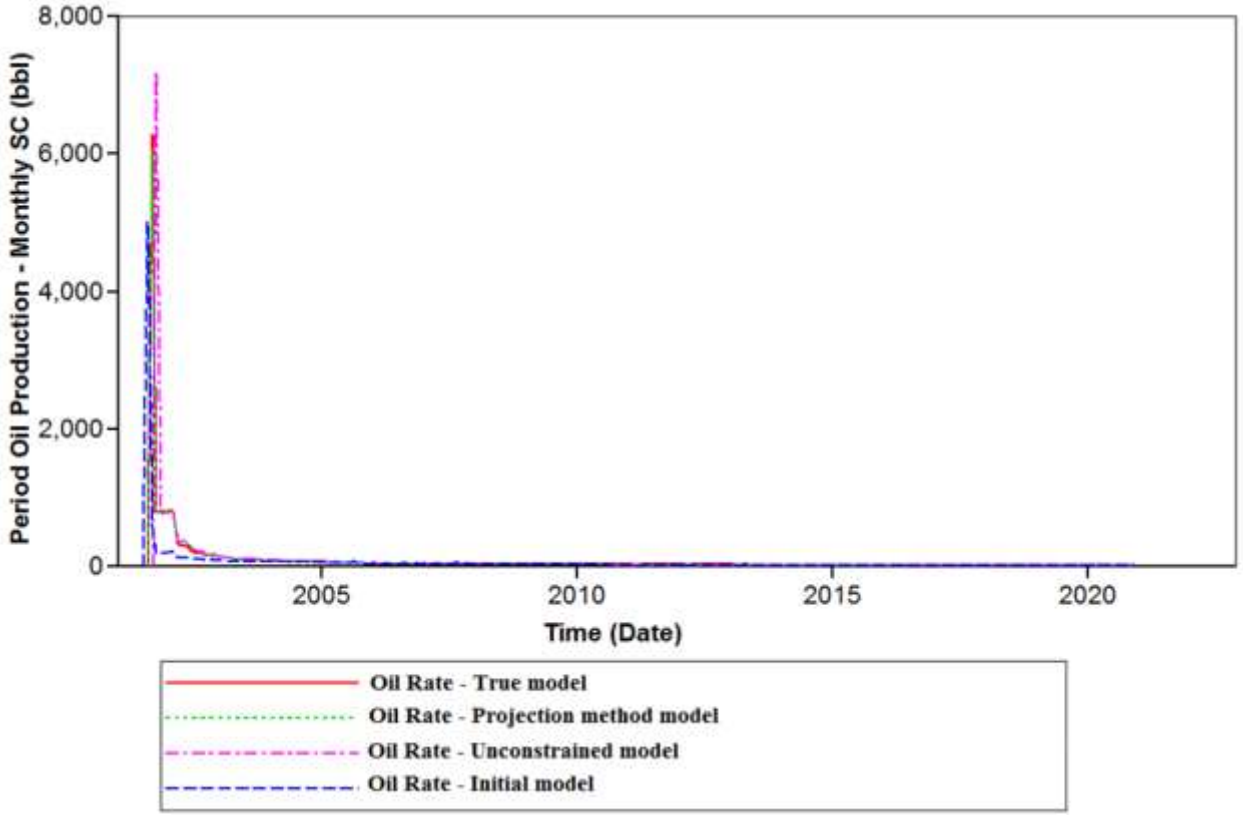

Fig 2.14 Comparison of the mean ensemble predictions for the monthly oil production with respect to the historical production data using the true model, mean of the initial and the estimated models at the production well Pro-1.

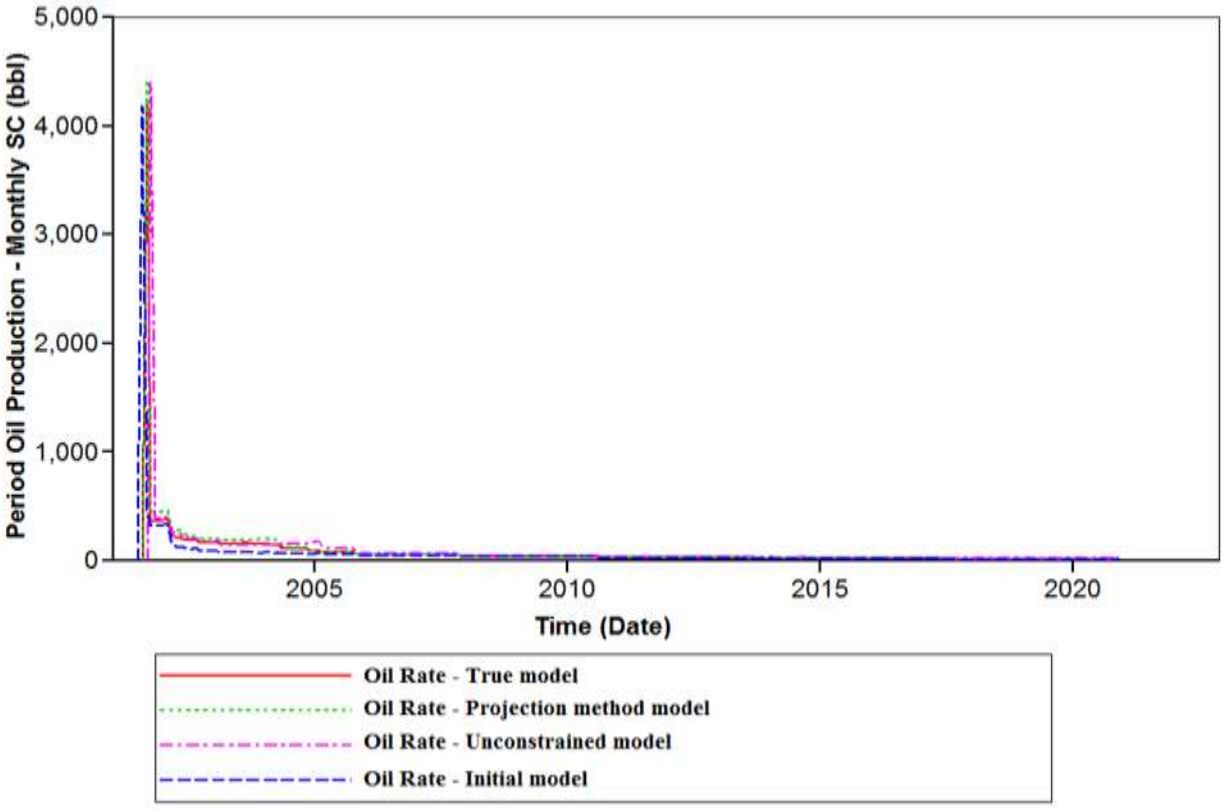

Fig 2.15 Comparison of the mean ensemble predictions for monthly oil production with respect to the historical data using the true model, mean of the initial and the estimated models at the production well Pro-2.

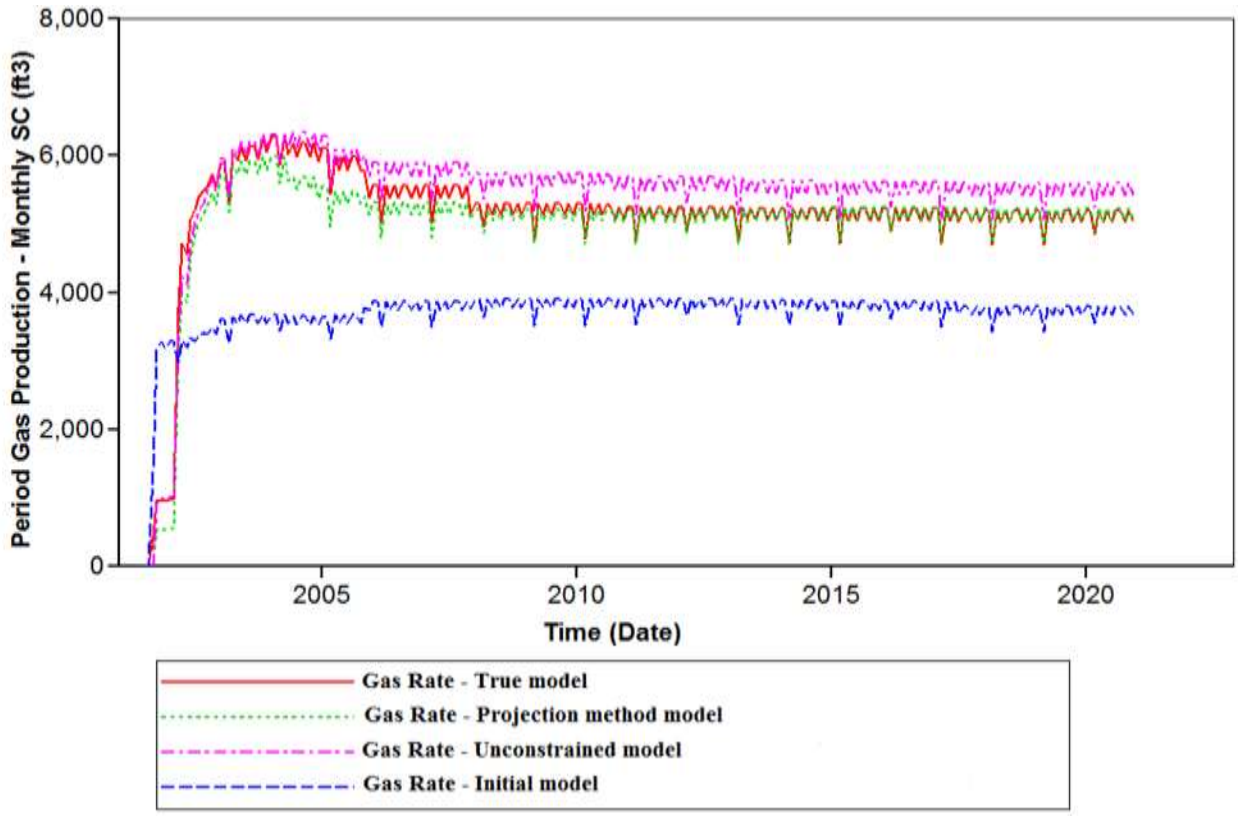

Fig 2.16 Comparison of the mean ensemble predictions for the monthly gas production with respect to the historical data using the true model, mean of the initial and the estimated models at the production well Pro-1.

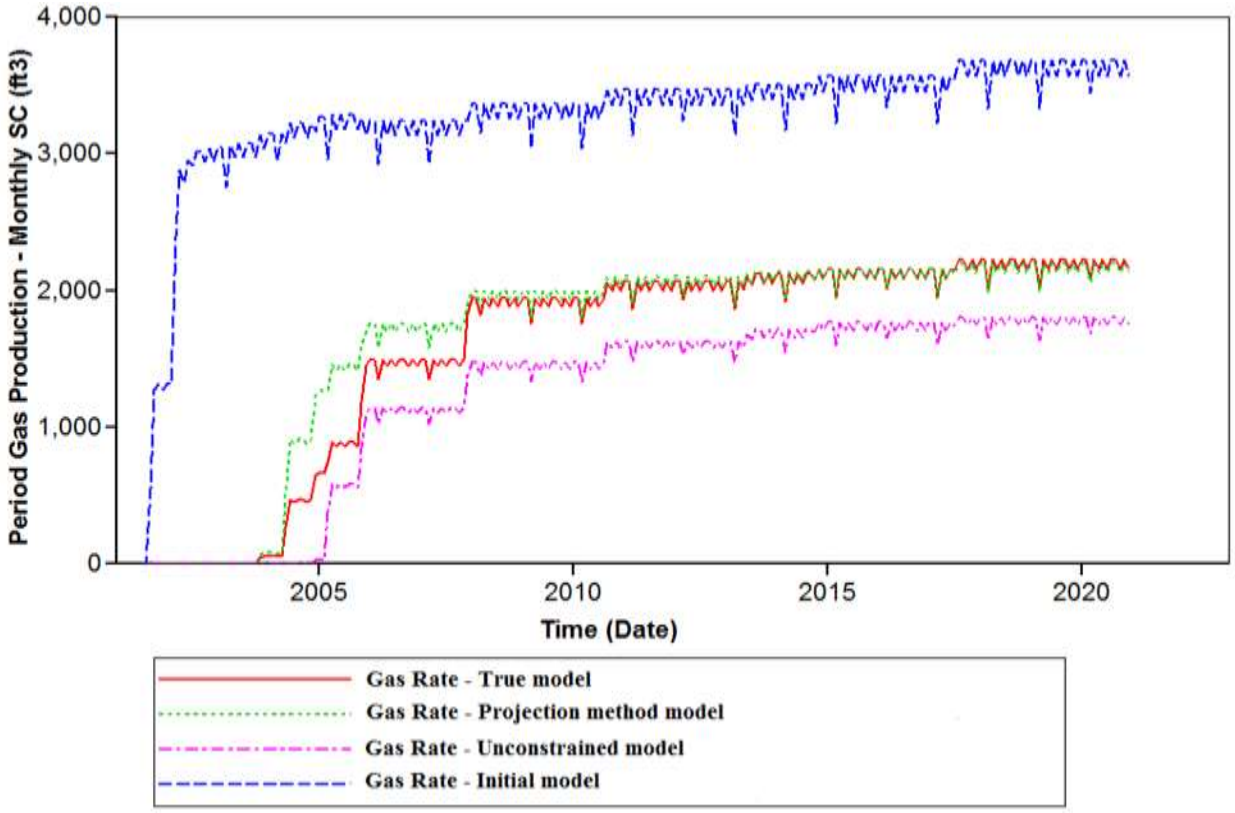

Fig 2.17 Comparison of the mean ensemble predictions for the monthly gas production with respect to the historical data using the true model, mean of the initial and the estimated models at the production well Pro-2.

From the above figures, it can clearly be seen that the soft constraint implementation lead to closer match of states and parameter maps with respect to the corresponding maps of true model.

2.5.2 HETEROGENEOUS 3D RESERVOIR MODEL:

A three-dimensional reservoir model of dimension 50 x 10 x 5 is created using the commercial simulator CMG STARS and is shown in **Fig 2.18**. The reservoir's dimension is 5000ft x1000ft x150ft. The data set for this model was taken from [41]. The permeabilities at all the grid block locations were taken from the above mentioned model. There are a total of 2500 permeability values and permeabilities in all directions were set to be equal. Since this is a highly heterogeneous model, the value of permeability is different in different grid blocks and their values range from 1000 to 3000 mD in this model. It is assumed that permeability information is available at certain spatial locations in the form of hard data. In this case, oil was produced by a steam assisted gravity drainage (SAGD) process. SAGD is a relatively modern method of producing oil from reservoirs,

where several pairs of horizontal wells are drilled instead of the conventional vertical wells. In this method, the steam is passed at high pressure through injection well and as the steam passes through the well, a steam chamber is formed around the wells, which heats the oil sands, thereby reducing its viscosity. Due to this reduced viscosity, the heated crude drains downwards to the second well, called the producer well, from where it is reaches the surface by natural pressure gradient set up in the well or by artificial lift techniques. In our model, there are two injector-producer well pairs as shown in **Fig 2.19**.

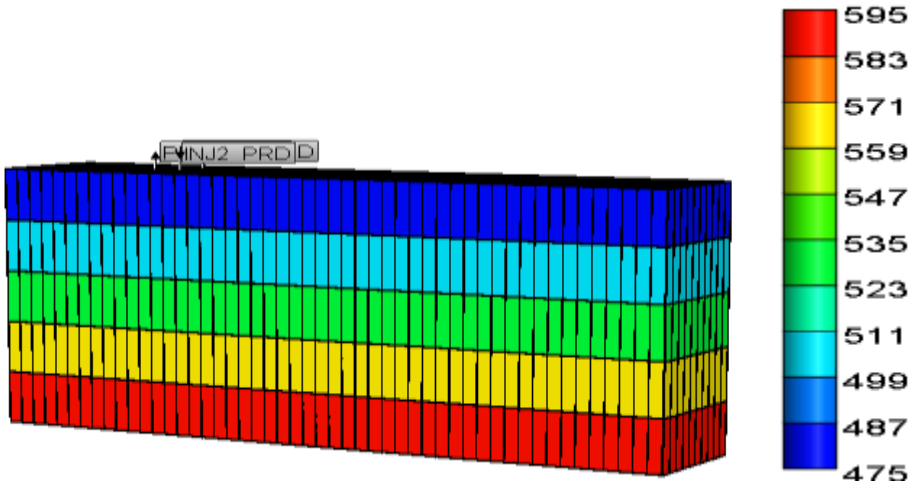

Fig 2.18 Three dimensional SAGD model

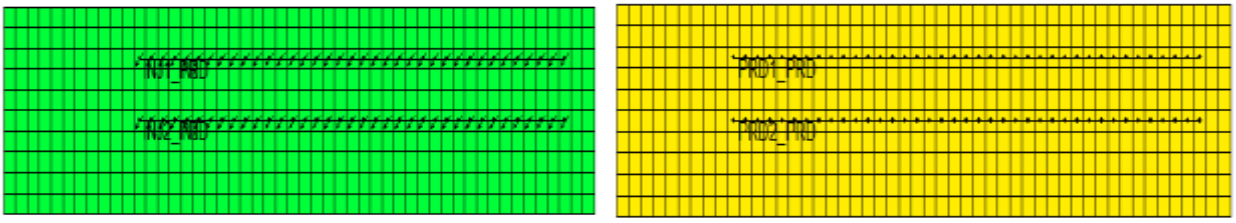

Fig 2.19 Third and fourth layer of the model representing the horizontal well pairs. The colors indicate the depth of each layer from the suface

The inputs used in the process were the steam injection rate and the steam quality. The steam was injected at 250 ^{0}C. The parameter to be estimated is permeability and the dimension of the parameter vector is 2500 x 1. The state vector consisted of three dynamic reservoir properties, namely, the oil saturation, temperature and the water saturation. Since there are 2500 grid blocks in the model, the total dimension of state vector is 7500 x 1. The production data vector consisted

of two components, namely the oil production of the entire field and the cumulative steam-oil ratio (SOR) of the entire field.

For the initial ensemble, realizations of the natural logarithm of the permeability fields were generated using the geostatistical simulation package SGeMS and the spatially distributed permeability values were obtained by the sequential Gaussian simulation algorithm. 50 realizations were used in each ensemble throughout this history matching process. The initial ensemble was constructed to honour both the reservoir hard and soft data. As was the case in 2D reservoir case study described earlier, history matching of the production data was carried out using both the conventional and the projection method-based EnKF algorithms. The update step of the EnKF was performed at 6 time instances. To be precise, it was carried out after 6 months for the three year time period from January 2001 – December 2003.

Fig 2.20 compares the permeability field of the third layer (injection well layer) of the estimated models with respect to the reference permeability field. It is interesting to note that there is a drastic change in the permeability values at the grid blocks defining this layer of the model after the implementation of the EnKF algorithm. In order to quantify the results obtained from these maps, their corresponding histogram representing the distribution of low, medium and high permeability regions in the entire reservoir is shown in **Fig 2.21**.

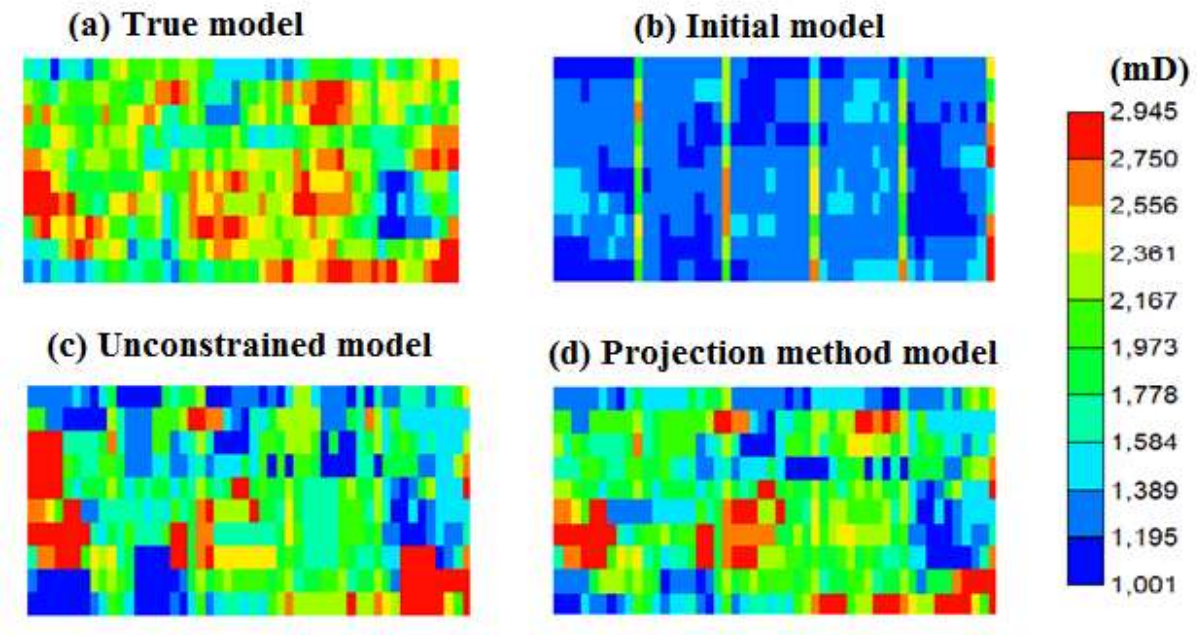

Fig 2.20 Permeability map comparison: Clockwise from top left corner – Reference permeability field of true model, initial permeability field, covariance localization-based permeability field and projection method-based estimated permeability field.

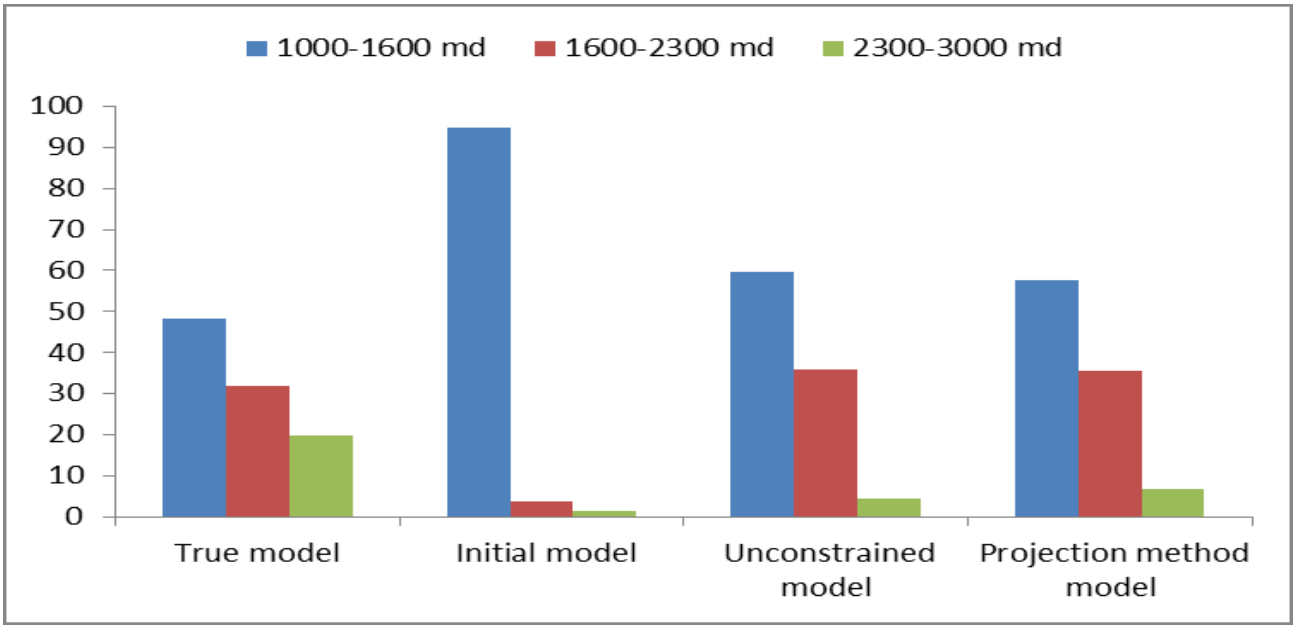

Fig 2.21 Comparison of the histogram of the permeability distribution for true, initial, unconstrained and the projection method models.

The histogram shown in **Fig 2.21** points to the fact that the integration of hard and soft data constraints into the estimation algorithm results in a better capture of the spatial distribution and histogram of the reference field. **Fig 2.22** and **Fig 2.23** compare the temperature profile after 10 years of SAGD operation in the reference, the initial and the estimated models. This temperature profile is commonly referred to as the steam chamber in the SAGD processes. These figures indicate that while the evolution of steam chamber in the reservoir is very slow for the initial model when compared to the true model, addition of constraints into the EnKF framework results in a steam chamber whose characteristics match very closely with respect to the true model. The evolution of steam chamber is quantified in **Fig 2.24**, which further lends support to the fact that the projection method-based EnKF method results in a better reproduction of the dynamics involved in SAGD process of the reference reservoir. **Fig 2.25** compares the mean estimated oil saturation fields of the reservoir using traditional and projection method-based EnKF methods with that of the reference model after 10 years of the SAGD process. **Fig 2.26** and **Fig 2.27** represent the history match between the estimated oil production and steam oil ratio for the entire reservoir field with their corresponding true values before and after history matching. It can clearly be observed that a very good match between the historical data and the production data corresponding to the estimated models using conventional and the projection method-based EnKF methods is obtained, demonstrating the efficacy of this algorithm. Moreover, as was observed in 2D case study, the projection method results in a better history match with the production data compared to the traditional method.

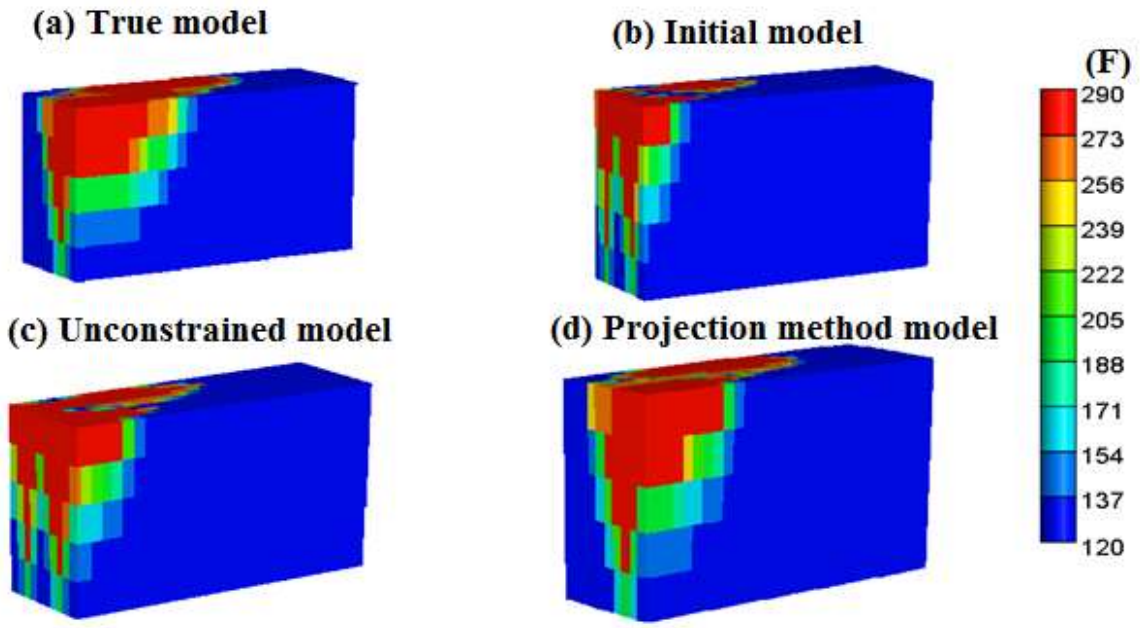

Fig 2.22 Comparison of the temperature distribution profile of SAGD process observed in a reservoir section cut out in the vertical plane perpendicular to the plane containing horizontal well pairs for different cases: Clockwise from top left corner: Temperature profile of the true reservoir model, mean temperature field obtained from the initial model, projection method model and the unconstrained model.

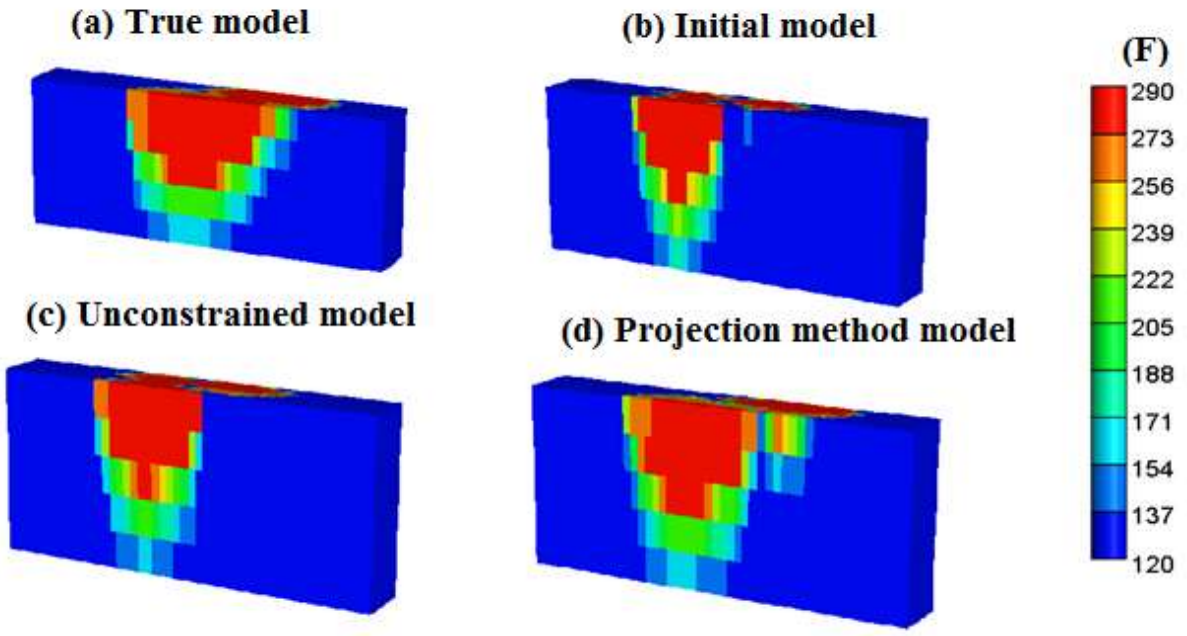

Fig 2.23 Comparison of the temperature distribution profile of SAGD process observed in a reservoir section cut out in the vertical plane containing one of the horizontal well pairs for different cases: Clockwise from top left corner: Temperature profile of the true reservoir model, mean temperature field obtained from the initial model, projection method model and the unconstrained model.

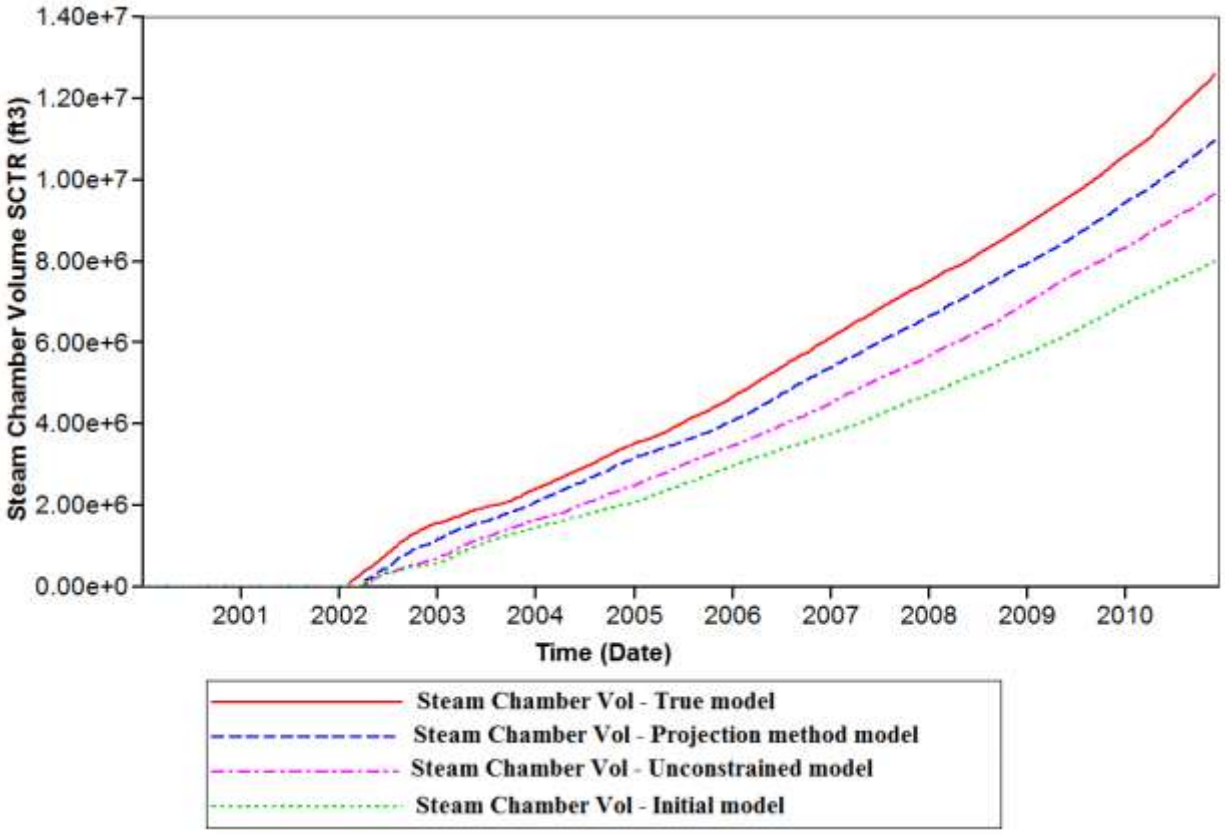

Fig 2.24 Comparison of the steam chamber evolution profile with the progress of SAGD process for initial, true, unconstrained and the projection method models.

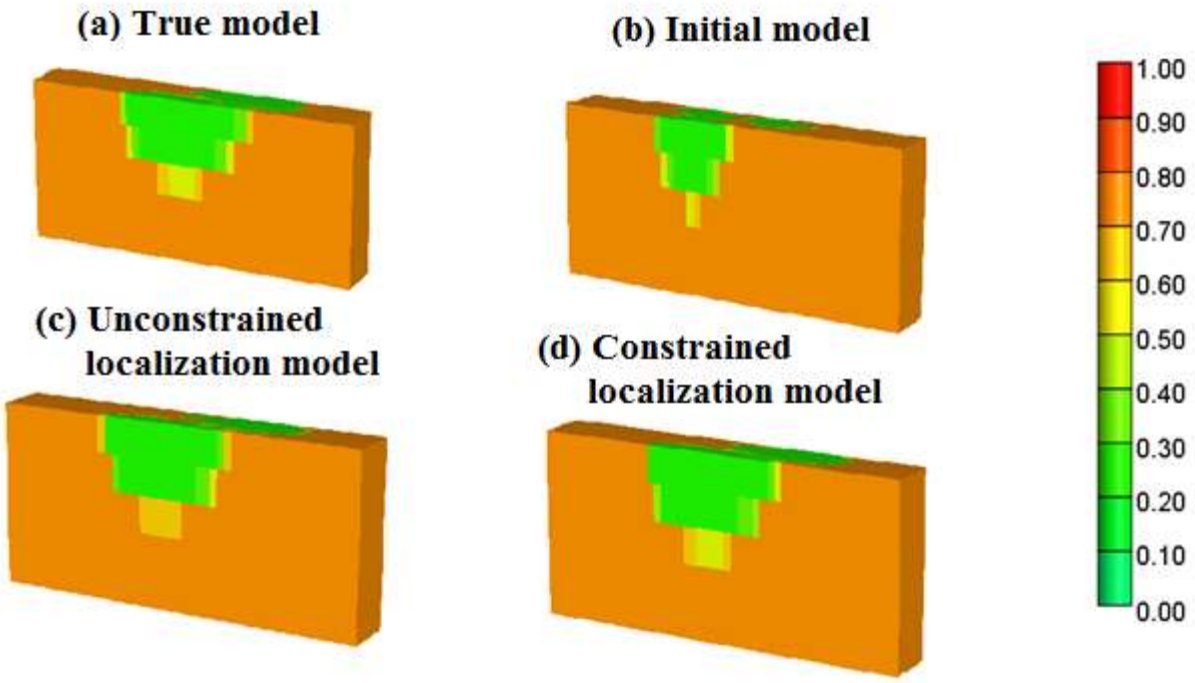

Fig 2.25 Comparison of the oil saturation profile of SAGD process observed in a reservoir section cut out in the vertical plane containing one of the horizontal well pairs for different cases: Clockwise from top left corner: Oil saturation profile of the true reservoir model, mean oil saturation fields obtained from the initial model, projection method model and the unconstrained model.

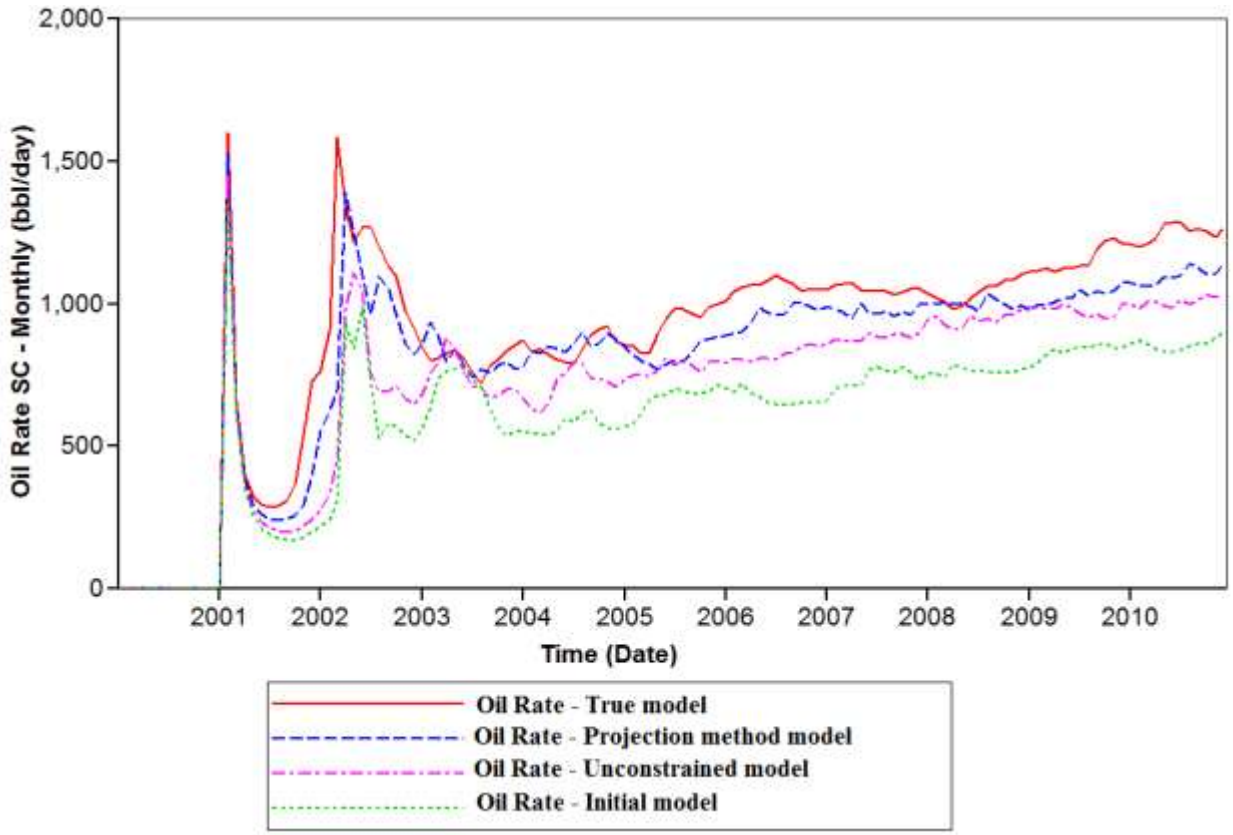

Fig 2.26 Comparison of the mean ensemble predictions for monthly oil production for the entire reservoir field with respect to the historical data using the true model, mean of the initial and the estimated models.

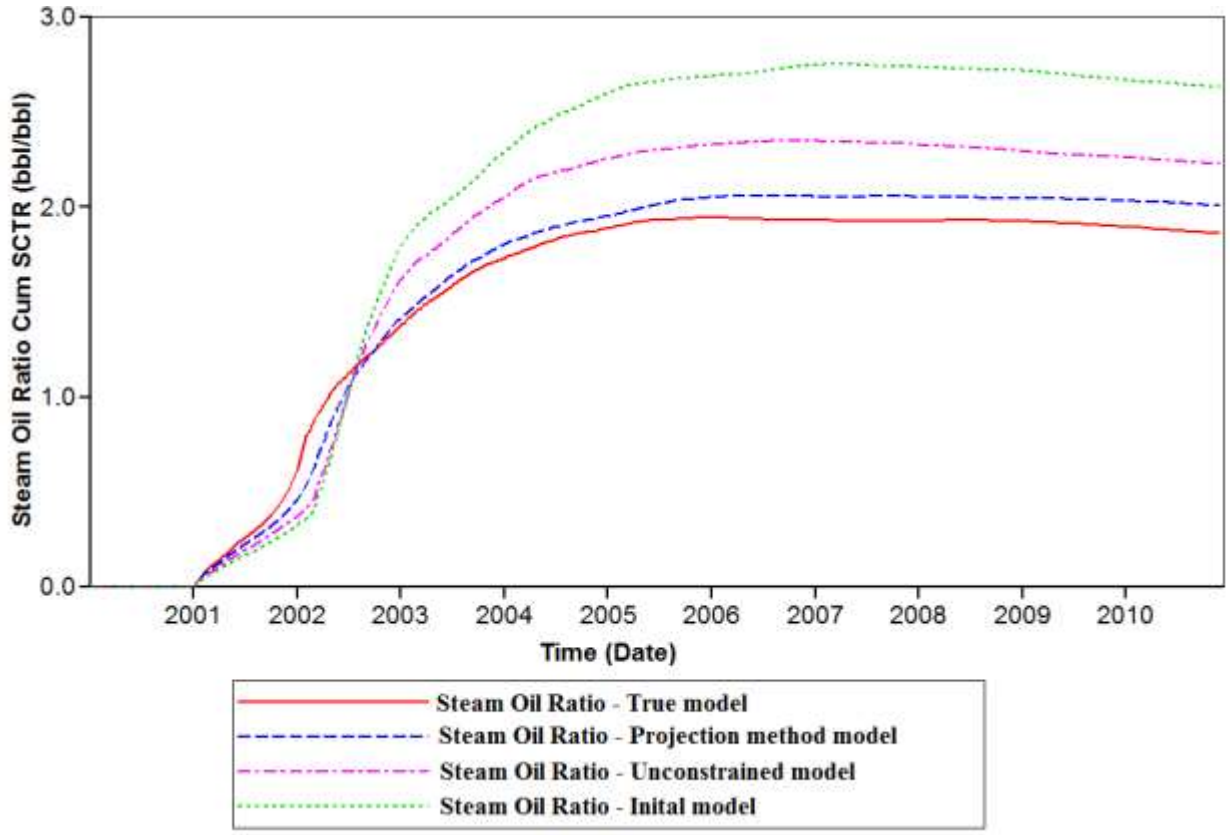

Fig 2.27 Comparison of the mean ensemble predictions for steam oil ratio for the entire reservoir field with respect to the historical data using the true model and the mean of the initial and the estimated models.

2.6 Conclusion

In this chapter, a novel projection method was proposed to integrate the prior geological information available in the form of hard and soft data into the traditional EnKF framework. The application of this proposed method to reservoir history matching problem was analyzed and compared with the performance of the conventional EnKF method using two synthetic heterogeneous reservoir models. It was found that the proposed projection method performed better in yielding permeability estimated consistent with the prior geological information and also led to a better matching with the historical reservoir production data.

Chapter 3

Covariance localization based EnKF for reservoir history matching

In the previous chapter, we implemented constraints in the conventional EnKF algorithm to arrive at geologically consistent estimates of reservoir parameters. In this chapter, the application of covariance localization to reservoir characterization is explored thoroughly. It can be observed from equation 2.22 that the reservoir model parameters and states are updated based on the Kalman gain K, which is dependent on $P_{k|k-1}^{e,\varepsilon}$, the cross covariance matrix between reservoir model states and reservoir production measurements.

Now, using this matrix $P_{k|k-1}^{e,\varepsilon}$ to compute K leads to two potential technical drawbacks. First, it induces spurious correlation between the production measurements at wells and reservoir properties at grid blocks that are very distant from these observation wells. This results in unrealistic physical updates of the reservoir properties at distant grid blocks. Second, estimating reservoir property at each and every grid block leads to a substantial increase in the computational time and effort required.

To lessen the severity of this erroneous long distance correlation in EnKF, reservoir engineers generally locate certain regions in a reservoir that have the greatest impact on the observation data at different production wells and concentrate on the estimation task only in these regions. In this way, physically meaningless updates to the reservoir properties at unimportant regions are prevented and the dimension of this parameter estimation problem is greatly reduced. This problem of parameter and state estimation in a reduced state-space model is known as parameterization or covariance localization.

However, updating only these regions and leaving the remaining portions without updating leads to a geological discontinuity and mismatch with the variogram obtained through the reservoir soft data. To address this problem, we implement sensitivity analysis-based covariance localization to update only the most important regions in the reservoir. After every time update through the EnKF,

we update the remaining portions through the geostatistical algorithm sequential Gaussian simulation so that the updated reservoir is at all times consistent geologically with the hard and soft data.

This chapter is organized as follows. Section 3.1 gives a brief literature review on the parameterization application to reservoir characterization. Section 3.2 explains our proposed methodology for the implementation of covariance localization. This is followed by results and detailed discussions presented in Section 3.3 and finally, conclusions in Section 3.4.

3.1 Literature review

As was pointed out in the introduction of this chapter, the EnKF-based parameter estimates may potentially depart from the prior information and also result in spurious correlation between grid block properties and the well data. Moreover, many possible combinations of these grid block values may yield the same set of historical production data, leading to ill-posedness [42]. To counter this ill-posedness, parameterization or covariance localization has been introduced in the history matching literature. In parameterization techniques, the reservoir grid block parameters are represented by a reduced set of parameters that capture most of the spatial variability. Research in the last decade has focused on coupling the EnKF with several parameterization techniques to reduce the dimension of the estimation problem and avoid ill-posedness. Jacquard et al [43] introduced the concept of zonation method to the reservoir parameterization literature. In this zonation method, the petroleum reservoir was assumed to be divided into several zones, with each zone being represented by uniform reservoir properties. This is the simplest but a very crude form of reservoir parameterization.

In the last two decades, more sophisticated parameterization techniques based on a set of mathematical transforms have been developed to obtain more accurate reservoir descriptions. One such commonly used metric is the discrete cosine transform (DCT), which has its roots in image processing and is widely applied to data compression applications [44]. It is a Fourier-based transform, which decomposes the spatially distributed reservoir parameters like permeability into the coefficients of the retained cosine basis functions [45]. The permeability values at each grid block is represented by a corresponding DCT coefficient. When applied along with the EnKF, the transform is applied to every realization of the ensemble and the most significant DCT coefficients and their basis functions that capture most of the spatial variation of permeability are retained.

Usually, the total number of DCT coefficients required to represent this spatial variation is considerably smaller than the total number of model parameters, thereby significantly reducing the dimension of the parameter estimation problem. It has been widely explored in the history matching problem in the recent past. Wang et al [46] applied DCT-based EnKF to estimate the permeability of fluvial channels. In another work, Wang et al [47] implemented DCT on an iterative EnKF framework to carry out reservoir history matching and inversion. Jafarpour et al [42, 48] also successfully coupled DCT-based EnKF for the history matching problem. Mathematically, DCT-based parameterization can be expressed through linear equations 3.1 and 3.2.

$$\theta_t = \emptyset_\theta \, \theta'_t \tag{3.1}$$

$$\theta'_t = \emptyset_\theta^T \theta_t \tag{3.2}$$

Eq 3.1 represents the inverse transformation from the set of *d* retained DCT basis function coefficients $\emptyset_\theta$ to the set of *n* grid block parameter values. Eq 3.2, on the other hand, is representative of the forward transformation of grid block parameters values to the DCT basis function coefficients.

Wavelet transform-based EnKF is another tool to implement covariance localization or parameterization for history matching. The wavelet transform is basically a linear transformation, resulting in the decomposition of the signal into completely different frequencies [49]. In wavelet transformation, a multiresolution technique is implemented, where different resolutions are used to analyze different frequencies. It has been explored widely for signal compression purposes [50]. In the past two decades, it has been used with great success for the reservoir history matching problem [14]. The multi-resolution wavelet transform was first proposed by Sahni et al [51] for the purposes of integrating historical data with the prior geostatistical information for reservoir history matching. Similar to the DCT methodology, the wavelet coefficients are calculated to represent the distribution of the spatially varying parameters in a reservoir like porosity or permeability. The main set of coefficients that capture most of the spatial variability are retained and used for the update step in the EnKF while the grid blocks characterized by very low values of these coefficients are not updated, thereby reducing the dimension of the reservoir characterization problem.

In addition to these transform based methods, singular value decomposition (SVD) and Karhunen-Loeve(KL)-based parameterization have been explored for reservoir history matching applications. KL-based parameterization was first introduced to the reservoir characterization literature by Gavalas et al [52] and was developed further by Oliver [53] and Reynolds et al [54]. This method is based on the eigen-decomposition of the covariance matrix of the spatially varying parameters in a reservoir. Although, it has been successful in arriving estimates with geologic spatial consistency with respect to prior soft data, it is difficult to apply it to large scale reservoirs due to heavy computations associated with the decomposition calculations [55]. Moreover, it has failed in preserving the multi-point statistics of the spatial parameters in many cases. Sarma et al [55] developed a kernel-based principal component analysis (KPCA) for parameterization in order to overcome the limitations of the KL-based approach.

Pilot point method is another tool to implement parameterization introduced by de Marsily et al [56] and later explored by a few researchers [57, 58, 59]. A certain number of grid blocks, i.e., pilot points, are chosen in a reservoir model depending on crucial factors like locations of wells, reservoir heterogeneity and prior geological information. The main characteristic feature of this method is that the petrophysical realizations of a spatially varying property such as porosity or permeability can be perturbed and still retain its spatial variability [60]. There are several ways to select these pilot points. In their work, Ramarao et al [57] suggested a sensitivity analysis study to determine the high sensitivity regions in the concerned reservoir model and use these regions to place the pilot points.

Some of the parameterization techniques involve distance-based localization, where only a few grid blocks that are close to the wells are updated. Houtekemar et al [25] first introduced the concept of localization principle by applying a distance-based cutoff to the Kalman gain matrix computed in the update step of the EnKF such that only grid blocks within this cutoff distance is updated [30]. Arroyo-Negrete et al [61] used a streamline simulation to get an idea about the region of influence. In their work, they arrived at the final region of influence by coupling the streamline simulation results with the prior geostatistical information regarding the maximum distance of correlation in different directions in a reservoir. Furrer et al [62] introduced non-distance based localization techniques to carry out parameterization by using a pseudo-optimal localization taper function.

3.2 Proposed methodology for covariance localization

It is a well-known fact that in a reservoir model, only the parameters in a fraction of the spatial locations will have an impact on the reservoir productivity measured at the production wells, and covariance localization seeks to identify these crucial regions of influence for each well in the reservoir system. In this work, we employ sensitivity analysis for covariance localization using the reservoir sensitivity analysis simulation package CMOST. Since reservoir systems are discretized into thousands of grid blocks, sensitivity calculations are not applied to every grid block. Instead, we coarsen the discretization only for the purposes of sensitivity calculations based on the range (the maximum spatial extent of the correlation in the parameters) of the horizontal and vertical variograms. Any hard data available for each of the coarsened regions is used to assign the values of the parameters in that region.

After determining this region of the highest sensitivity, the EnKF update is performed in the grid blocks defining this region. However, performing an update only in these regions will lead to geological discontinuity and mismatch of the variogram and correlogram with respect to the reference (true) variogram/correlogram. In order to overcome this limitation, the parameter estimates of the remaining grid blocks (outside the region of influence) are estimated using sequential Gaussian simulation (SGS) [63]. SGS is a widely used method for randomly generating an ensemble of equiprobable spatial distributions of the reservoir property of interest that are consistent with a specified variogram. During this step, the EnKF updated values are used as hard data and exported to the geostatistical software SGeMS to perform SGS. This operation makes sure that the reservoir is all times consistent with the reference variogram. This method of implementing covariance localization is advantageous for two reasons. First, as with any conventional method of parameterization, the size of the parameter vector used in the EnKF calculation is considerable reduced, thereby reducing the computational load. Second, this method also yields geostatistically consistent estimates of reservoir properties such as permeability.

The SGS algorithm, which is used to generate realizations of the parameter of interest (permeability) consistent with the known properties (variogram) of its distribution and conditioned by hard data available at a few locations, typically consists of five steps. First, a point is chosen at random in the unknown data locations. The mean and variance of this unknown data point is then estimated using a kriging procedure. In this work, we employ ordinary kriging, which assumes the

mean of the property being estimated to be known and constant only in the local neighborhood of the points to be estimated [30]. Kriging is a regression-based interpolation method that estimates properties at interpolatory locations by assigning weights to the known property values at a few data points. Points closer to the location with the unknown values are assigned higher weights, and vice versa. In kriging, the data $Z \equiv (Z(s_1), \dots, Z(s_n))$ can be thought to be the observations of a random or stochastic process at known locations $s_1, \dots, s_n$. In our case, Z represents the permeability, and is assumed to follow

$$Z(s) = \mu + \delta(s) \tag{3.3}$$

where δ is a zero-mean stochastic process with known covariance function C. To predict the data at a particular location s_0 based on a set of known values at locations $s_i, i = 1, \dots, n$, the kriging estimator can be written as

$$Z^*(s_0) = m(s_0) + \sum_{i=1}^{n} l_i[Z(s_i) - m(s_0)] = [1 - \sum_{i=1}^{n} l_i]m(s_0) + \sum_{i=1}^{n} l_i Z(s_i) \tag{3.4}$$

Here, l_i represent the weights assigned to each of the known locations in determining the value of the property at the location s_0. Applying the conditions that the mean is constant in the local neighborhood of s_0 and the sum of the kriging weight is 1, we obtain the ordinary kriging estimator to be

$$Z^*(s_0) = \sum_{i=1}^{n} l_i Z(s_i) \tag{3.5}$$

The best linear unbiased predictor is obtained by minimizing $E[Z(s_0) - \sum_{i=1}^{n} l_i Z(s_i)]^2$, and the weights are be obtained by using the method of Lagrange multipliers, which provides an estimate of the variance of the kriging estimator [64].

In the third step of SGS, the value of the parameter at this location is chosen by random sampling from a normal probability distribution whose mean and variance are obtained from the kriging procedure described in the second step. In the fourth step, this data point is now added to the conditioning data used to simulate the permeability in the remaining locations with unknown values. This process is repeated until all the data points are simulated.

SGS is used to generate an ensemble of equiprobable realizations based on the random sampling described above. A key assumption is for the data to follow a normal distribution; however, if this assumption is not met, a normal score transformation can be used.

3.3 Results and discussion

3.3.1 Heterogeneous 2-D reservoir

The reservoir model considered for this study is the same as the one described in previous chapter. However for the sake of completeness, the model is shown below in **Fig 3.1**. This model is of dimension 100 x 1 x 20. The values of permeability are different in each block due to the heterogeneity of the reservoir. There are three wells in total – one injector well placed at the center of the reservoir and two producer wells, placed symmetrically on either side of the injector well.

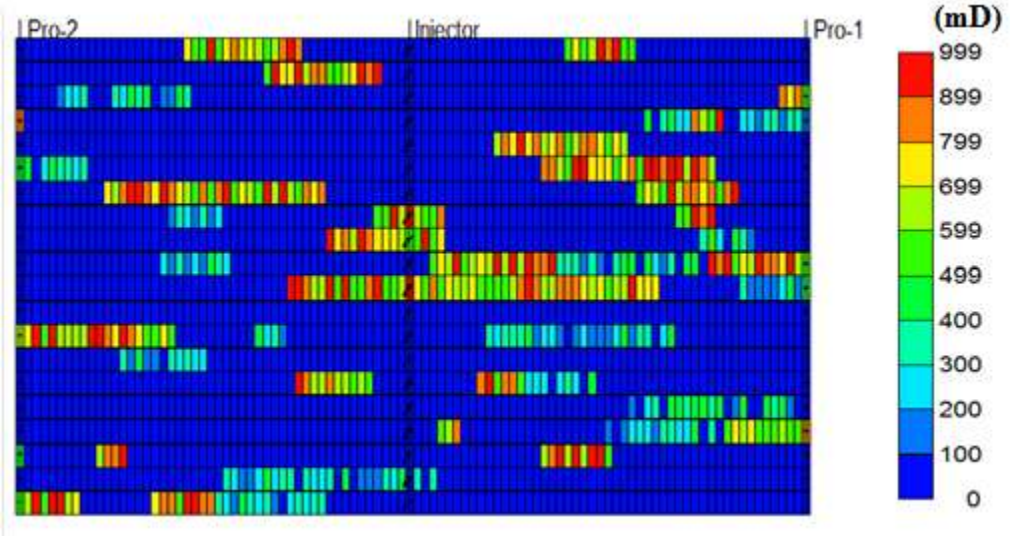

Fig 3.1 2-D heterogeneous reservoir (color map represents the permeability)

In order to perform covariance localization, a sensitivity analysis study was performed and regions of influence for the two producing wells were identified. The EnKF operation was centered only on these regions and the remaining regions were updated using the geostatistical algorithm sequential Gaussian simulation in SGeMS. The regions of influence are shown in **Fig 3.2**. This region of influence in the reservoir was characterized by a total of 1200 grid blocks. Hence the dimensions of the state and parameter vectors are 4800 x 1 and 1200 x 1 respectively. We can see here that the dimension of the estimation vector has drastically reduced compared to the dimension of the estimation vector used in non-localization based EnKF method in Chapter 2 (6000 x 1 and

2000 x 1). This results in great reduction in the computational load present in the EnKF calculations.

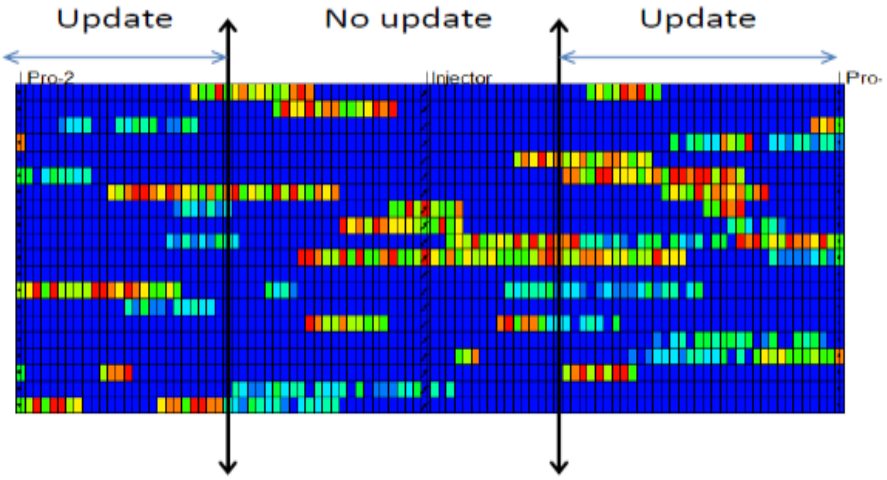

Fig 3.2 Regions of influence in the reservoir for covariance localization

The operating conditions used for this reservoir simulation are exactly the same as those used in the previous chapter. The problem has been posed as a joint state and parameter estimation problem, where only the parameters are updated explicitly in the EnKF update step and the states are updated using the confirming option explained in the previous chapter in section 2.3. The states include the oil saturation, the water saturation and the pressure while parameter of interest is the spatially varying permeability. The historical production data was collected at 14 time instances, like in the previous 2D case study.

For the generation of initial ensemble of permeability field, the geostatistical simulation package SGeMS was used, where the spatial distribution was generated by the sequential Gaussian simulation algorithm. While generating the initial ensemble, the distribution obtained was forced to honour the permeability values represented by the hard data at the hard data locations.

Fig 3.3 represents compares the permeability of the true model, the initial model, the one obtained after estimation using the traditional covariance localization-based EnKF and the one obtained after estimation using the geostatistics-based localization EnKF method. On observing these maps closely, it can be inferred that the constrained localization algorithm has resulted in a very good reproduction of the spatial locations of the high and low permeability regions present in the

reference reservoir model. On the other hand, the spatial variability characteristics of the permeability field of the initial model are very different when compared to that of the reference model. The vast improvement in the ability to reproduce the spatial heterogeneity and variability characteristics of the reference model indicates a significant correction applied to the initial model with each time step to account for the historical measurement data. In the case where the localization was performed without any soft constraint implementation, the middle portion of the reservoir was not updated and looks exactly the same as the middle portion of the initial model. This is because, in the traditional method of localization, only the sensitive regions in the reservoir are updated using the EnKF update equation. However, when the remaining regions are also updated by integrating the updated portion with geostatistics, i.e., the constrained localization method, then the overall estimated field will be very similar to the true field and more consistent with the reservoir soft and hard data.

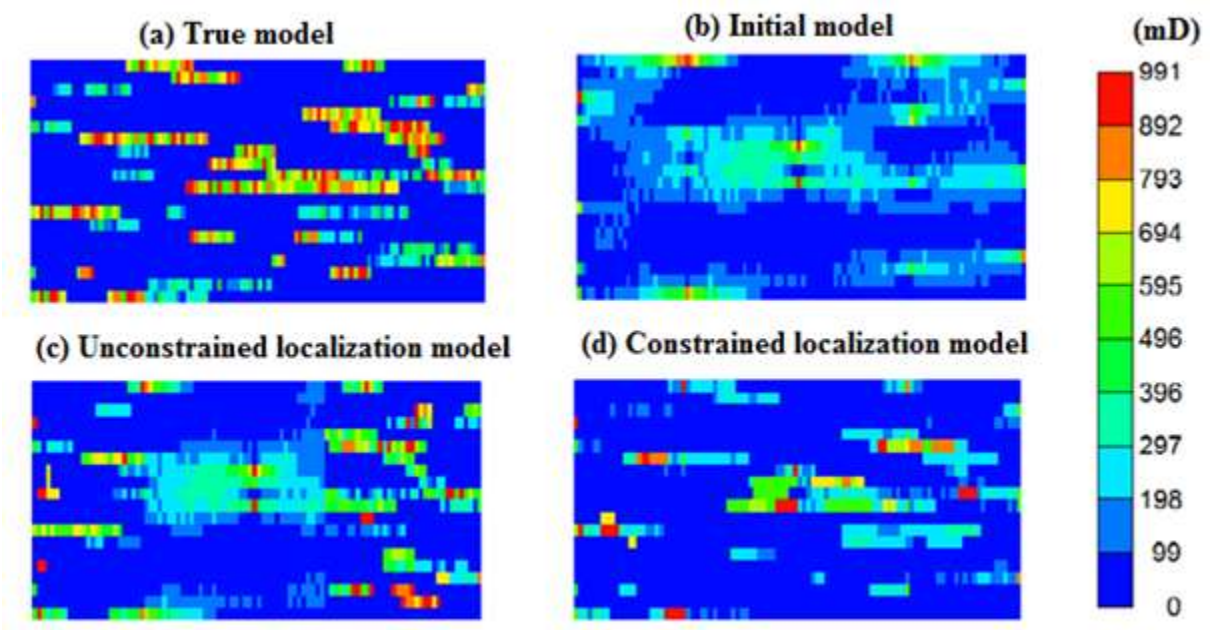

Fig 3.3 Permeability map comparison: Clockwise from top left corner – Reference permeability field of true model, initial permeability field, unconstrained covariance localization-based permeability field and geostatistics-based covariance localization estimated permeability field.

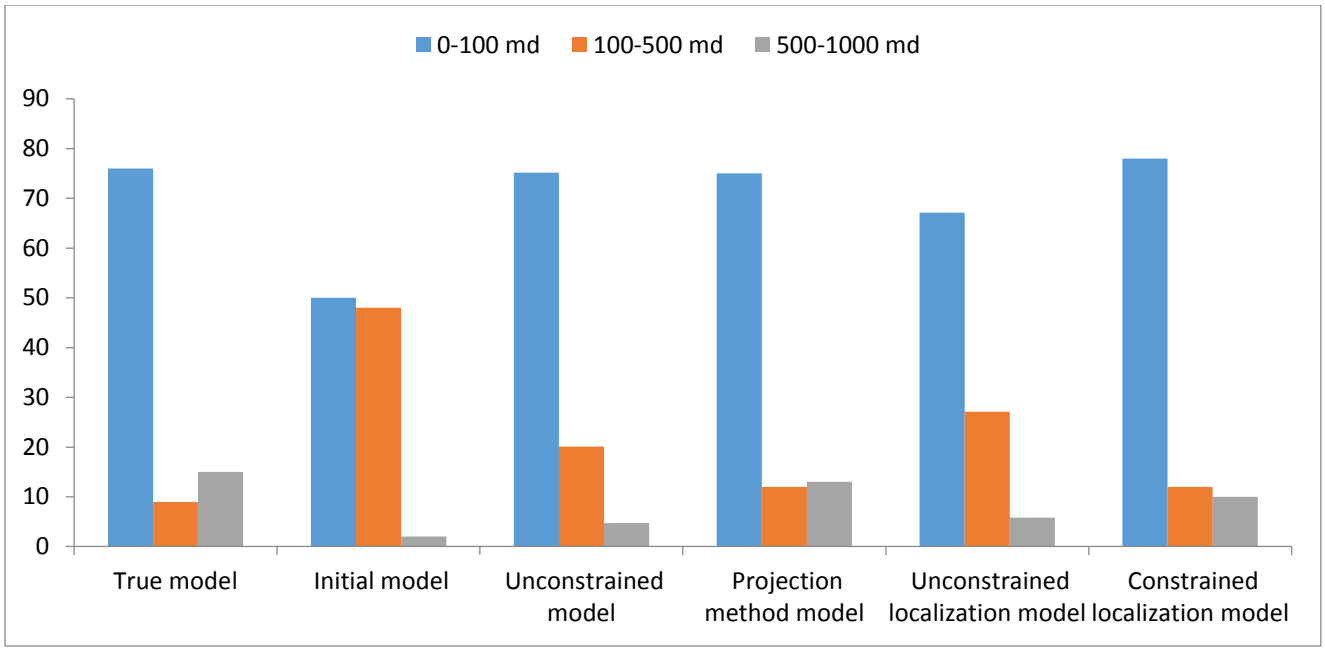

Fig 3.4 Comparison of the histogram of permeability distributions for true, initial, unconstrained, projection method, unconstrained localization and constrained localization models.

Fig 3.4 gives the comparison of the distribution of the low, medium and high permeability regions of the true model, initial model and the model obtained using the projection and the covariance localization-based methods in order to quantify the colour maps shown in **Fig 3.3**. It can be observed from this figure that with the implementation of the EnKF, the distribution of the estimated permeability is in good agreement with the true permeability distribution and the covariance localization methodology captures the spatial variability of the permeability to a slightly better extent when compared to the projection methodology.

Figures 3.5, 3.7 and 3.9 show the comparison of gas saturation, oil saturation and pressure distribution of the reservoir respectively at the last time instant, i.e., 7300 days respectively obtained using the true model, the initial model and the estimated models using conventional localization and proposed localization methods. These contour plots further brings out the efficacy of the proposed localization technique in reproducing the saturation and pressure profiles with the progress of the waterflooding process better than the conventional localization technique. The results from these contour plots are quantified by **Fig 3.6** and **Fig 3.8**. These figures compare the evolution of the mean reservoir oil saturation and gas saturations for different estimated models

with the progress of the oil recovery process. In order to identify the best among all methods explored in this work, we have also included the results obtained from the unconstrained EnKF and the projection method-based EnKF methods. From these figures, it can be concluded that the proposed localization estimation technique performs best in this history matching exercise.

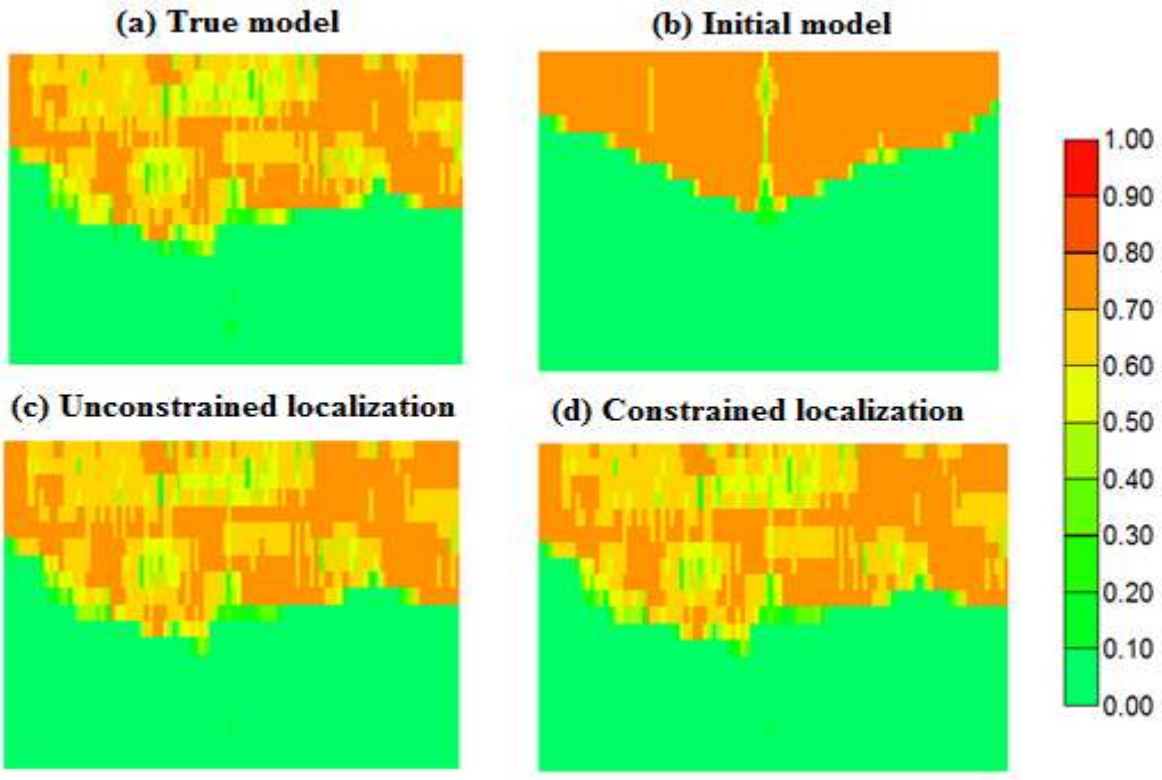

Fig 3.5 Comparison of constrained vs. unconstrained localization estimation with respect to gas saturation at the last time instant. Clockwise from top left corner: Gas saturation corresponding to true model, mean gas saturation fields of the initial model, constrained localization-based EnKF model and unconstrained localization model.

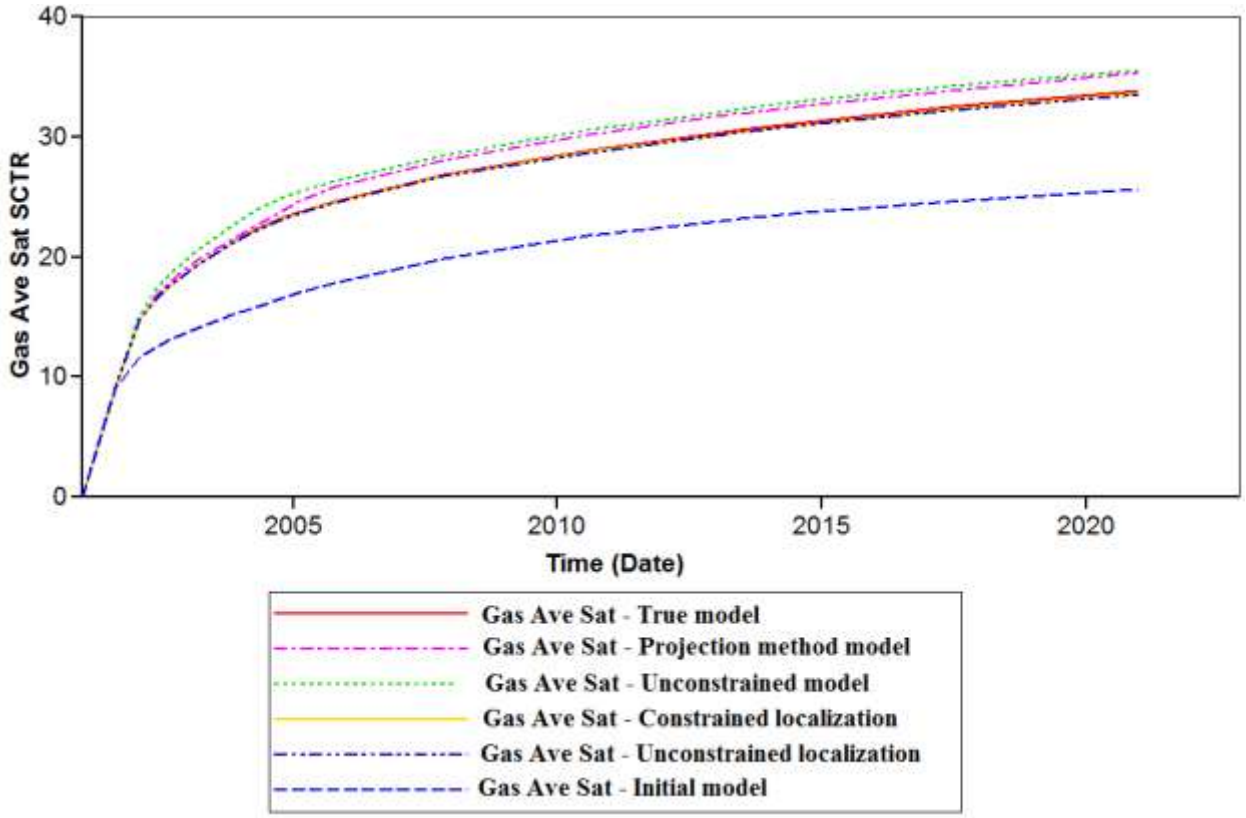

Fig 3.6 Comparison of the average gas saturation in the entire reservoir with the progress of the waterflooding process for true model, initial model, projection method-based EnKF and unconstrained EnKF model.

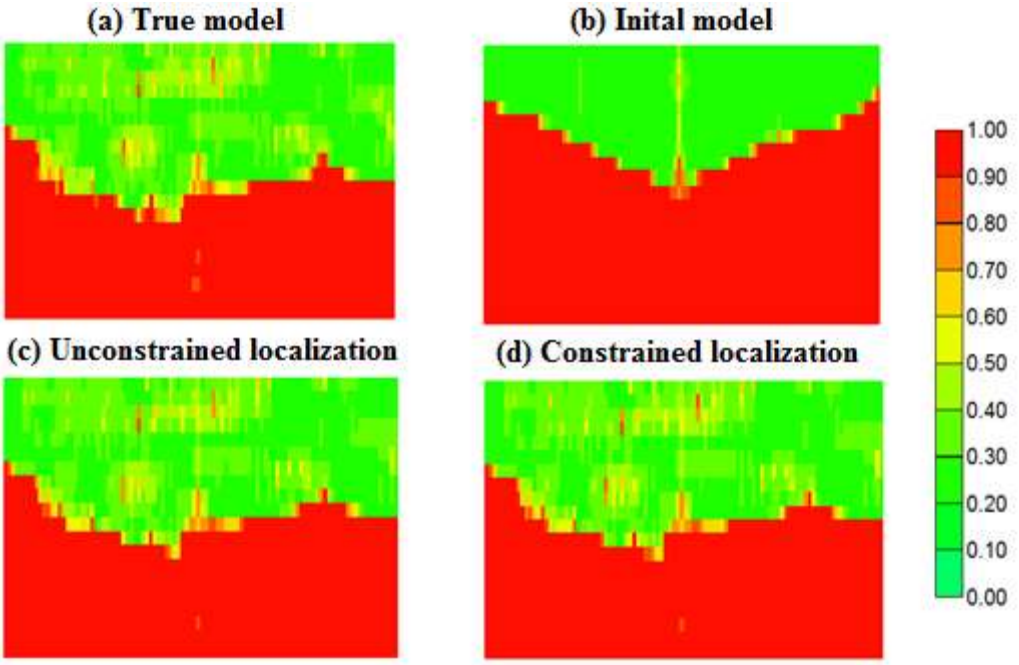

Fig 3.7 Comparison of constrained vs. unconstrained localization estimation with respect to oil saturation at the last time instant. Clockwise from top left corner: Oil saturation corresponding to true model, mean oil saturation fields of the initial model, constrained localization-based EnKF model and unconstrained localization model.

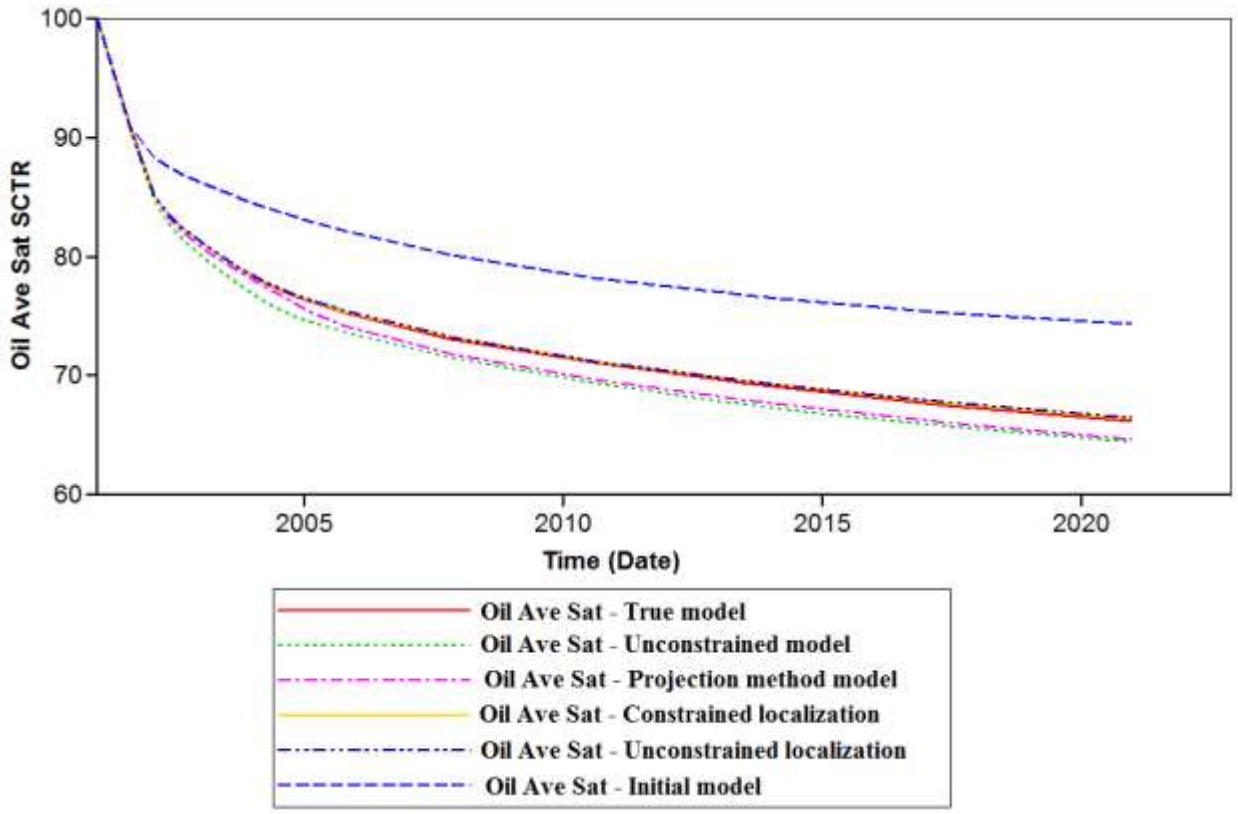

Fig 3.8 Comparison of the average oil saturation in the entire reservoir with the progress of the waterflooding process for true model, initial model, projection method-based EnKF and unconstrained EnKF model.

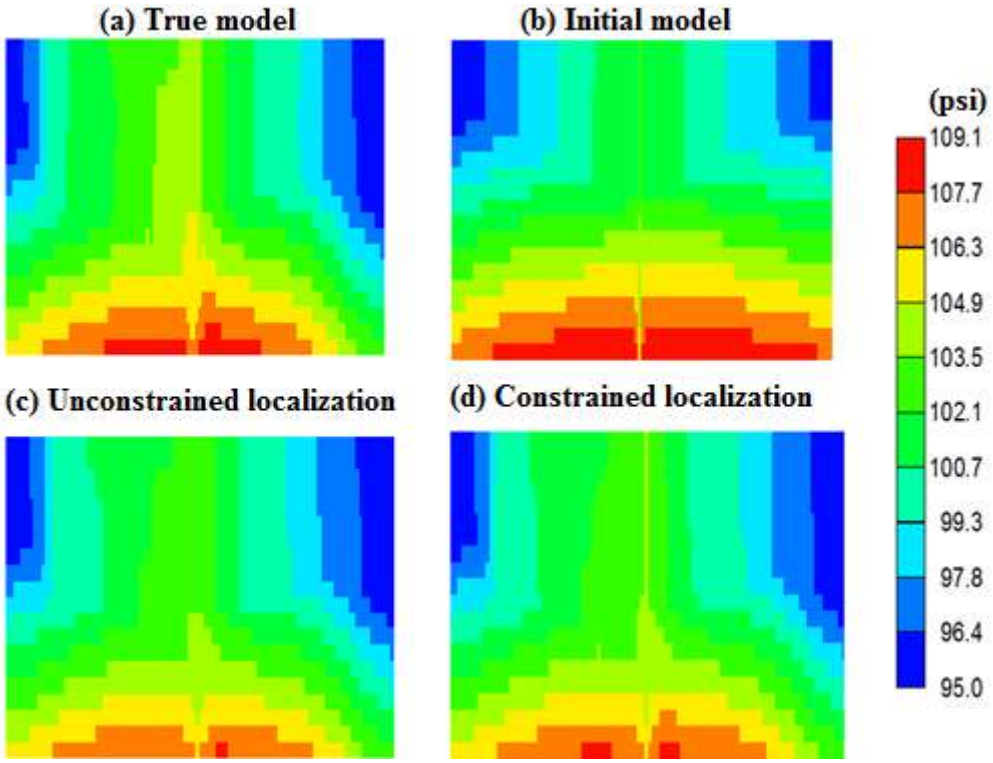

Fig 3.9 Comparison of constrained vs. unconstrained localization estimation with respect to oil saturation at the last time instant. Clockwise from top left corner: Oil saturation corresponding to true model, mean gas saturation fields of the initial model, constrained localization-based EnKF model and unconstrained localization model.

Fig 3.10, Fig 3.11, Fig 3.12 and Fig 3.13 represent the comparison of the ensemble predictions obtained from diferent estimation methodologies and the historical production data obtained from the two production wells. To be precise, the history matching of the monthly oil production obtained from the wells Pro-1 and Pro-2 are shown in **Fig 3.10** and **Fig 3.11** respectively. **Fig 3.12** and **Fig 3.13**, on the other hand, show the history matching results of the monthly gas production obtained from the wells Pro-1 and Pro-2 respectively. It can be clearly seen from these figures that compared to the initial model, the oil production of the final estimated models is in very good agreement with the true reservoir's oil production. The success of the EnKF in matching the historical production data can be observed, demonstrating the efficacy of this algorithm. This successful performance can be attributed to the correction step of the EnKF algorithm, where the available online measurements from the production wells reduce the uncertainty in the reservoir parameters with each data assimilation step. Moreover, these figures indicate that the proposed

localization technique performed better than the conventional localization method for this reservoir case study followed by the projection method, which in turn performed better than the conventional EnKF method.

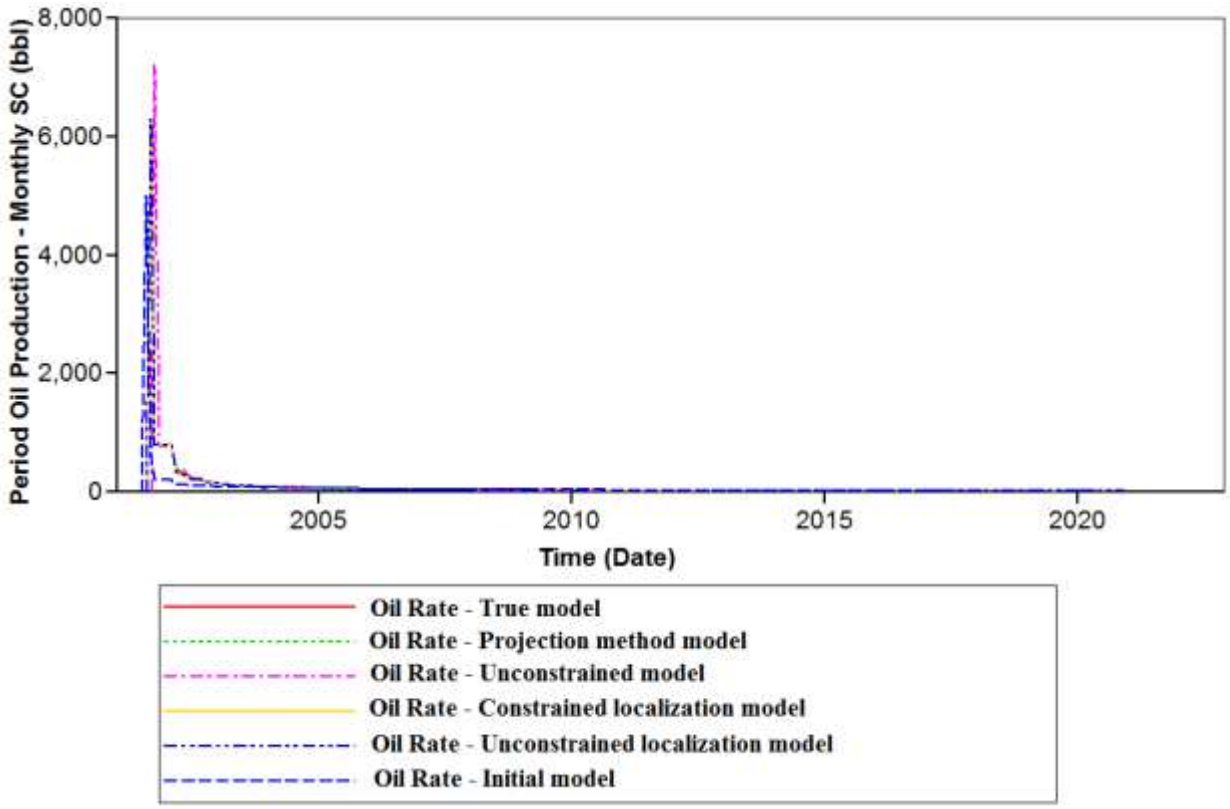

Fig 3.10 Comparison of the mean ensemble predictions for the monthly oil production with respect to the historical production data using the true model, mean of the initial and the estimated models at the production well Pro-1.

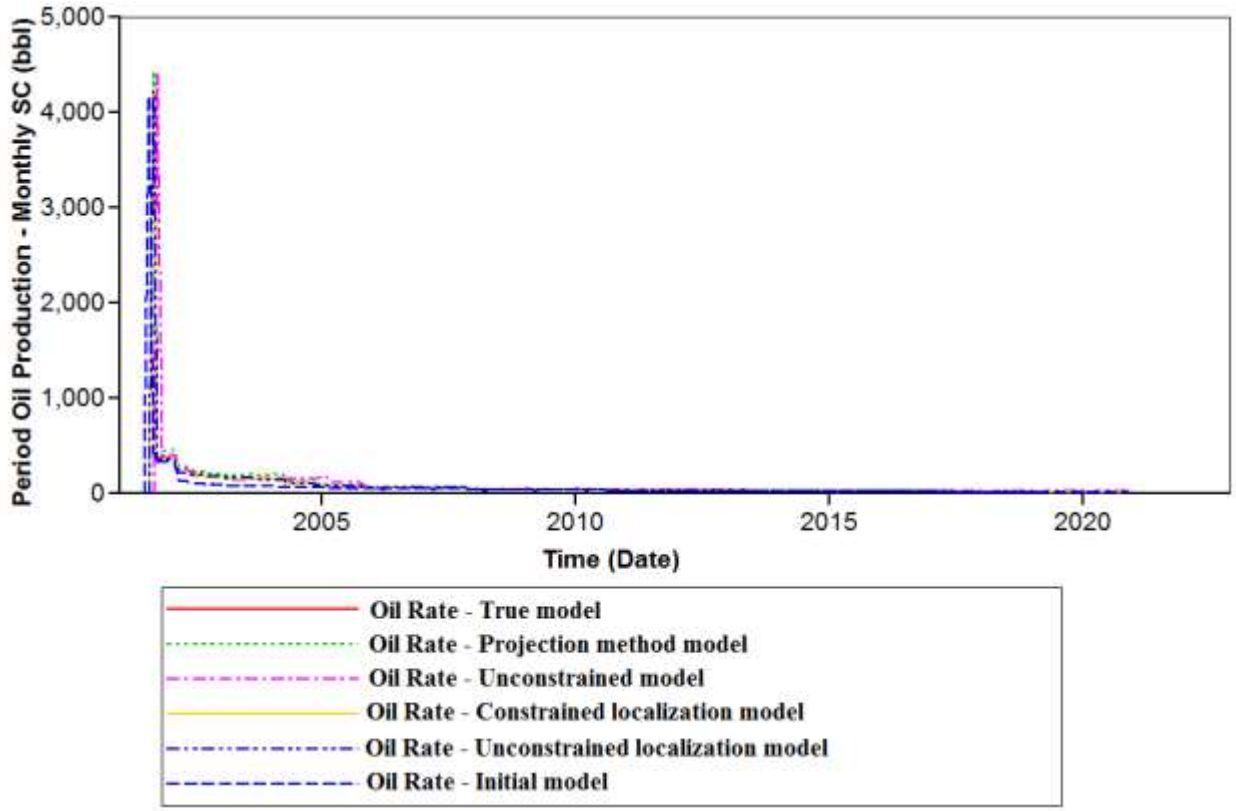

Fig 3.11 Comparison of the mean ensemble predictions for the monthly oil production with respect to the historical production data using the true model, mean of the initial and the estimated models at the production well Pro-2.

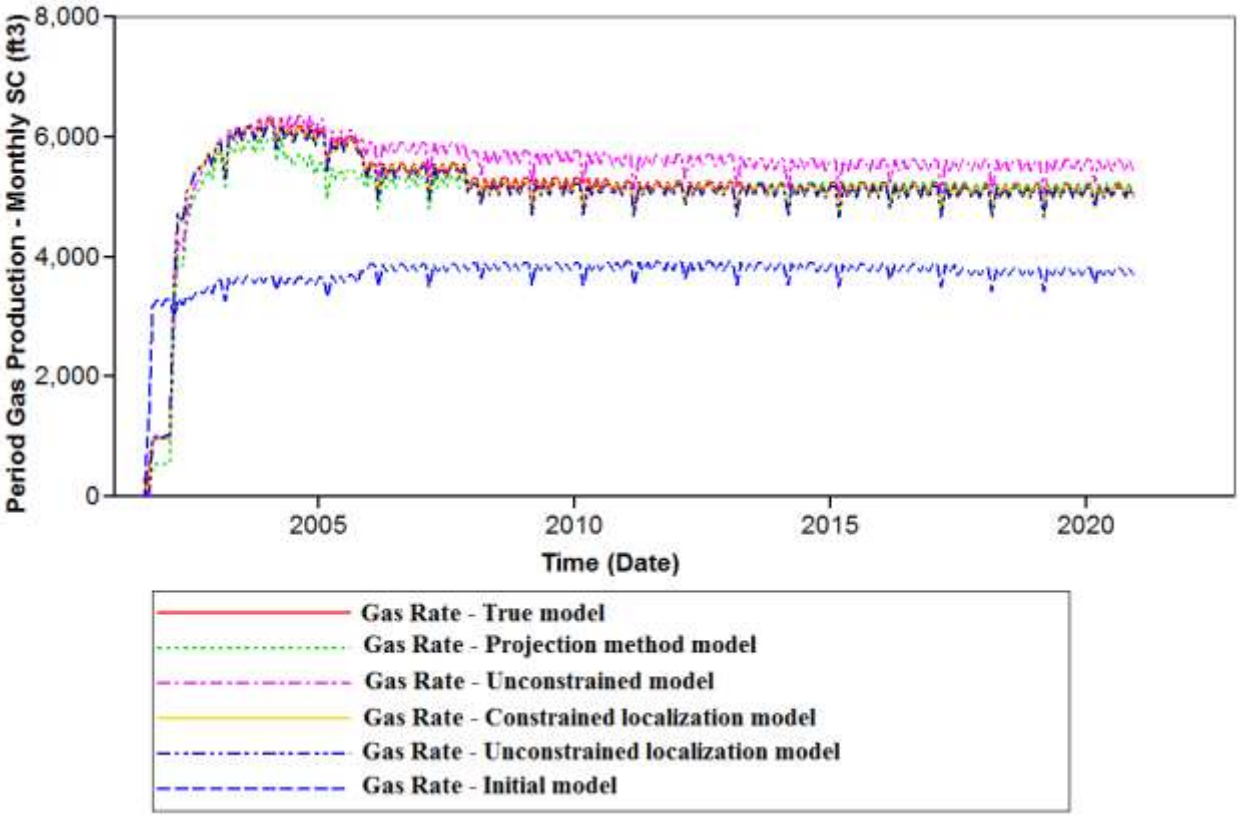

Fig 3.12 Comparison of the mean ensemble predictions for the monthly gas production with respect to the historical production data using the true model, mean of the initial and the estimated models at the production well Pro-1.

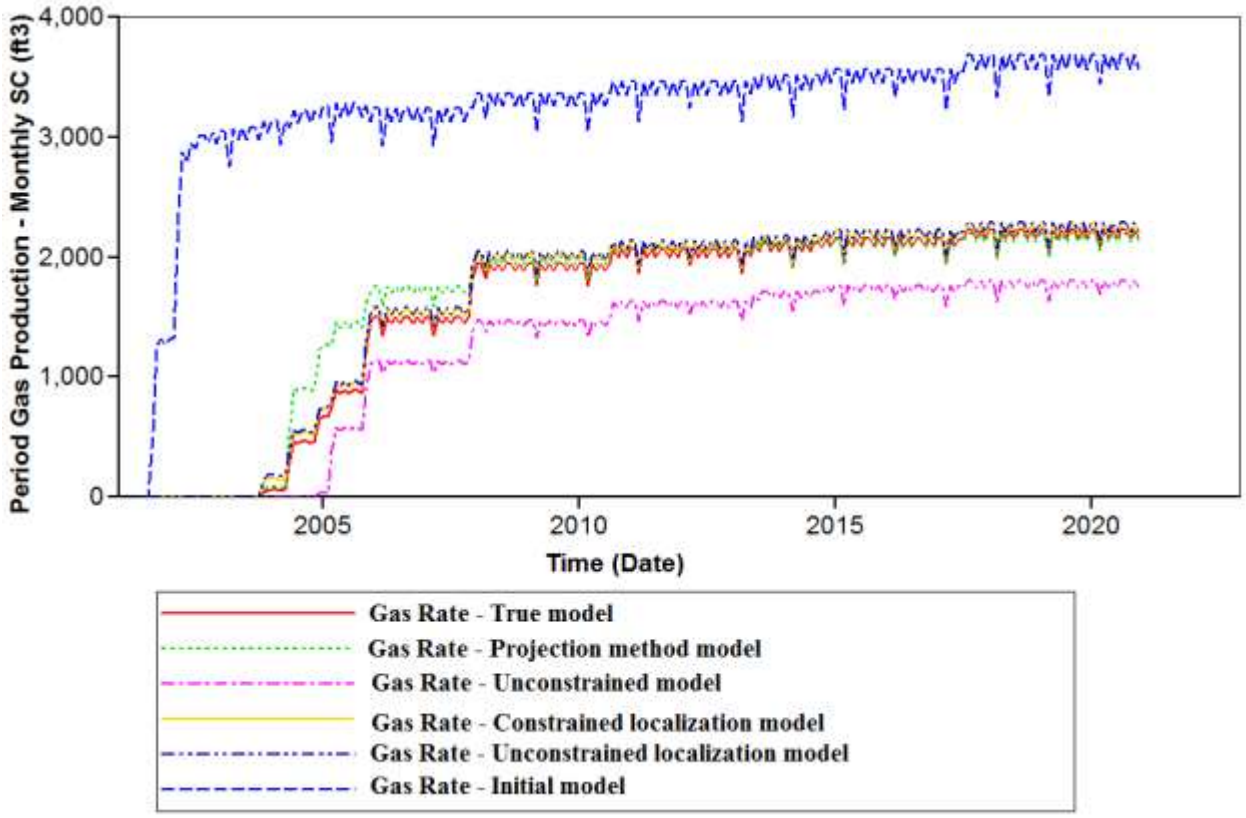

Fig 3.13 Comparison of the mean ensemble predictions for the monthly oil production with respect to the historical production data using the true model, mean of the initial and the estimated models at the production well Pro-2.

3.3.2 3D SAGD reservoir model

For this study, the reservoir model considered is exactly the same as the one considered in the previous chapter. Although the representation of the model was shown in the previous chapter, for the sake of completeness, it is also shown below in **Fig 3.14.** The history matching was posed as a joint state and parameter estimation problem through the EnKF. The reservoir's dimension is 5000ft x 1000ft x 150ft. The data for this model was taken from [41]. The permeability values at all the grid block locations were taken from the above mentioned model. There are totally 2500 permeability values and the permeability in all directions were set to the same value. Since this is a highly heterogeneous model, the value of permeability is different in different grid blocks. The values of permeability range from 1000 md to 3000 md in this model. It is assumed that permeability information at certain spatial locations is available in the form of hard data.

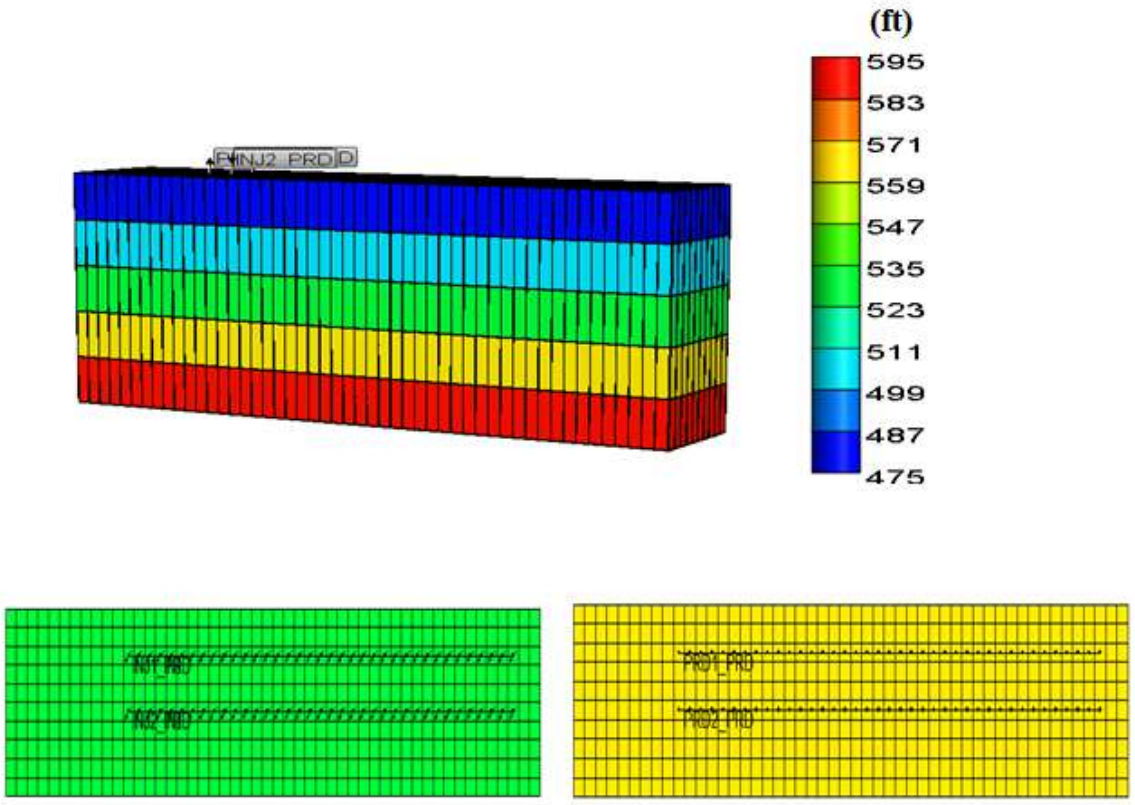

Figure 3.14 3D SAGD reservoir model and two layers representing the horizontal well pair placement

In order to perform covariance localization, sensitivity analysis was conducted to identify regions of influence for the two horizontal producing wells. It was found out that except for the top and bottom layers, other layers affected the production data at the producing wells significantly. Therefore, the EnKF update operation was focused only on the grid blocks comprising these regions. After every update step of the EnKF, the top and bottom layers were modified using sequential Gaussian simulation so that these two layers are at all times geologically consistent with the remaining three regions. In this way, the variogram of the estimated model will be in very good agreement with the variogram obtained as a part of the soft data information. This region of influence was comprised of 1200 grid blocks. Hence the dimensions of the state and parameter vectors are 4800 x 1 and 1200 x 1 respectively. This considerable decrease in the size of the estimation vector greatly reduces the computational load that is present in the conventional EnKF method calculations.

Fig 3.15 shows the comparison of permeability map of the third layer of the reservoir between the true model, initial model and the ones obtained using the conventional and the proposed method of localization-based EnKF for reservoir history matching. It can be observed that the EnKF algorithm has greatly improved the permeability estimates compared to the initial model. Similar to the results obtained from the 2D case study described in section 3.3.1, the permeability field estimated using the proposed methodology has resulted in better reproduction of the spatial heterogeneity characteristics present in the reference model when compared to that reproduced by the conventional localization estimates. In order to quantify these colour maps, a comparison of the histograms of these estimated models was performed and is shown in **Fig 3.16**. In this histogram comparison, it is easy to conclude that the proposed localization method performs best in yielding geologically consistent estimates. Although the unconstrained localization method also performs fairly well in reproducing the high and low permeability regions present in the reference model, it fails to reproduce the histogram of the reference field. This is because of the presence of certain insensitive regions in the reservoir that do not get updated during the entire course of the EnKF process.

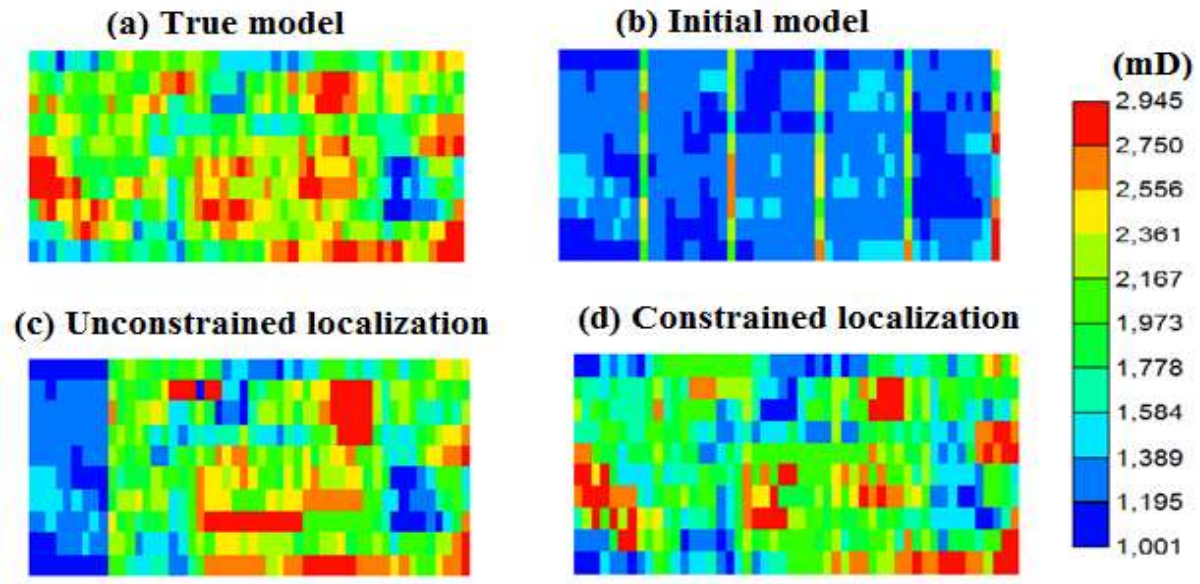

Figure 3.15 Permeability map comparison: Clockwise from top left corner – Reference permeability field of true model, initial permeability field, constrained covariance localization-based permeability field and the unconstrained localization-based estimated permeability field.

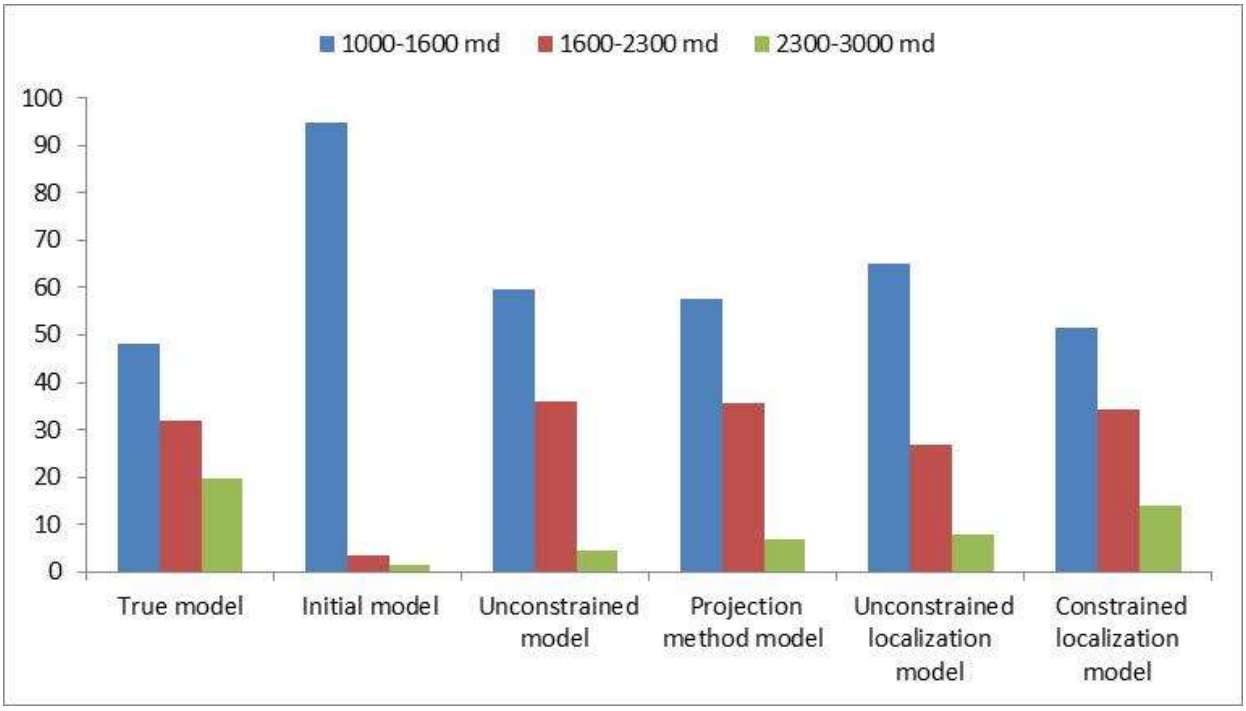

Figure 3.16 Comparison of the histogram of permeability distributions for true, initial, unconstrained, projection method, unconstrained localization and constrained localization models.

Fig 3.17 and **Fig 3.18** show the temperature distribution of the estimated models in comparison with that of the true model for this SAGD process to further illustrate the fact that implementation of constraints into the algorithm leads to more accurate reservoir characterization. **Fig 3.19** quantifies these contour maps by comparing the evolution rate of the steam chamber i.e., increase in the steam chamber volume, observed in the reference and the estimated models with the progress of the SAGD process. On a similar note, Fig 3.20 shows a comparison of the oil saturation profile of SAGD process observed after 10 years in a reservoir section cut out in the vertical plane containing one of the horizontal well pairs for the different estimated models.

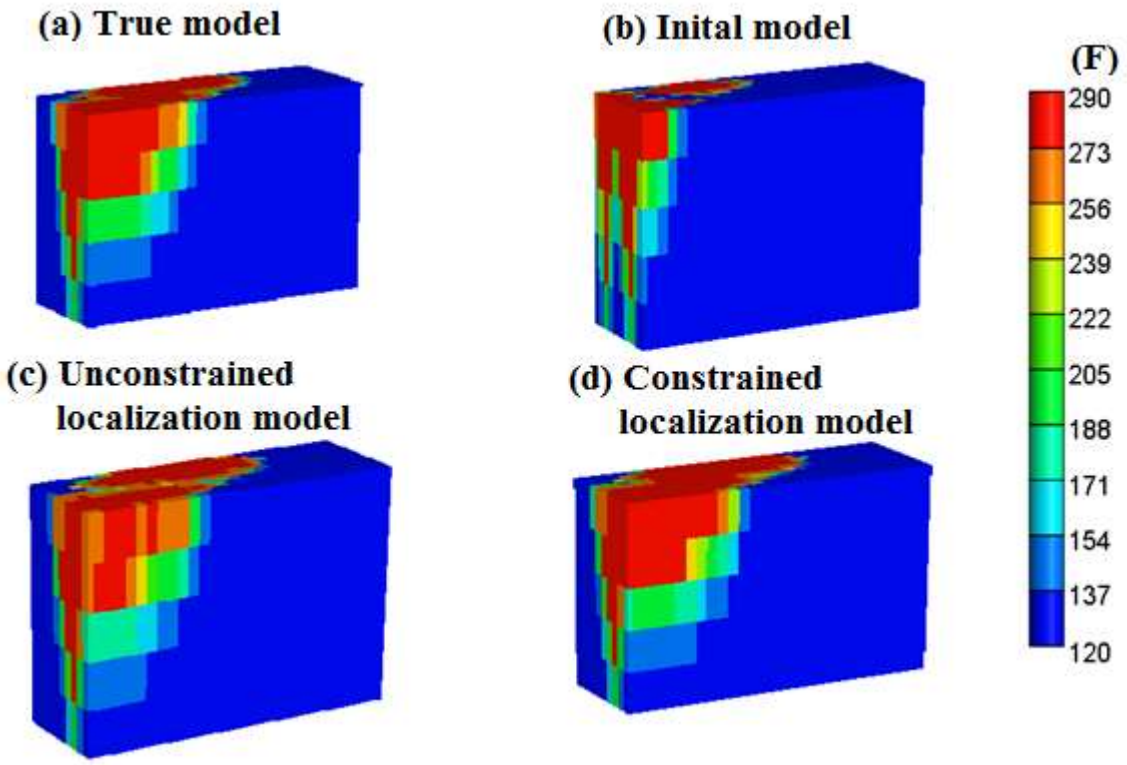

Figure 3.17 Comparison of the temperature distribution profile of SAGD process observed in a reservoir section cut out in the vertical plane perpendicular to the plane containing horizontal well pairs for different cases: Clockwise from top left corner: Temperature profile of the true reservoir model, mean temperature field obtained from the initial model, constrained localization model and the unconstrained localization model.

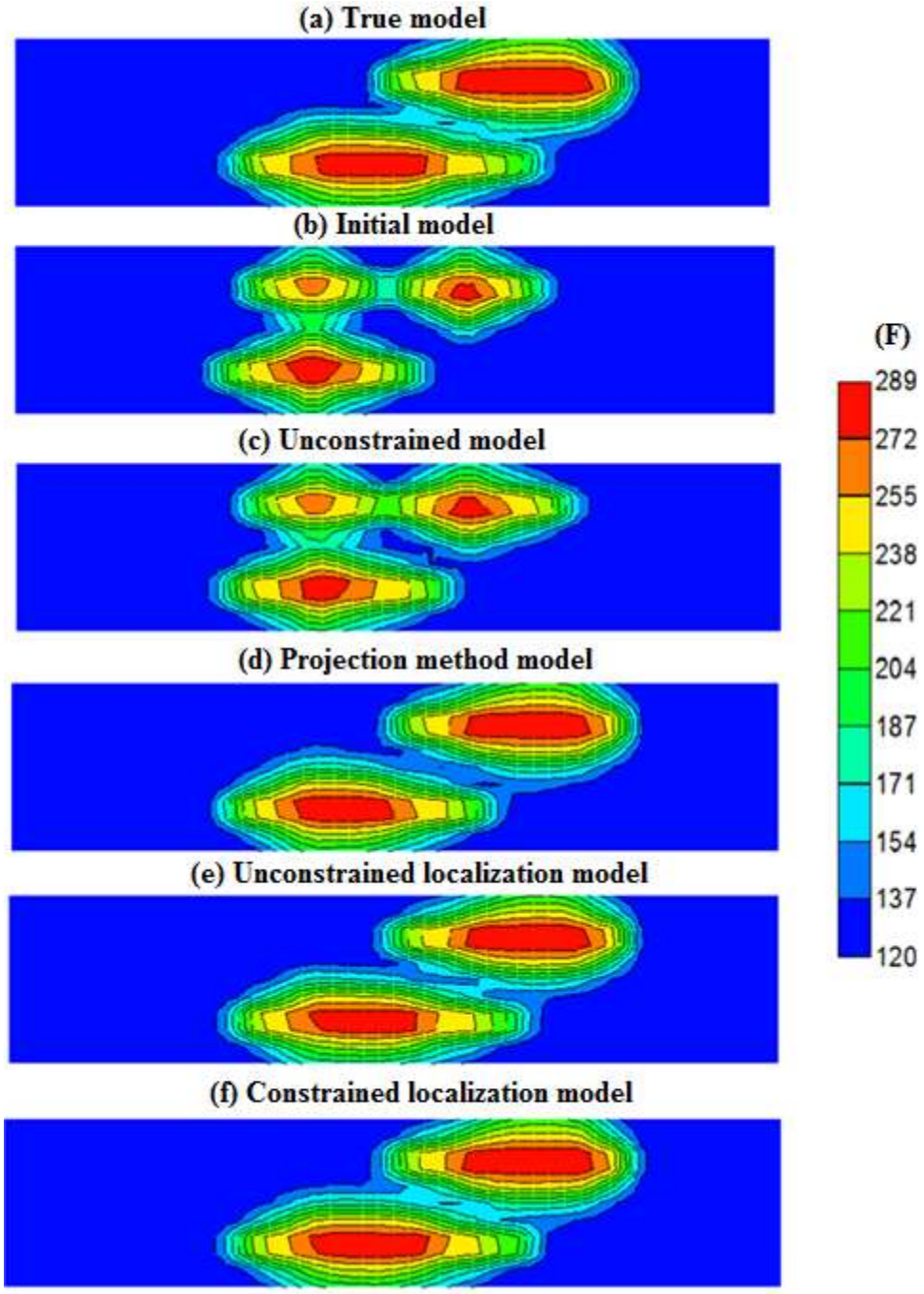

Figure 3.18 Comparison of the temperature distribution profile of SAGD process observed in the third layer of the reservoir (injection well layer) for different cases: Temperature profile of the true reservoir model, mean temperature field obtained from the initial model, and the mean temperature field of the estimated models.

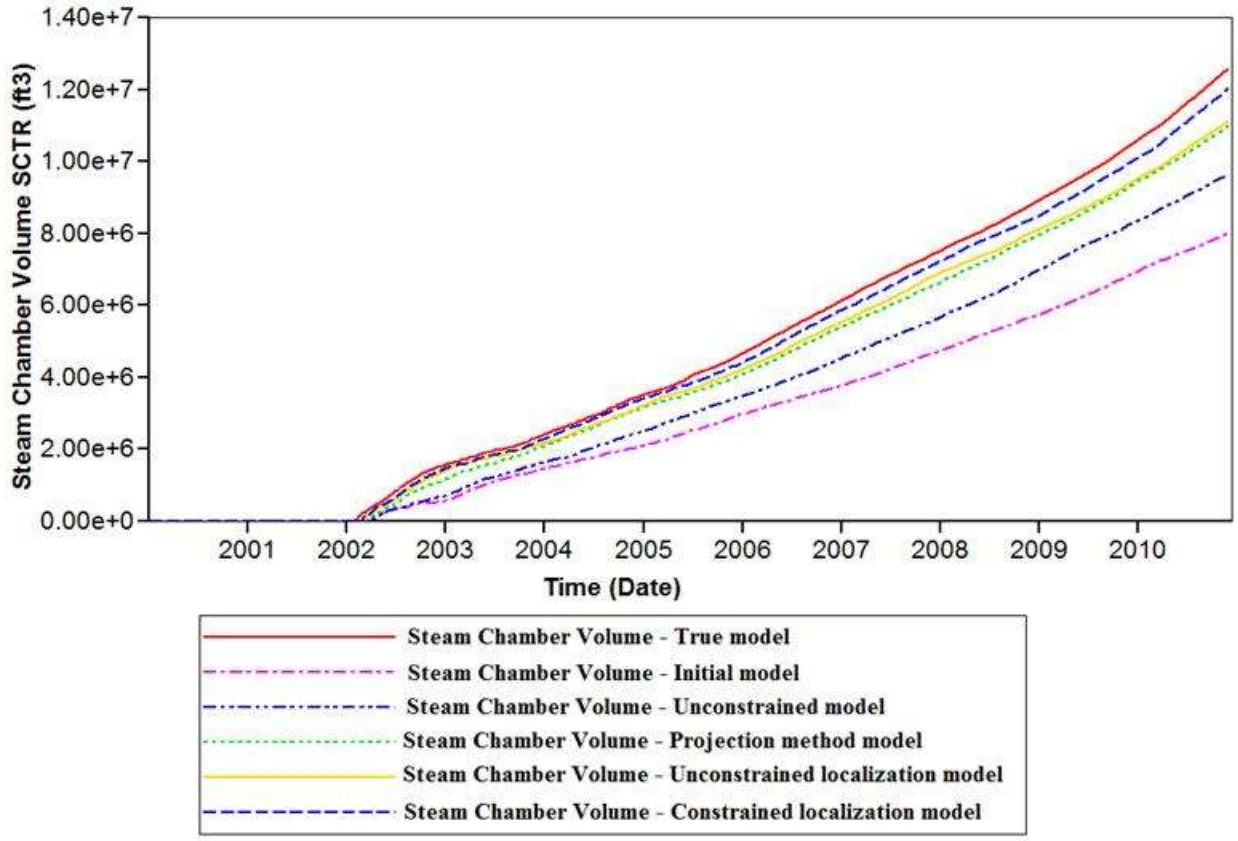

Figure 3.19 Comparison of the evolution of the steam chamber with the progress of SAGD process for different models.

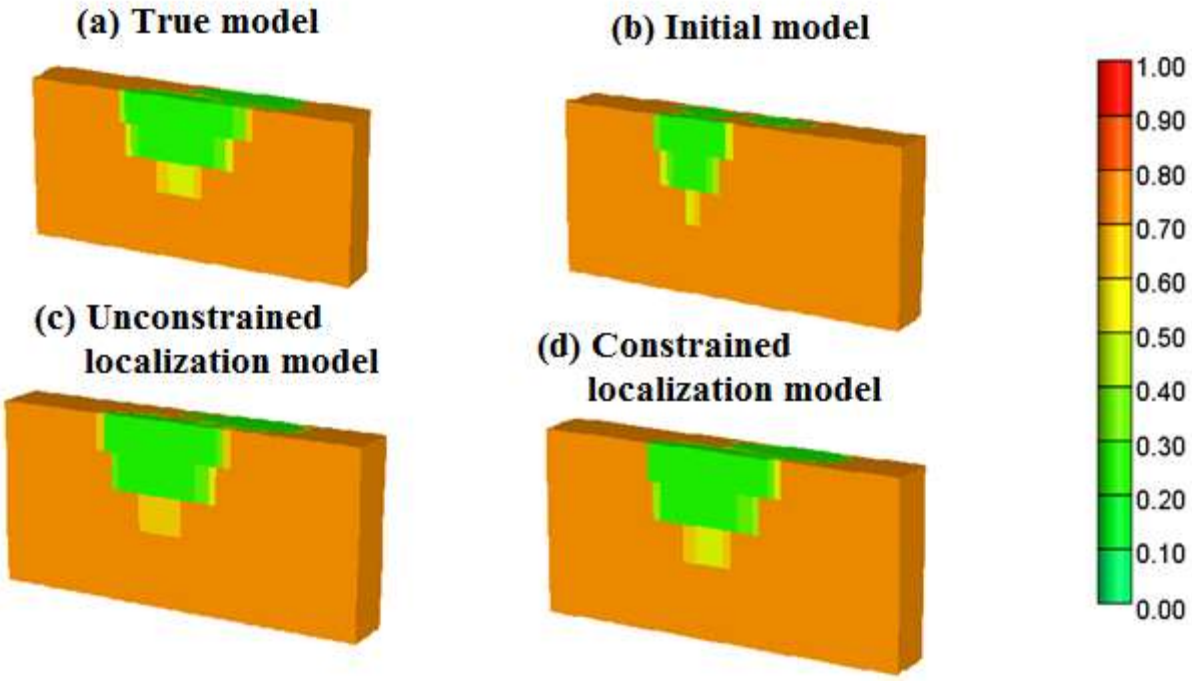

Figure 3.20 Comparison of the oil saturation profile of SAGD process observed in a reservoir section cut out in the vertical plane containing one of the horizontal well pairs for different cases: Clockwise from top left corner: Oil saturation profile of the true reservoir model, mean oil saturation fields obtained from the initial model, constrained localization method model and the unconstrained localization method model.

Fig 3.21 and **Fig 3.22** represent the history match of the oil production and the cumulative steam oil ratio for the entire reservoir field obtained from the estimated reservoir model when compared to the true reservoir model. It can be observed that with the addition of constraints into the estimation algorithm, better history matching is obtained. Moreover, as was observed in the case of 2D case study, the geostatistics-based localization algorithm performed best in matching the historical production data followed by the conventional localization method and the projection method-based EnKF method.

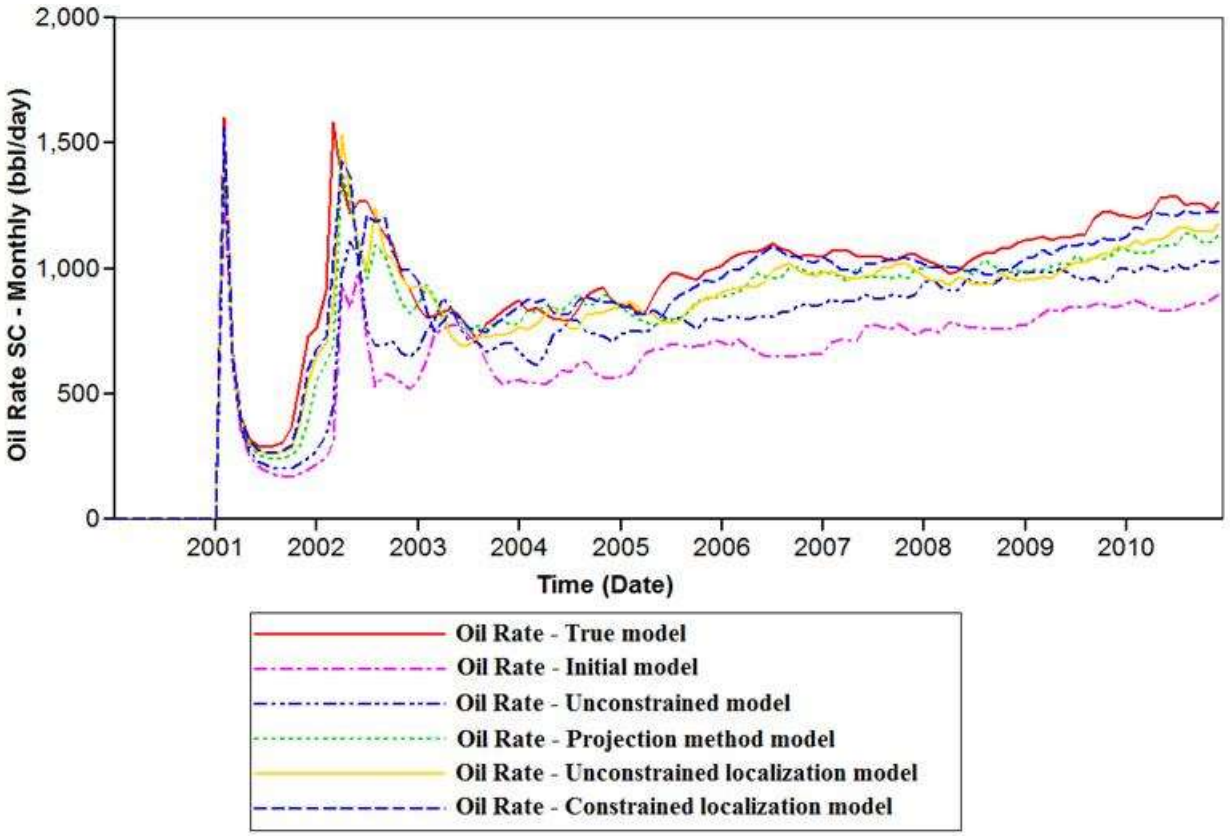

Figure 3.21 Comparison of the mean ensemble predictions for monthly oil production for the entire reservoir field with respect to the historical data using the true model, mean of the initial and the estimated models.

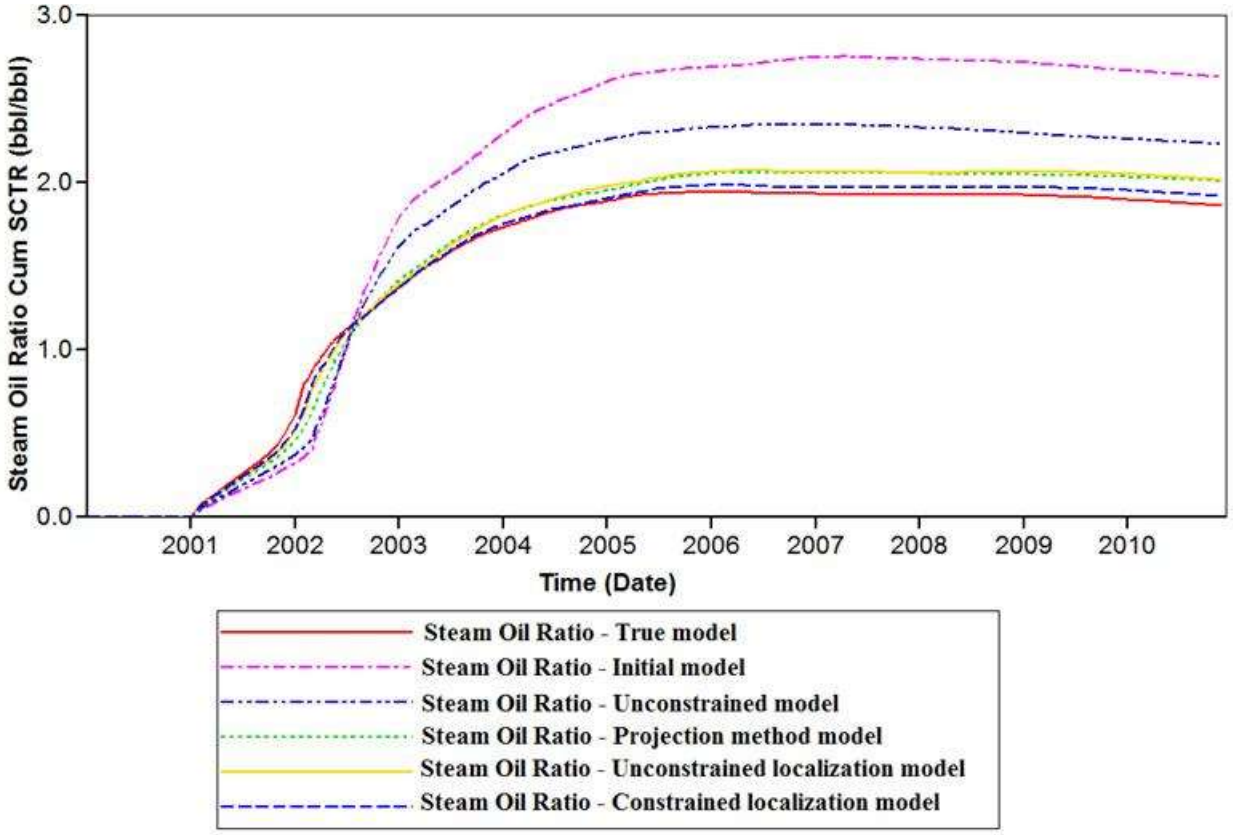

Figure 3.22 Comparison of the mean ensemble predictions for steam oil ratio for the entire reservoir field with respect to the historical data using the true model, mean of the initial and the estimated models.

3.4 Conclusion

In this work, the high efficacy achieved in history matching of reservoirs using covariance localization-based EnKF has been demonstrated in detail. Two highly heterogeneous and synthetic reservoir models were used for this study to apply the EnKF algorithm for reservoir history matching problem. The shortcomings of the conventional EnKF implementation were overcome by coupling the covariance localization-based EnKF with geostatistics. The advantages of this implementation were clearly seen in this chapter as it reduced the computational time by approximately 50% and also yielded more realistic and geostatistically consistent estimates of the reservoir permeability.

Chapter 4

Reservoir history matching using particle filtering

Chapter 2 and Chapter 3 addressed the shortcomings of the conventional method of the EnKF implementation for reservoir history matching applications so that geologically consistent estimates of the spatially varying reservoir parameters such as permeability are obtained. Although the EnKF is currently the most explored metric for reservoir characterization, it is important to understand that all distributions involved in an EnKF workflow is assumed to be Gaussian. The use of non-Gaussian distributions for reservoir parameters in the EnKF framework will not yield stable results and it may potentially fail to give any meaningful estimates. It is well known that the distributions of parameters such as porosity and permeability in a reservoir do not necessarily follow a Gaussian distribution in realistic scenarios. Hence, it is of great importance to carry out characterization procedures, taking into account these non-Gaussian distributions.

To suppress this limitation of the EnKF or any other Kalman filter variants, several sequential Monte Carlo-based Bayesian estimation methods have been developed in the last few decades with an aim to estimate nonlinear model states and parameters, characterized by their non-Gaussian distribution. The particle filter (PF) is one such method based on the Bayesian estimation, and has been successfully used in many applications. The particle filter is very similar to the EnKF in that they are both based on the Monte-Carlo simulations of states and parameters. However, unlike the EnKF, the particle filter differs in the update step where the parameters are evolved from one assimilation step to another by a completely Bayesian statistical update. In this chapter, we present the application of the particle filtering methodology to reservoir history matching. The efficacy of this method is demonstrated using two synthetic heterogeneous reservoir models considered in the previous chapters. Both unconstrained and covariance localization-based particle filtering are implemented on these reservoir models. The benefit of localization-based filtering in significantly reducing the computational burden as well as yielding better estimates are clearly observed.

Section 4.1 presents a survey of literature on the particle filter and its application to high dimensional problems such as reservoir parameter estimation. Section 4.2 provides a detailed

description of the particle filtering framework. Application of the particle filter to the two synthetic reservoir models is then analyzed in detail in Section 4. 3 and this is followed by a brief summary in Section 4.4.

4.1 Introduction

As mentioned before, a major assumption of the EnKF is not valid when the prior probability density functions (pdf) of the states and parameters are not Gaussian. For a nonlinear system, since the pdfs are generally not Gaussian, they should be classified as sub-optimal nonlinear filters [65]. In order to get around this problem, particle filters are widely used in systems that are characterized by the presence of nonlinearities in the state space model.

Particle filtering is a sequential Monte Carlo technique (SMC), first introduced by Gordon et al [66]. Ever since its inception, particle filtering has been used increasingly to obtain the solutions of the optimal states and parameters of complicated nonlinear dynamic systems [67]. Unlike the popular Kalman filter (KF) or any of its variants such as the extended Kalman filter (EKF), the unscented Kalman filter (UKF) and the EnKF, the particle filter methodology can be applied to any nonlinear process models, whose states follow a non-Gaussian distribution. The main drawback of the particle filter is the high computational effort that is required to arrive at estimates of states and parameters. However, due to rapid advancements in high speed computation, the particle filter has been now been successfully applied to on-line process monitoring of chemical processes such as in polymerization process [68], fermentation process [69], target tracking, robotics, computer vision and econometrics [70]. In recent years, particle filters have also been applied to geophysical models [71].

In the particle filter, the posterior pdf is used to store all the information about the states involved in the process. The uncertain states are initially generated through a stochastic Monte Carlo sampling, similar to the EnKF, giving rise to their corresponding posterior pdfs at the time instant before any measurement data has been assimilated. These samples or ‘particles’ are then propagated forward through the dynamic process model until the first assimilation time, resulting in the evolution of the states in accordance with the state transition function of the process, constituting the prediction step of the particle filter. These evolved states give rise to their corresponding prior pdfs. When the first measurement is available, then these particles are ranked

and weighed based on their likelihood function value with respect to the most recent available measurement. After ranking these particles, new particles are generated from this sample based on the weights of individual particles using several techniques such as the sequential importance sampling (SIS) and the sequential importance resampling (SIR). A detailed mathematical description of the SIR and the SIS filters is provided in Section 4.2.

The classic drawback of the particle filters is the degeneracy of the particles after certain number of assimilation steps, leading to impoverishment of the sample. Another drawback is that it is not as effective for simultaneous state and parameter estimation as it is for state estimation. This is because of the static nature of parameters, which does not allow them to evolve with each time step, thereby leading to parameter degeneracy after some time. To get around this problem, Kitagawa et al [72] suggested the inclusion of parameters in the extended state vector. However, taking into consideration the exponential forgetting of any joint state-parameter filter, this approach will lead to sample parameter degeneracy with successive resampling steps [73, 74]. Kitagawa et al [72] and Higuchi et al [75] suggest the addition of artificial random noise to the parameters in the extended state vector to prevent the degeneracy. This approach has been coupled with the auxiliary SIR by Liu et al [76] and also with the Rao-Blackwellised particle filter by Gustaffson et al [77]. Although this approach diminishes the particle degeneracy, it leads to variance inflation as pointed by Liu et al [76]. As a correction for this problem, they proposed a kernel smoothing-based SIR filter for use in the joint state and parameter estimation.

Although the particle filtering has been used successfully in large scale problems, it has hardly been explored for reservoir history matching applications. Heimhuber et al [17] present history matching results using the polynomial chaos expansion-based bootstrap particle filters. Luo et al [18] compare the EnKF and PF for reservoir history matching applications.

4.2 Particle filter methodology

To understanding the mathematical foundation behind a general SMC technique, let us consider a stochastic system comprising of only states represented by the following equations.

$$X_k = f(X_{k-1}) + W_k \tag{4.1}$$

$$Y_k = g(X_k) + V_k \tag{4.2}$$

$$V_k \sim N(0, R) \tag{4.3}$$

where

X_k: State variables of interest at a given time instant k. They are generally dynamic in nature such as the pressure, the oil saturation and the water saturation in a reservoir system.

f : State transition function which relates the state variables at a given instant to the state variables at the previous instant.

Y_k : The dynamic measurement data obtained at the time instant k. In a reservoir, these may include the oil production rate, the steam oil ratio, the gas production rate, the monthly oil production, the bottom-hole pressure, water cuts, oil cuts and the cumulative liquid production.

W_k: The process noise for the system.

V_k: The measurement noise associated with the process.

To get a basic grasp of the SMC method, the sequential importance sampling algorithm (SIS) is explained below, since SIS represents one of the most fundamental SMC methods. This sampling method has been in use since the last five decades [78]; however, it is not widely used now due to its computationally intensive nature.

As with any Monte Carlo-based technique, the states involved in the process are represented by a set of particles at any time instant k. Let the particles at time instant k be represented by X_k^i , $i = 1, 2, 3, 4, \ldots, N$, posterior density of a state at time instant k be represented by $p(x_k|Y_k)$ and the joint posterior density of the state be $p(x_k|Y_k)$. Let the weights corresponding to the individual particle be represented as w_k^i, $i = 1, 2, 3, 4, \ldots, N$. The joint pdf of the states can be approximated by equation 4.4.

$$p(x_k|Y_k) \approx \sum_{i=1}^{N} w_k^i \delta(X_k - X_k^i) \tag{4.4}$$

In importance sampling, the samples are drawn from the importance density $q(X_k|Y_k)$ to approximate the exact distribution $p(X_k|Y_k)$, since it is unknown. Now, the weights of the particles are given by the probabilistic equation 4.5.

$$w_k^i \alpha\, p\left(X_k^i \,|Y_k\right) \mid q\left(X_k^i \,|Y_k\right), \quad i = 1, 2, 3, 4, \ldots., N \tag{4.5}$$

Since the importance density is a known distribution, drawing samples from it is very similar to drawing samples from the actual posterior distribution. Assuming that the posterior density at time instant *k-1* is known, then when the measurement Y_k is available, the importance density is determined by equation 4.6.

$$q\left(X_k^i \,|Y_k\right) = \; q(x_k \mid X_{k-1}, Y_k)\; q(X_{k-1} \,|Y_{k-1}) \tag{4.6}$$

The posterior density is then given by the following equation:

$$p(X_k \,|Y_k) = \; p(y_k \mid X_k, Y_{k-1})\; p(X_k \mid Y_{k-1}) \;/\; p(y_k \mid Y_{k-1}) \tag{4.7}$$

Hence, the weight equation can be derived as:

$$w_k^i \alpha\, p\left(X_k^i \,|Y_k\right) \mid q\left(X_k^i \,|Y_k\right) = \; w_{k-1}^i\, p\left(y_k | x_k^i\right)\, p\left(x_k^i | x_{k-1}^i\right) |\; q\left(x_k^i \,|X_{k-1}^i, Y_k\right) \tag{4.8}$$

Now, the approximation of the posterior density can be given by equation 4.9.

$$p(x_k \,|Y_k) \approx \; \sum_{i=1}^{N} w_k^i \delta(\, x_k - x_k^i) \tag{4.9}$$

The main drawback of the SIS particle filter is the requirement of an extremely large number of particles in order to avoid the occurrence of particles with zero weights. As the number of particles N increases, the true posterior density will be obtained. The sequential importance resampling (SIR) filter was proposed by Gordon et al [64] to get rid of the degeneracy problem of SIS filters and is currently the most popular sampling method used in the update step of the particle filter. In the SIR method, a set of N particles are sampled from the posterior distribution such that each of the particles in the resulting sample have an equal weight of *1/N*. These are represented as *{* $x_k^i, \frac{1}{N}$ *}*. Hence, the SIR can be represented by the equations 4.10 and 4.11.

$$q(x_k |\, X_{k-1}^i, Y_k) = \; p(x_k^i \,| x_{k-1}^i) \tag{4.10}$$

$$w_k^i \;\alpha\; w_{k-1}^i \;\; p(y_k | x_k^i) \tag{4.11}$$

Fig 4.1 shows the schematic representation of the SIR-based particle filter.

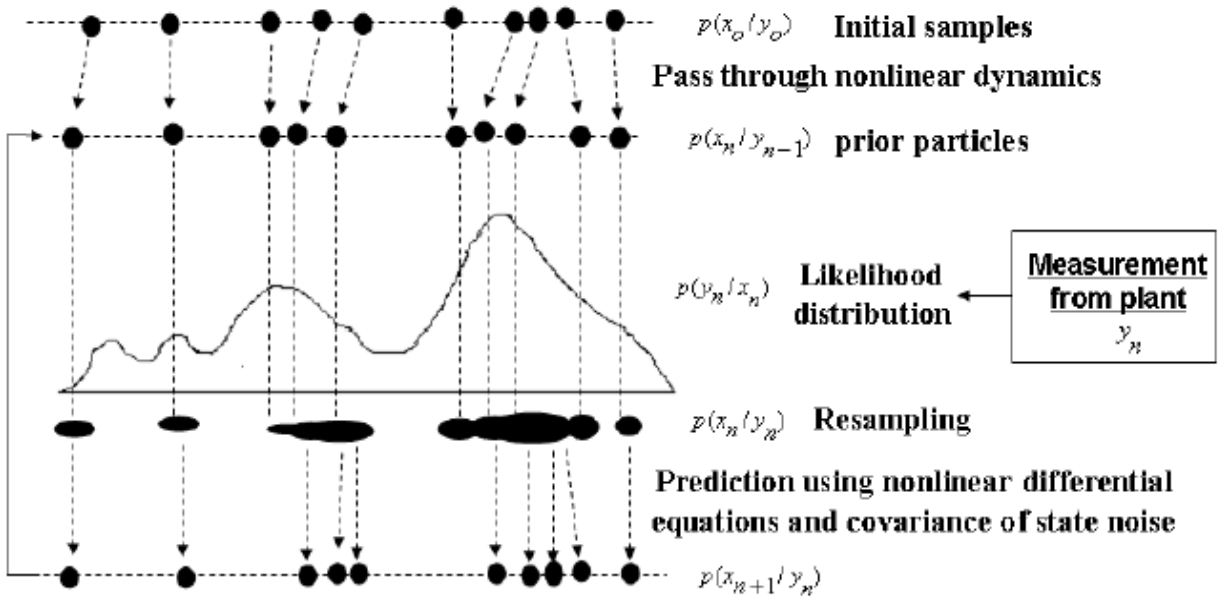

Fig 4.1 Schematic representation of SIR filters

As can be seen from the figure, the initial particles of the states generated through a stochastic Monte Carlo sampling is propagated through the system dynamics to obtain transitions particles, constituting the importance particles with a characteristic importance distribution. The importance weights are then calculated using the likelihood function and incoming measurements. This is followed by a resampling step, where a new set of particles are generated such that all of them have equal weight and these particles generally correspond to those in the region of high probability. These particles will then serve as the prior particles for the next time update step and the same process is repeated again until the last assimilation step.

Although the particle filtering methods explained above seems to be simple, it fails dramatically when a few unknown static parameters are involved in the process. When static parameters are involved in the state space model and are updated based on the above-mentioned algorithms, the static parameters will not move to new positions in the parameter space with each assimilation step. In other words, they do not get updated. Moreover, within a few assimilation steps, degeneracy of the particles associated with these parameters may occur, thereby leading to the failure of the filter. Gordon et al [64] suggested adding some random artificial perturbations to the particles of the states in order to avoid the problem of degeneracy. Several other authors followed suit by extending this idea to add artificial random noise to the static parameters as well. However,

this process led to the artificial loss of information as pointed out by Liu et al [76]. To address this limitation, they suggested a novel algorithm that combines the SIR filter with a kernel smoothing method so that this artificial loss of information is averted. For this work, we have used the method proposed by Liu et al [76] to overcome the limitation of the particle filter for parameter estimation and the detailed description of its algorithm is explained below.

When both the states and parameters have to be estimated such as in reservoir characterization, Bayes' rule will imply the following relation:

$$p(x_k, \theta_k|Y_{1:k}) \; \alpha \; p(Y_k \; |x_k, \theta_k, Y_{1:k}) \; p(x_k|\theta_k, Y_{1:k}) \; p(\theta_k|Y_{1:k-1}) \tag{4.12}$$

where θ_k is the vector of reservoir model parameters such as the porosity and permeability. In order to facilitate the joint state and parameter estimation of reservoir properties, an augmented vector consisting of both the dynamic states and the static parameters is used and a Gaussian random walk model (see equation 4.13) is employed to evolve the parameter estimates during the prediction stage of the particle filter.

$$\theta_k = \theta_{k-1} + s_k \tag{4.13}$$

where s_k is the random noise for the random walk model following a Gaussian distribution defined by equation 4.14.

$$s_k \sim N(0, CV_k) \tag{4.14}$$

where CV_k is the covariance matrix. The last term in equation 4.12 $p(\theta_k|Y_{1:k-1})$ is usually approximated by a mixture of particles as shown in equation 4.15 [79].

$$p(\theta_k|Y_{1:k-1}) \sim \sum_{i=1}^{N} \mathrm{w}_{k-1}^{\mathrm{i}} \; N(\; \theta_k \mid \theta_{k-1}^{\mathrm{i}}, CV_k) \tag{4.15}$$

Assuming that the sample mean and the covariance matrices of the parameters with weights $\{\theta_{k-1}^{\mathrm{i}}, \mathrm{w}_{k-1}^{\mathrm{i}} \, , i = 1, 2, 3, \ldots \ldots N\}$ computed from the ensemble at time instant *k-1* are represented as μ_{k-1}^{θ} and V_{k-1}, Liu et al [76] concluded that covariance inflation occurs, since they found that the distribution in equation 4.15 is characterized by a covariance of $V_{k-1} + CV_k$. In order to avoid this variance inflation, kernel smoothing was proposed by Liu et al [76]. Here, a kernel smoother is used with the smoothing parameter $0 < h < 1$.

$$p(\theta_k|Y_{1:k-1}) \sim \sum_{i=1}^{N} w_{k-1}^{i}\, N(\theta_k \mid m_{k-1}^{i}, h^2 V_{k-1}) \quad (4.16)$$

In the above equation, m_{k-1}^{i} represent the kernel locations and are determined by using a shrinkage rule [76] provided in mathematical form in equation 4.17. This shrinkage rule makes sure that the particles are distributed very close to their mean values.

$$m_{k-1}^{i} = \left(\sqrt{1-h^2}\right)\theta_{k-1}^{i} + \left(1 - \left(\sqrt{1-h^2}\right)\right)\mu_{k-1}^{\theta} \quad (4.17)$$

In general, the smoothing parameter h is obtained from a tuning exercise. It is usually chosen to be around 0 – 0.2 if the parameters are known to static or slightly time-varying and around 0.8 – 1.0 if they are known to be strongly time-varying. For this work, we have used the algorithm used by Thomas [80] to combine the SIR resampling with the kernel smoothing, which is explained below in 6 steps.

1. At t= 0, Monte Carlo samples for the states $\{x_{t=0}^{i}\} : p(x_0)$ and parameters $\{\theta_{t=0}^{i}\} : p(\theta_0)$ are drawn for all $i = 1, 2, 3, \ldots\ldots N$.
2. Parameter samples are drawn for the time k+1 represented as $\{\theta_{k+1}^{i}\}$: $N(\theta_{k+1} \mid m_k^i, h^2 V_k)$ and m_k^i is calculated using equation 4.17 for all $i = 1, 2, 3, \ldots\ldots N$.
3. State samples at time instant *k+1*, $\{x_{k+1}^{i}\} : N(x_{k+1} \mid \mu_k^i, \theta_{k+1}^{i})$ are then drawn using the state transition function in the state space model (equation 4.1).
4. Weights are computed using equation 4.18.

$$w_{k+1}^{i} = \frac{p(y_{k+1}|x_{k+1}^{i},\theta_{k+1}^{i})}{\sum_{i=1}^{N} p(y_{k+1}|x_{k+1}^{i},\theta_{k+1}^{i})} \quad (4.18)$$

5. The samples θ_{k+1}^{i} and x_{k+1}^{i} are then resamples with resampling using SIR technique to get N samples of the states and parameters representing the posterior distribution.
6. Steps 2 to 5 are repeated until the end of the particle filtering process for this application.

4.3 Results and discussions

A two-dimensional reservoir model of dimension 100 x 1 x 20 is created using the commercial simulator CMG IMEX as shown in **Fig 4.2**. The model consists of one injector well placed at the center of the well and two producer wells located at either side of the injector. The data set for this model was taken from 2000 SPE Project [41]. Initially, it is assumed that the reservoir is fully saturated with oil, i.e., the oil saturation S_o = 1.0 and values of the gas saturation S_g and water

saturation S_w being equal to zero. The value of permeability ranges from 0 to 1000 mD in this model. It is assumed that certain information is available in the form of hard data. The values of permeability is assumed to be known in a total of 100 grid block locations at i=1, 25, 50, 75, 100 and the corresponding vertical direction.

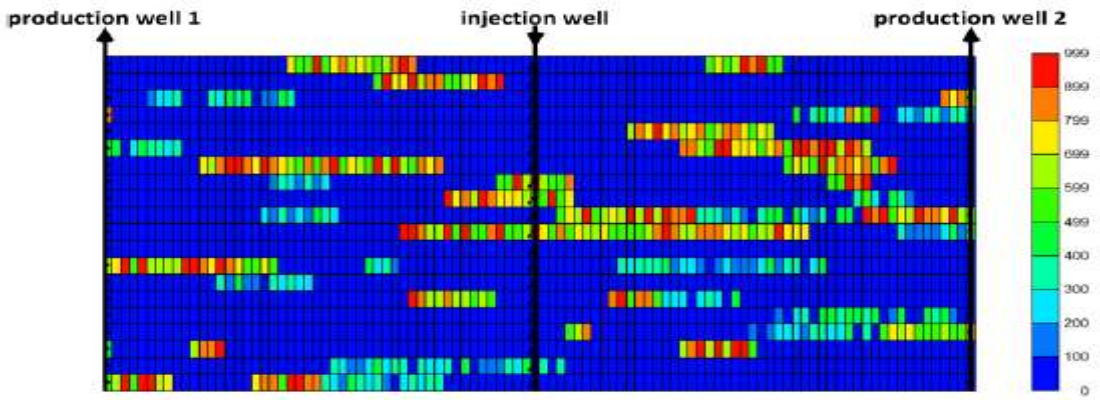

Fig 4.2 Two dimensional reservoir model

Here, the oil was produced by a waterflooding process. In a waterflooding process, water is injected in order to increase the reservoir pressure leading to increased oil production from the reservoir. The input used in the process was water injection rate and its mole fraction in the injection phase. The parameter to be estimated is permeability. The state vector consisted of three components, namely, oil saturation, water saturation and pressure. The production data vector consisted of two components, namely the oil production at well 1 and the oil production at well 2.

For the generation of the initial ensemble of the natural logarithm of the permeability field, the geostatistical simulation package SGeMS was used, where the spatial distribution was generated by a sequential Gaussian simulation algorithm. While generating the initial ensemble, the distribution obtained was made to honour the permeability value represented by the hard data at the hard data locations. For this method, an ensemble was made of 150 such realizations/particles.

To implement covariance localization, a sensitivity analysis was conducted to determine the region of influence in the reservoir. This study was done using the simulation package CMOST. **Fig 4.3** represents the regions of influence in the two-dimensional reservoir under consideration for this case study. The state vector consisted of two dynamic reservoir properties, namely the gas saturation and the oil saturation while the parameter vector consisted of the permeability values at

the grid blocks. Hence, in the conventional implementation of the particle filter, the dimensions of the state and parameter vectors are 4000 x 1 and 2000 x 1 respectively. On the other hand, the corresponding dimensions for localization-based particle filter are 2400 x 1 and 1200 x 1. This reduction in the dimension of the estimation vector greatly reduces the computational load involved in the estimation framework and also lessens the severity of the particle degeneracy problem described in the previous section.

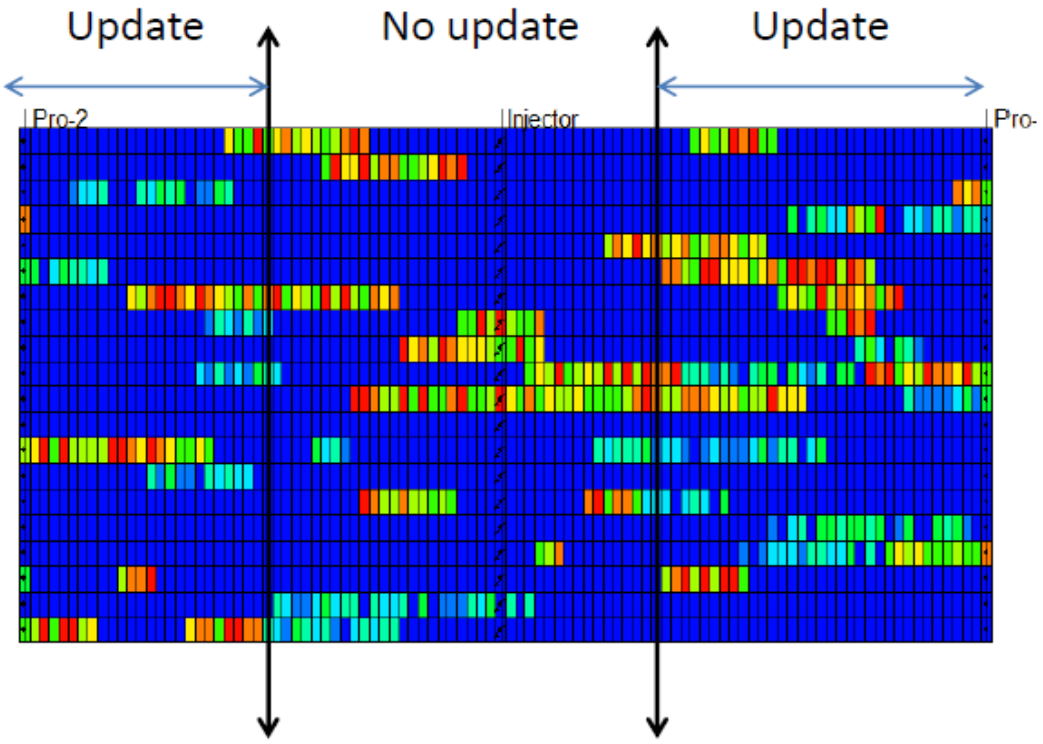

Fig 4.3 Region of influence in the reservoir

Fig 4.4 compares the permeability maps of the estimated model with respect to the true model. We can infer from this figure that although, the particle filtering has not resulted in a very good estimate of the permeability field compared to the reference permeability field, the use of the covariance localization has given rise to a field with a reasonable resemblance to the reference field. However, compared to the EnKF, the accuracy of estimation of the particle filter is not so good; this can be attributed to the presence of a large number of states and parameters in the reservoir, leading to degeneracy of the particles after assimilation of a certain number of

measurements. Moreover, since the number of particles constituting an ensemble is three times more than that used for the EnKF ensemble, particle filter is more computationally expensive when compared to the EnKF. Fig 4.4 also implies that the localization based particle filtering technique yields estimates more consistent with the reference field compared to the estimated field obtained using the conventional unconstrained particle filtering method.

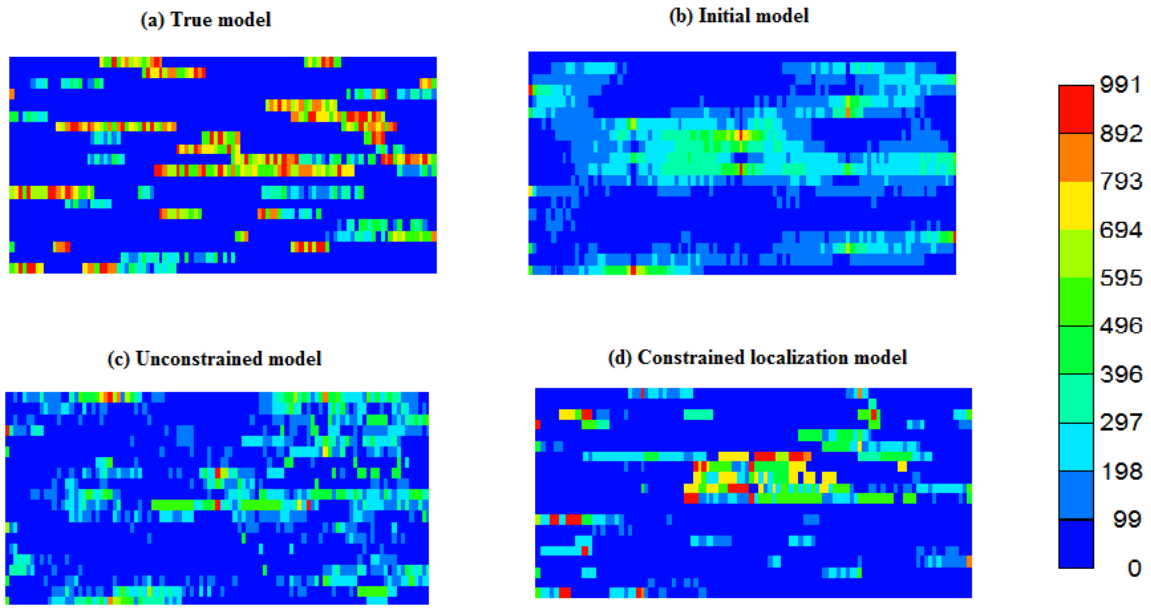

Fig 4.4 Permeability map comparison: Clockwise from top left corner – Reference permeability field of true model, initial permeability field, covariance localization-based permeability field unconstrained estimated permeability field.

The simulations were done for a period of 7300 days and there were 14 data assimilation steps in total for this study. **Fig 4.5** and **Fig 4.7** compare the oil saturation profile and the gas saturation profile respectively in the reservoir at the last time instant (t=7300 days) obtained by using the true reference model, the initial model and the two estimated models. To order to quantify the results revealed by these contour plots, we have shown the comparison of the evolution of the average oil and gas saturation (see **Fig 4.6** and **Fig 4.8**) in the entire reservoir field with the progress of the waterflodding process for the reference and the estimated models. **Fig 4.9** and **Fig 4.10** compare the ensemble predictions of the oil production with respect to the historical production data at wells Pro-1 and Pro-2 respectively. These figures imply that the localization-based particle filtering performs better than the conventional particle filtering algorithm.

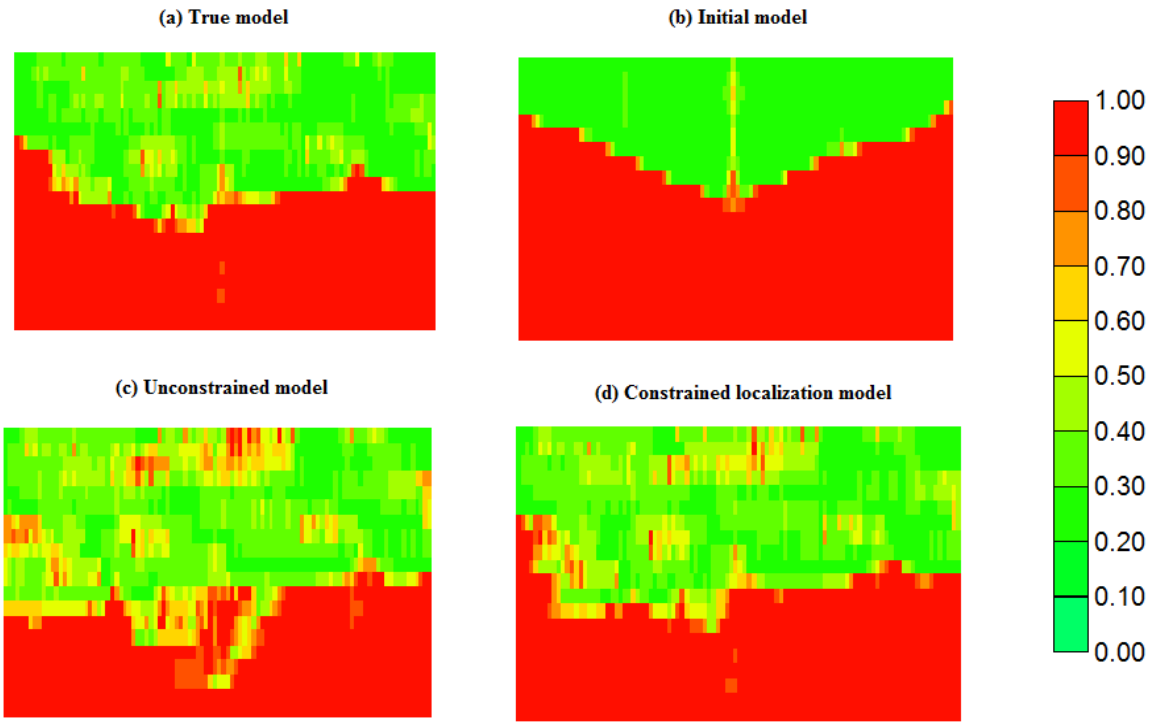

Fig 4.5 Comparison of constrained vs. unconstrained localization estimation with respect to oil saturation at the last time instant. Clockwise from top left corner: Oil saturation corresponding to true model, mean oil saturation fields of the initial model, constrained localization-based EnKF model and unconstrained model.

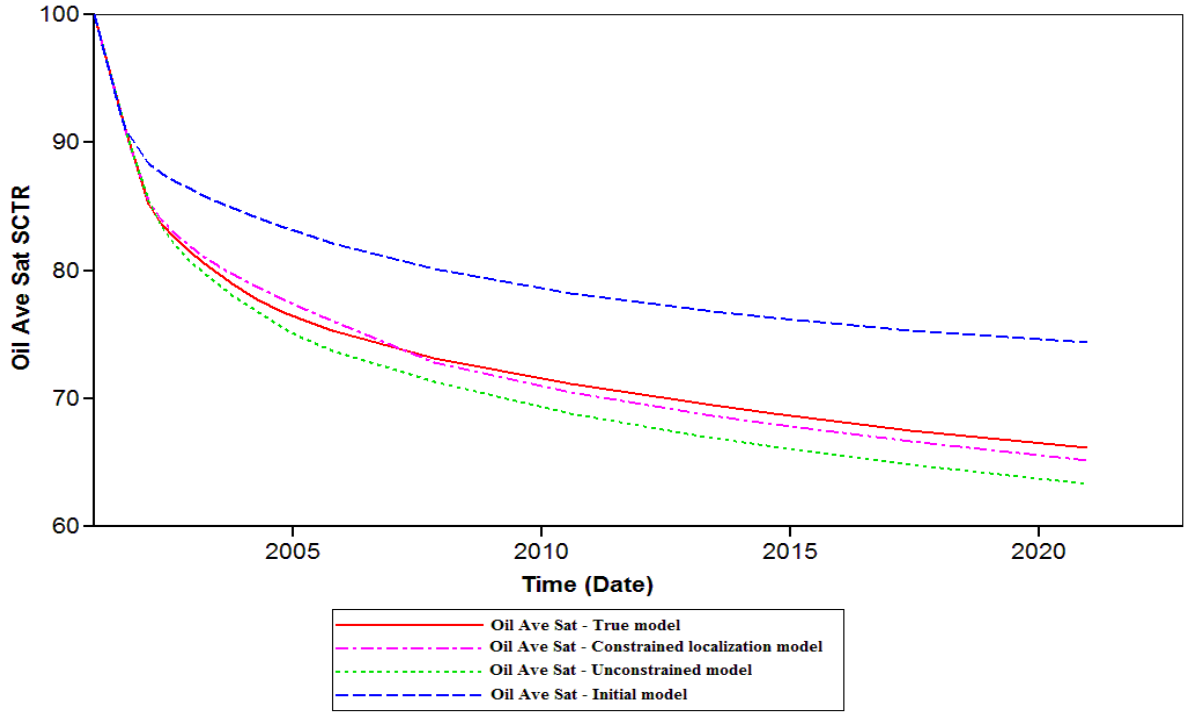

Fig 4.6 Comparison of the average oil saturation in the entire reservoir with the progress of the waterflooding process for true model, initial model, localization based EnKF and unconstrained EnKF model.

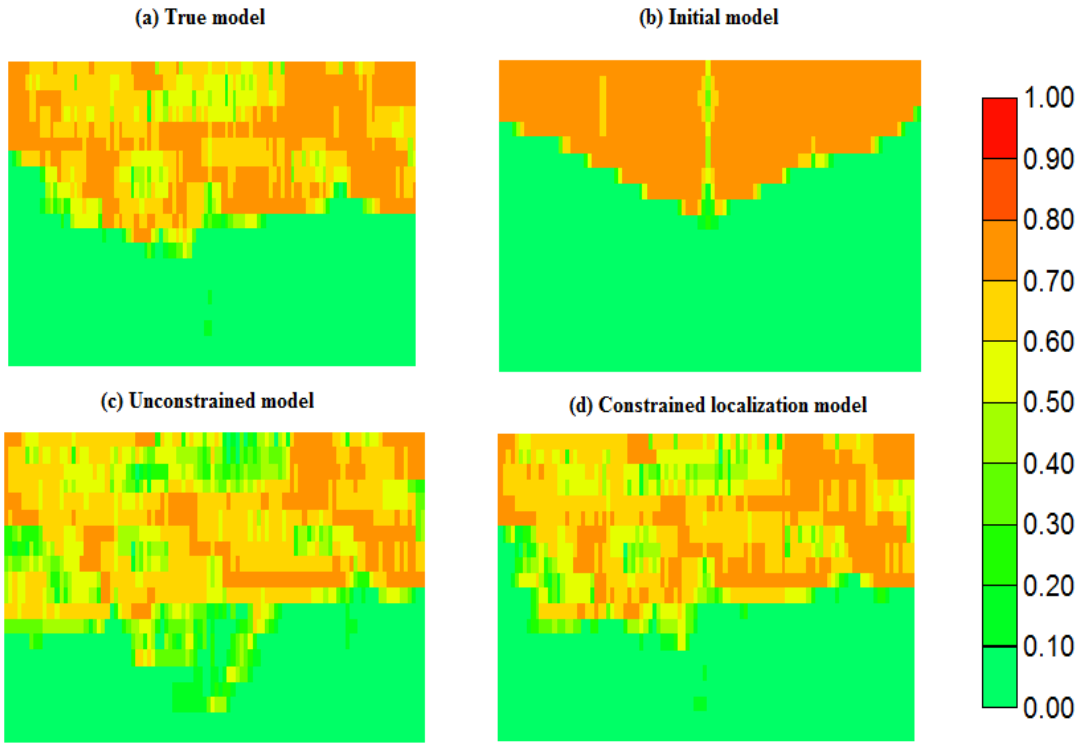

Fig 4.7 Comparison of constrained vs. unconstrained localization estimation with respect to gas saturation at the last time instant. Clockwise from top left corner: Gas saturation corresponding to true model, mean gas saturation fields of the initial model, constrained localization-based EnKF model and unconstrained model.

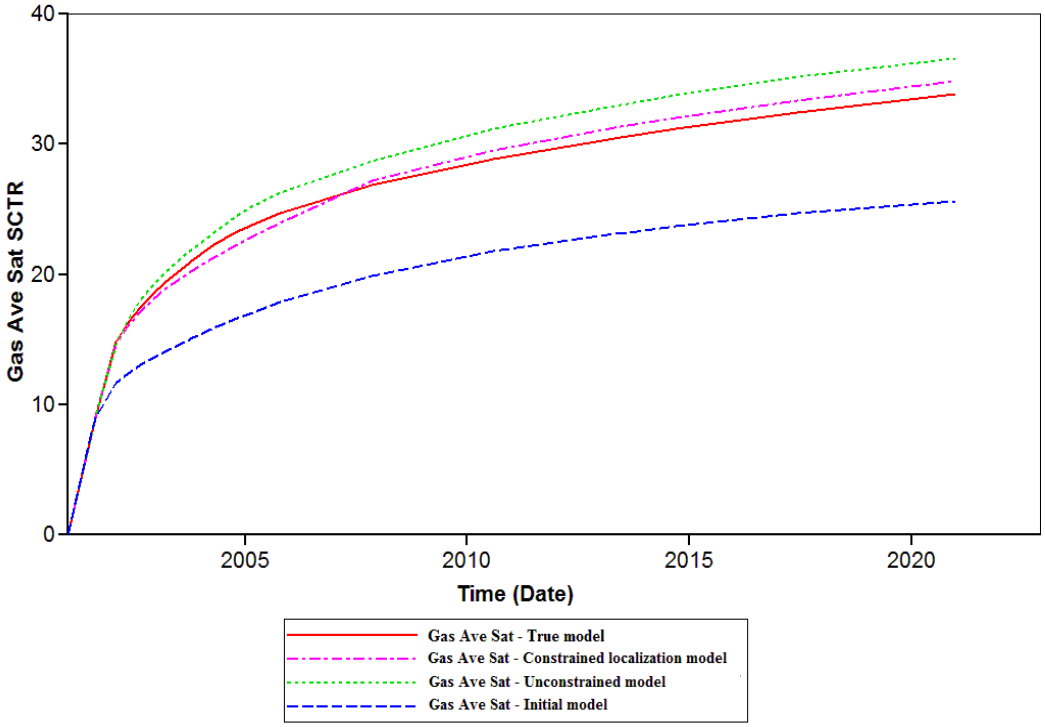

Fig 4.8 Comparison of the average gas saturation in the entire reservoir with the progress of the waterflooding process for true model, initial model, localization based EnKF and unconstrained EnKF model.

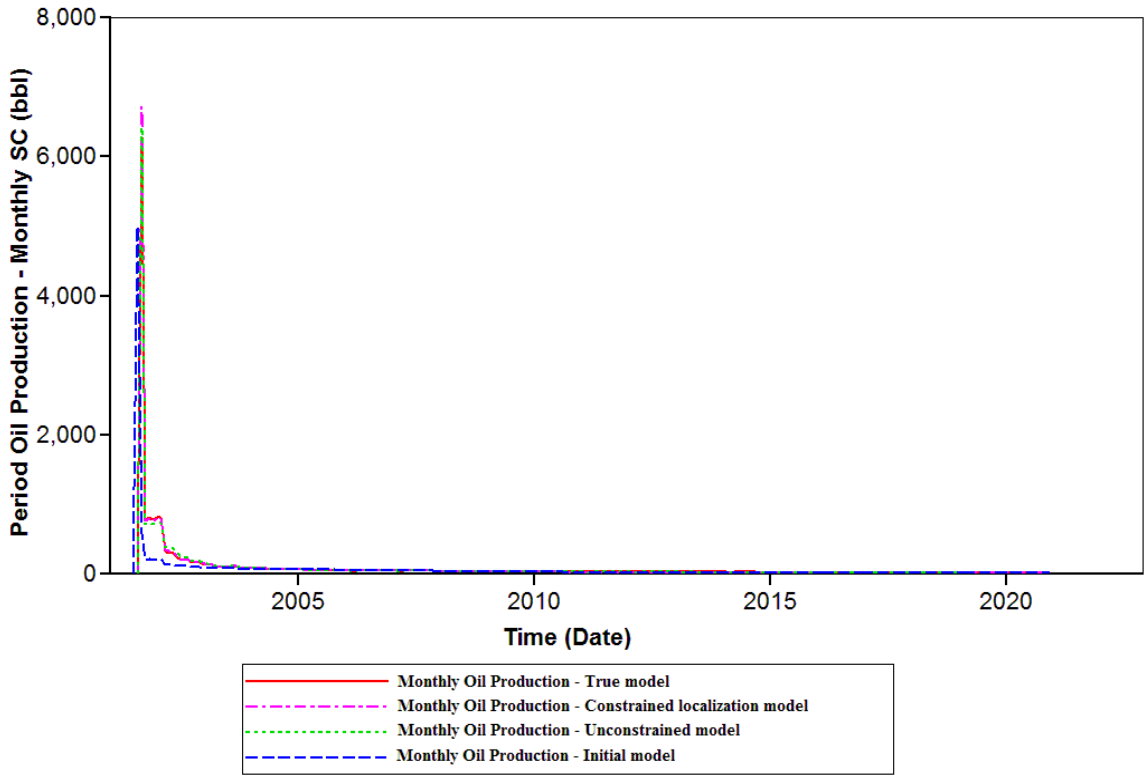

Fig 4.9 Comparison of the mean ensemble predictions for the monthly oil production with respect to the historical production data using the true model, mean of the initial and the estimated models at the production well Pro-1.

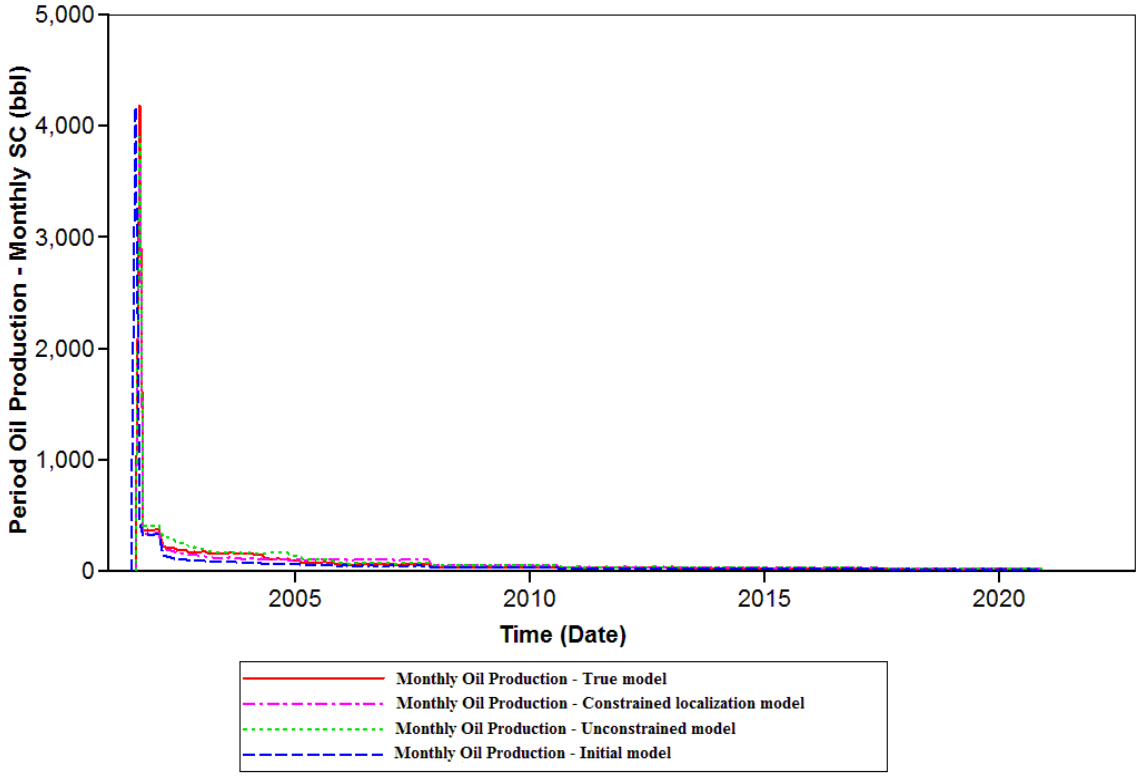

Fig 4.10 Comparison of the mean ensemble predictions for the monthly oil production with respect to the historical production data using the true model, mean of the initial and the estimated models at the production well Pro-2.

4.3.2 3D SAGD reservoir model

For this study, the reservoir model considered is exactly same as the one considered in the previous chapter. Although the representation of the model was shown in the previous chapter, for the sake of completeness, it is also shown below in **Fig 4.11.** The history matching was posed as a joint state and parameter estimation problem through the particle filtering method. The reservoir's dimension is 5000ft x 1000ft x 150ft. The data set for this model was taken from [41]. The permeabilities at all the grid block locations were taken from the above mentioned model. There are totally 2500 permeability values and permeabilities in all directions were set to be equal. Since this is a highly heterogeneous model, the value of permeability is different in different grid blocks. The value of permeability ranges from 0 to 1000 md in this model. It is assumed that permeability information at certain spatial locations is available in the form of hard data.

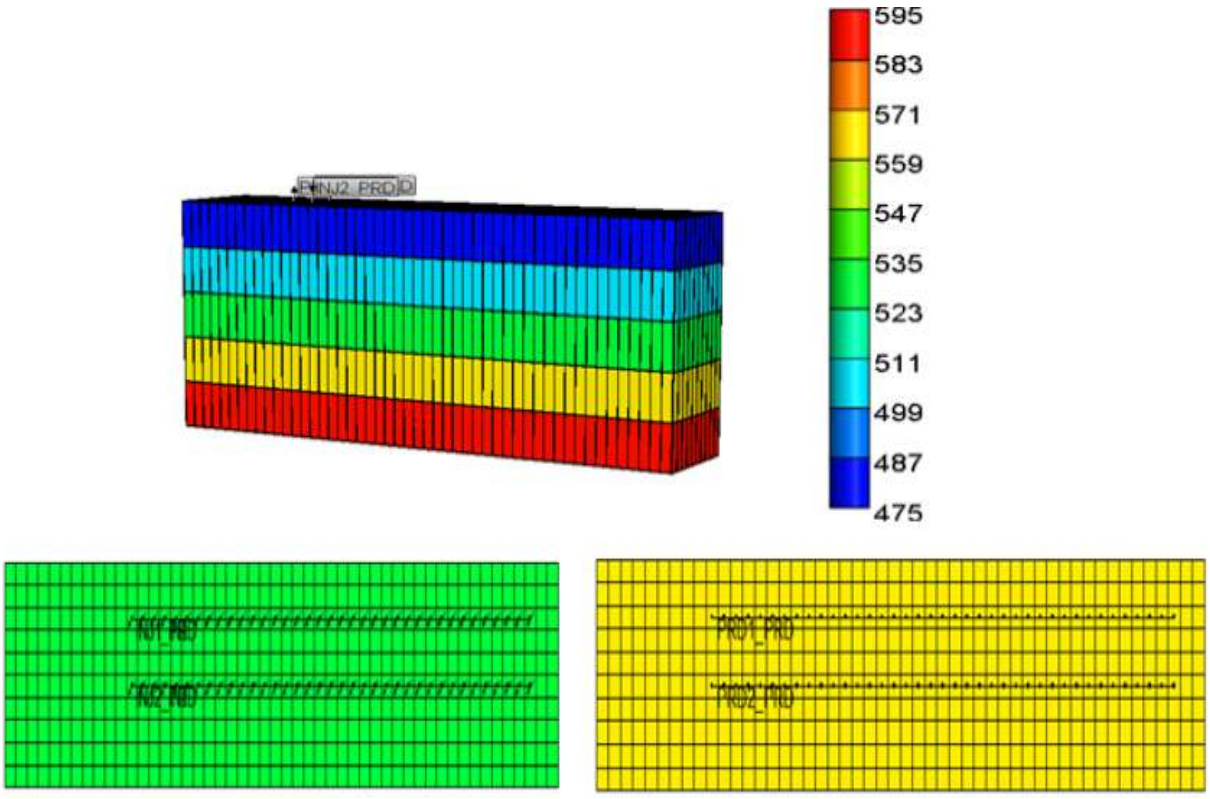

Fig 4.11 3D SAGD reservoir model and two layers representing the horizontal well pair placement

In order to perform covariance localization, a sensitivity analysis study was conducted to identify regions of influence for the two horizontal producing wells. It was found out that expect the top and bottom layers, other layers affected the production data at the producing wells significantly. Therefore, the particle filtering update operation was focused only on the grid blocks comprising these regions. After every update step of the particle filtering, the top and bottom layers were modified using the sequential Gaussian simulation so that these two layers are at all times geologically consistent with the remaining three regions. In this way, the variogram of the estimated model will be a very good match with respect the variogram obtained as a part of soft data information. The state vector was comprised of two dynamic reservoir properties, namely the oil saturation and temperature at the reservoir grid blocks, while the parameter vector comprised of the permeability values at the grid blocks. For the conventional particle filtering framework, the dimensions of the state and parameter vectors were 5000 x 1 and 2500 x 1 respectively. On the other hand, the corresponding dimensions for the localization-based particle filtering method were

2400 x 1 and 1200 x 1 respectively. This considerable reduction in the dimension of the estimation vector greatly reduces the computational load and also lessens the particle denegeracy problem generally prevalent in the particle filtering application to large scale systems.

Fig 4.12 shows the comparison of permeability map of the third layer of the reservoir between the true model, the initial model and the ones obtained using the unconstrained model and the covariance localization-based model. It can clearly be observed that the particle filtering algorithm has greatly improved the permeability estimates compared to the initial model, although not to the same extent observed in the EnKF implementation.

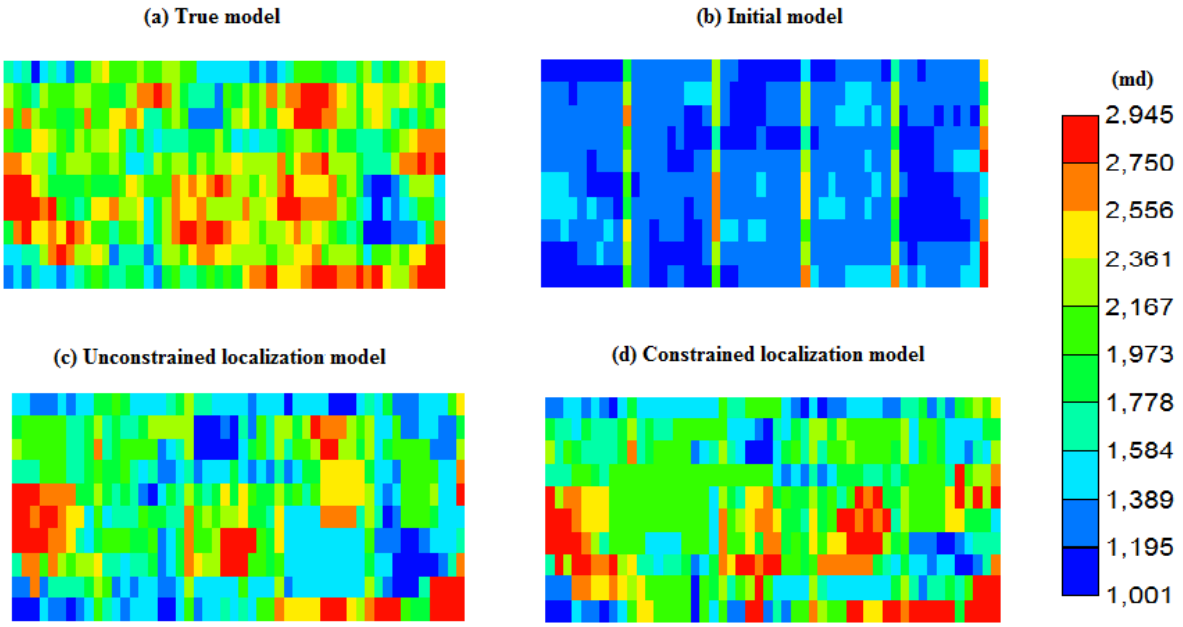

Fig 4.12 Permeability map comparison: Clockwise from top left corner – Reference permeability field of true model, initial permeability field, covariance localization-based permeability field and unconstrained estimated permeability field.

It can clearly be seen from the above figure that with the assimilation of production data, the particle filter yields an estimate of permeability closer to the true model. Moreover, when the covariance localization is applied to the estimation problem, the permeability match is very good. However, it is important to note that the estimate obtained from this method is not as good as the estimates obtained by using the EnKF. This is because of the fact that particle filter algorithm

works on a resampling technique, where the samples for successive prediction step are drawn from the importance distributions. This may lead to degeneracy of the sample.

Fig 4.13 compares the steam chamber profile for the SAGD process in the injection well layer (layer 3) after 10 years of SAGD operation for the true, the initial, unconstrained and localization-based models. **Fig 4.14** also gives a similar comparison of the steam chamber but in a perpendicular direction to that shown in **Fig 4.13**. **Fig 4.15** gives a quantitative comparison of the steam chamber evolution for the reference and the estimated models. It can be observed from these three figures that the localization-based particle filtering method results in a better reproduction of the reservoir characteristics as that of the reference model. **Fig 4.16** compares the mean oil saturation profile for the SAGD process in the injection well layer (layer 3) after 10 years of SAGD operation for the true, the initial, the unconstrained and the localization-based models. In order to quantify the results obtained from this figure, the evolution of the average oil saturation in the entire field was also observed and is shown in **Fig 4.17**. The prediction of the particles in the ensemble for the two estimated models are compared with the actual historical production data and are shown in **Fig 4.18** and **Fig 4.19**. These figures further indicate that the localization-based particle filtering results in better estimates of the reservoir permeability.

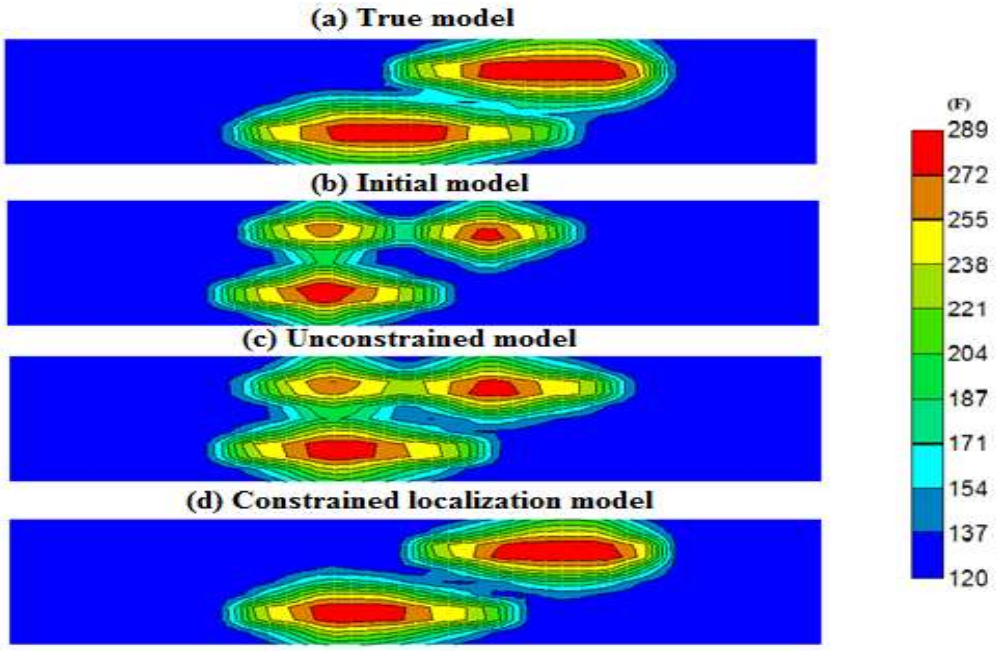

Fig 4.13 Steam chamber in the third layer of the SAGD model for true, initial, unconstrained and the constrained localization models.

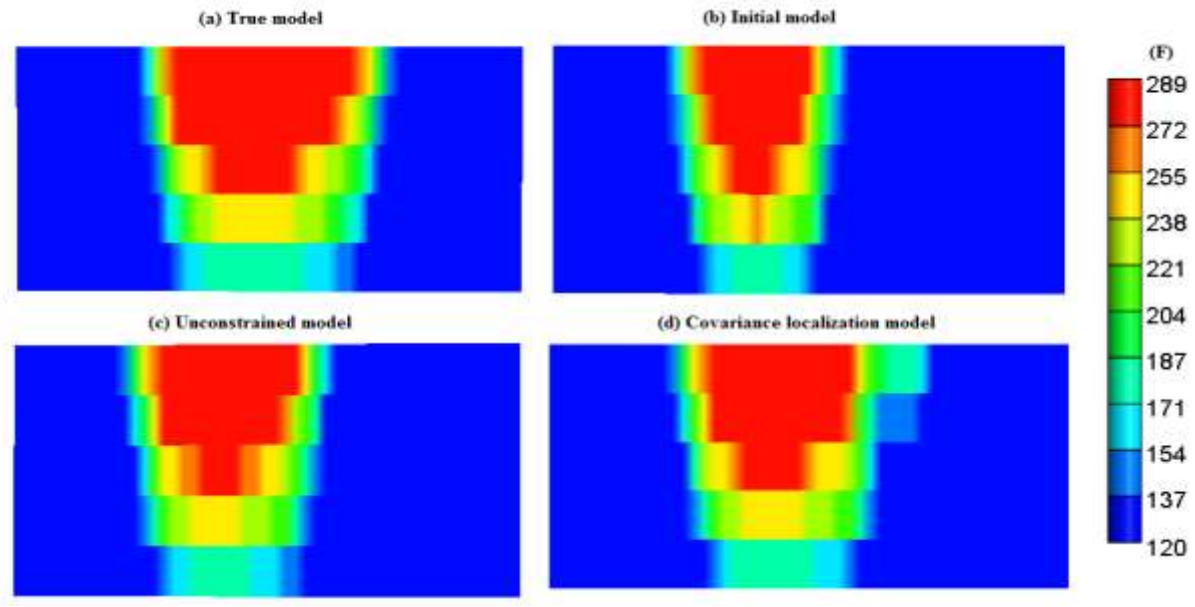

Fig 4.14 Steam chamber at the last time instant (t=10 years) for true, initial, unconstrained and covariance localization models.

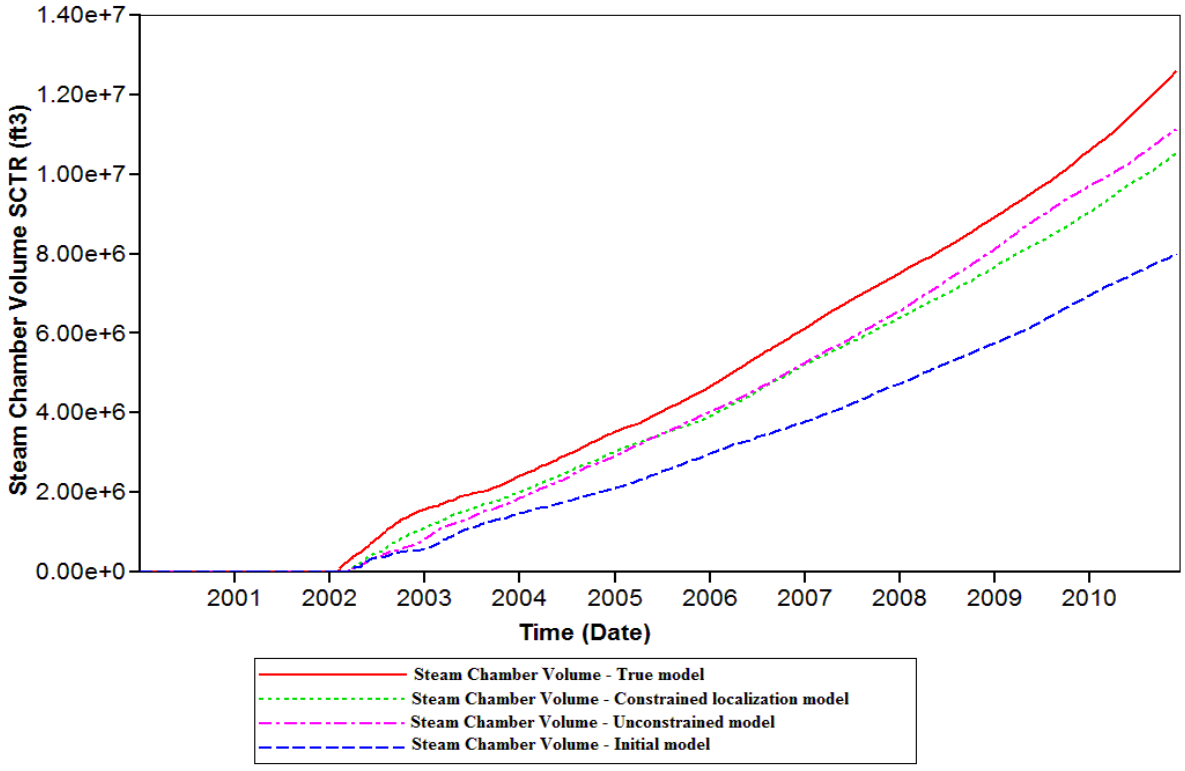

Fig 4.15 Evolution of the steam chamber volume with the progress of SAGD process for true, initial, unconstrained and constrained localization models.

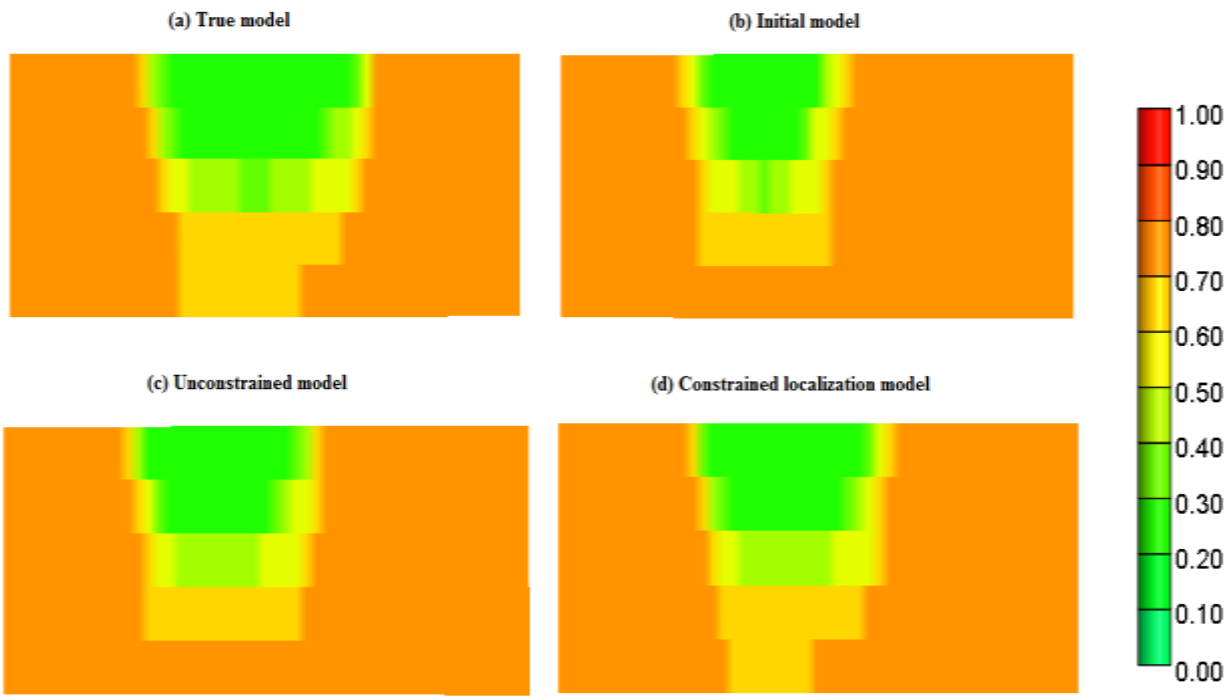

Fig 4.16 Oil saturation profile at the last time instant (t=10 years) for true, initial, unconstrained and localization models.

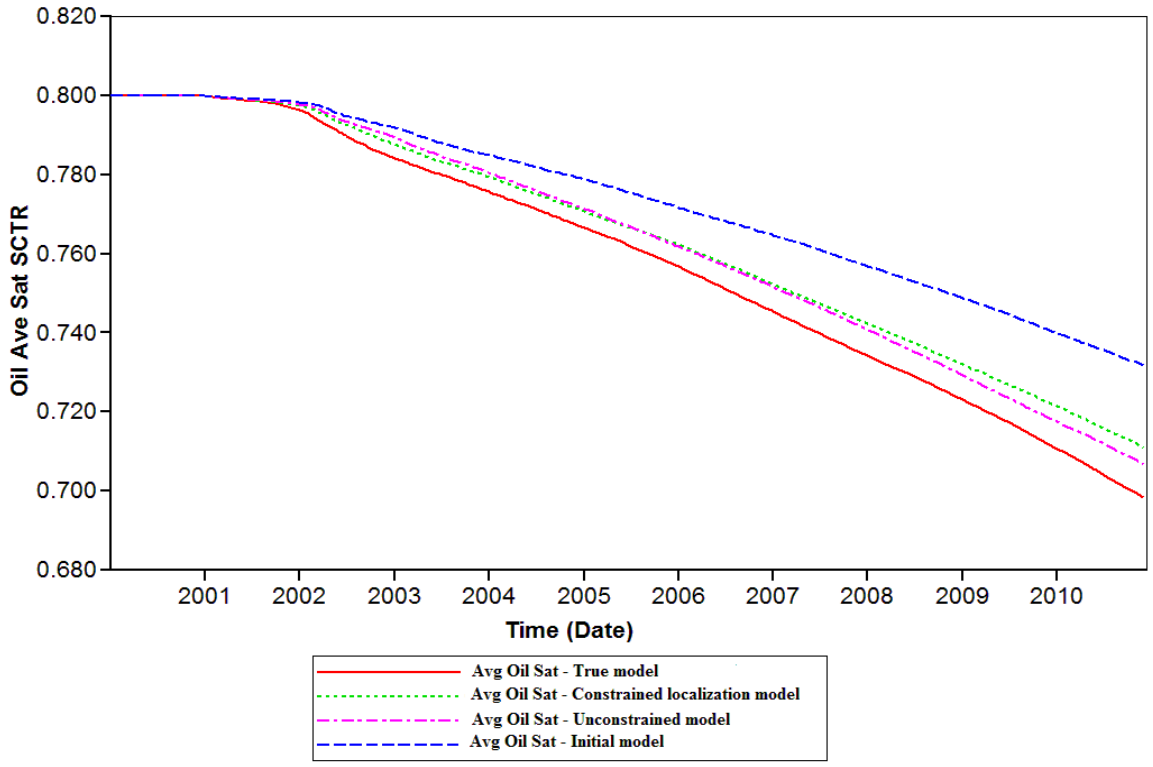

Figure 4.17 Comparison of the average gas saturation in the entire reservoir with the progress of the waterflooding process for true model, initial model, localization-based EnKF and unconstrained EnKF model.

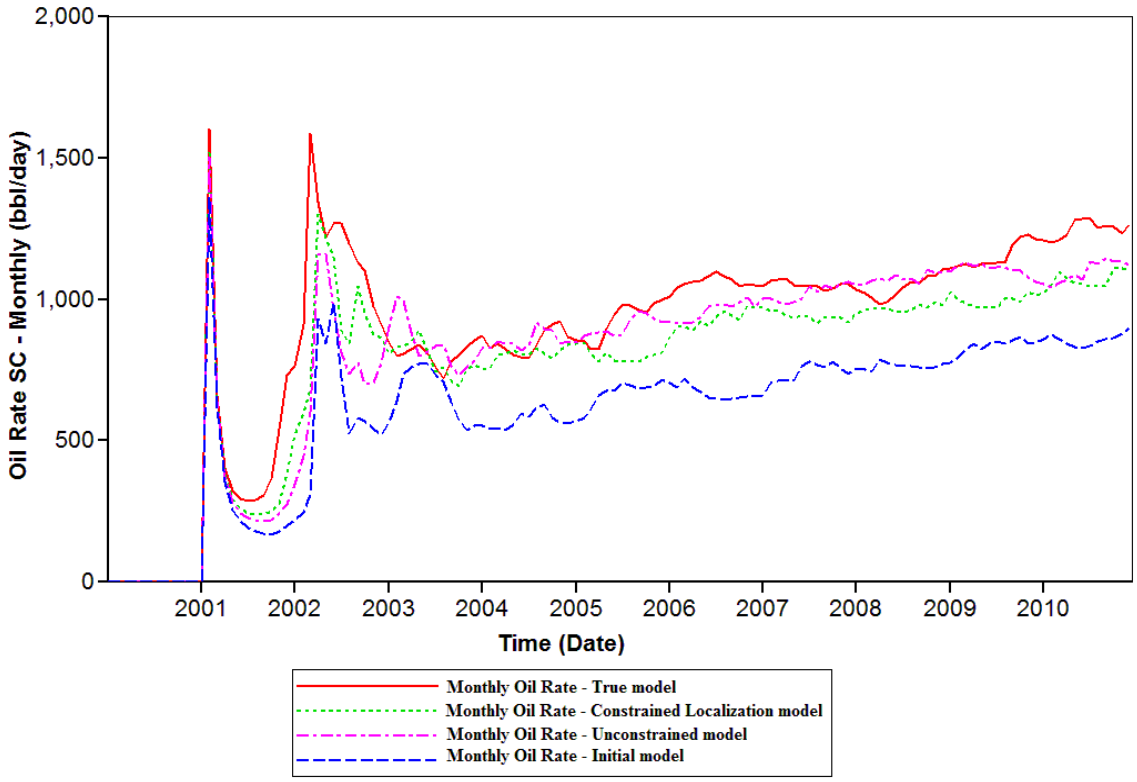

Fig 4.18 Comparison of the mean ensemble predictions for the monthly oil production for the entire reservoir field with respect to the historical production data using the true model, mean of the initial and the estimated models.

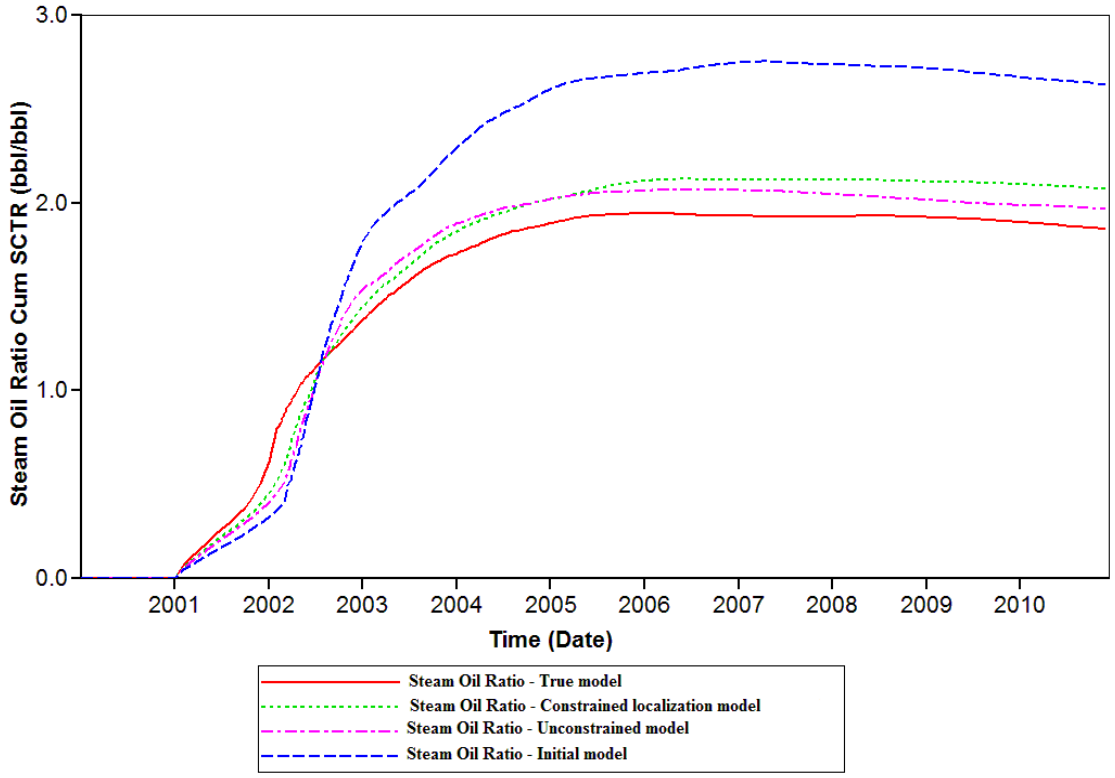

Fig 4.19 Comparison of the mean ensemble predictions for the monthly oil production for the entire reservoir field with respect to the historical production data using the true model, mean of the initial and the estimated models.

4.4 Conclusions

This chapter focused on the application of the particle filter to reservoir history matching. A reservoir model is highly nonlinear and characterized by a set of complicated partial differential equations explaining the flow of fluids in a porous bed of rocks defining a reservoir. As with any nonlinear model, the distribution of the model parameters is generally non-Gaussian in nature. Since the EnKF fails to obtain reasonable estimates when the distributions involved in the model are non-Gaussian, we attempted to use a completely Bayesian-based filter – the particle filter to estimate reservoir parameters. In this method also, the covariance localization was coupled with the particle filter and was found to perform better than the filter without any localization.

Chapter 5

Conclusions and future work

In this work, the challenging problem of reservoir characterization and history matching was analyzed using two sequential recursive estimation techniques – the ensemble Kalman filter (EnKF) and the particle filter (PF).

The first part of the thesis addressed some of the main shortcomings of the conventional method of the EnKF implementation. It is a well-known fact that some prior information about any petroleum reservoir is always available in the form of hard and soft data, which gives some details regarding the spatial connectivity and variability of reservoir parameters such as porosity and permeability. The EnKF, formulated on the grounds of the Monte Carlo Bayesian statistics and the Kalman filter (KF), arrives at estimates of parameters based on statistical error analysis and hence could potentially yield reservoir parameter estimates that are not geologically realistic and consistent. The main motivation of this thesis was to modify this conventional EnKF by incorporating geostatistics into the EnKF estimation framework using constraints so that we get estimates that are consistent with prior information – hard and soft data.

This was achieved in Chapter 2 using a novel projection method. In this method, the correlogram was used as the prior soft data information about the reservoir and the estimates obtained from the EnKF were projected onto the correlation structure indicated by this correlogram after each data assimilation step. By the application of this method to two synthetic heterogeneous reservoir models, it was observed that it is possible to preserve some of the EnKF statistics and at the same time, introduce geostatistical constraints to also preserve the spatial variability details.

The other half of the first part dealt with the spurious correlation induced by the Kalman gain computations in the EnKF update step, potentially leading to the erroneous update of parameters. As a result of this spurious update, there are high chances that values of the petrophysical parameters may depart from the geological realism and be physically meaningless. To solve this issue, a covariance localization-based EnKF was implemented on two synthetic reservoir models to understand its advantages in reservoir history matching. In this method, certain regions in the reservoir that were highly sensitive to production data were identified through a sensitivity analysis study. In this way, the EnKF was used to update only these regions to avoid spurious correlation.

Moreover, the remaining regions were updated based on a geostatistical algorithm (sequential Gaussian simulation) to make sure that geological spatial continuity and connectivity is retained. Due to the reduced number of parameters that are of interest for the EnKF, it was noted that the computational time involved in this study was considerably reduced. Also, it was observed that this coupling of geostatistics with the localization-based EnKF captures the spatial variability of permeability better than the projection method.

The second and the final part of the thesis focused on the application of the particle filter to reservoir history matching. A reservoir model is highly nonlinear characterized by a set of complicated partial differential equations explaining the flow of fluids in a porous bed of rocks defining a reservoir. As with any nonlinear model, the distribution of the noise is generally non-Gaussian in nature. Since the EnKF fails to obtain reasonable estimates when the distributions involved in the model are non-Gaussian, we attempted to use a completely Bayesian-based filter – the particle filter to estimate reservoir parameters. In this method also, covariance localization was coupled with the particle filter and was found to perform better than the filter without any localization.

5.1 Future work

There is plenty of scope to improve the current history matching algorithms to achieve accurate reservoir characterization.

- The current literature is extensive with several attempts made on the application of the EnKF to the history matching problem. However, methods such as the Gaussian sum filters, the particle filters and the expectation maximization (E-M) algorithms have been explored very little.
- It is also highly recommended to improve the results obtained by implementing the particle filters by means of bootstrapping them with the EnKF, i.e, use the proposal distributions obtained from the EnKF for resampling steps in the particle filter.
- Another challenge that can be addressed is the integration of 4D seismic data into the projection method proposed in this work.
- Thanks to the rapid advancement in sensor technology, it is now possible to place online sensors in the wells used in the oil recovery process. This could prove to be absolutely helpful for SAGD reservoir characterization. Using the temperature data from these sensors

placed at different intervals along the horizontal wells, it is possible to extrapolate values of temperature at unsampled locations using SAGD steam chamber dynamics. These values can, in turn, be used as a constraint while solving the joint reservoir state and parameter estimation problem.

- The well placement optimization problem can be coupled with the reservoir characterization procedure in order to optimize the reservoir performance.

References

1. Oliver D.S., Chen Y., 2011, "Recent progress on reservoir history matching: a review", Computatational Geosciences, 15 (1):185-221.
2. Chen, Z., 2007, "Reservoir Simulation : Mathematical Techniques in Oil Recovery", SIAM
3. Kalman, R.E., 1960, "A New Approach to Linear Filtering and Prediction Problems", Journal of Basic Engineering, 82 (1):35-45.
4. Welch, G., Bishop, G., 2006, "An Introduction to the Kalman Filter", UNC-Chapel Hill, TR 95-041, July 24, 2006.
5. Romeu, R. K., 2010, "History matching and forecasting", Journal of Petroleum Technology, April, 80.
6. Romero, C.E, Carter, J.N, 2001, "Using genetic algorithms for reservoir characterization", Journal of Petroleum Science and Engineering, 31(2-4):113-123.
7. Feraille, M., Roggero, F., Manceau, E., Hu, L.Y., Zabalza Mezghani, I., Reis, L.C, 2003, "Application of advanced history matching techniques to an integrated field case study (SPE 84463). In: Proceedings of the SPE Annual Technical Conference and Exhibition, Denver, Colorado, 5-8 October 2003.
8. Christie, M., Demyanov, v., Erbas, D, 2006, "Uncertainty quantification for porous media flows", Journal of Computational Physics, 217 (1):143-158.
9. Chu, L., Reynolds, A.C., Oliver, D.S., 1995, "Computation of sensitivity coefficients for conditioning the permeability field to well test data", In situ, 19 (2):179-223.
10. Evensen, G., 1994, "Sequential data assimilation with a nonlinear quasi-geostrophic model using Monte Carlo methods to forecast error statistics", Journal of Geophysics, 99 (C5):10.143 – 10.162.
11. Lorentzen, R. J., Fjelde, K. K., Froyen, J., Lage, A. C. V. M., Naevdal, G., Vefring, E. H., 2001, "Underbalanced and low-head drilling operations: Real time interpretation of measured data and operational support", In *SPE* Annual Technical Conference and Exhibition, New Orleans, Louisiana. Society of Petroleum Engineers Inc.
12. Gosselin, O., et al, 2003, "History Matching Using Time-Lapse Seismic (HUTS)", presented at the SPE Annual Technical Conference and Exhibition, Denver 5-8 Oct. 2003, Paper: SPE 84464.

13. Skjervheim, J.A., Evensen, G., Aanonsen, S.I., Rudd, B.O., Johansen, T.A., 2005, "Incorporating 4D Seismic Data in Reservoir Simulation Models Using Ensemble Kalman Filter", presented at the 2005 SPE Annual Technical Conderence and Exhibition, Dallas, Texas, 9-12 Oct, 2005. Paper: SPE 95789.
14. Lu, P., 2001, "Reservoir Parameter Estimation using Wavelet Analysis", Ph.D. dissertation, Stanford University, May 2001.
15. A. Panwar, J.J. Trivedi, Siavash Nejadi, 2012, "Importance of Distributed Temperature Sensor (DTS) Data for SAGD Reservoir Characterization and History Matching within Ensemble Kalman Filter (EnKF) Framework", In: Proceedings of the SPE Latin America and Caribbean Petroleum Engineering Conference, Denver, Mexico City, Mexico, 16-18 April 2012, Paper: SPE 153659.
16. Abacioglu, Y., Oliver, D.S., Reynolds, A., 2001, "Efficient reservoir history matching using subspace vectors", Computational Geosciences, 5 (2):151-172.
17. Heimhuber, R., 2012, "Efficient History Matching for Reduced Reservoir Models withPCE-based Bootstrap Filters", Diploma thesis, University of Stuttgart.
18. Luo, X., Hoteit, I., Duan, L. , Wang, W. 2011, "Review of nonlinear Kalman, ensemble and particle filtering with application to the reservoir history matching problem". In: Nonlinear Estimation and Applications to Industrial Systems. Control, Nova Publishers.
19. Chitralekha, S.B., Trivedi, J.J., Shah, S.L., 2010 "Application of Ensemble Kalman Filter for Reservoir Characterization and History Matching of Unconventional Oil Reservoirs", SPE International, Paper : SPE 137480.
20. Lu, P., Roland, N. H., 2000, "A Multiresolution Approach to Reservoir Parameter Estimation Using Wavelet Analysis", In: Proceedings of the SPE Annual Technical Conference and Exhibition, Dallas, Texas, 1-4 October 2000, Paper: SPE 62985.
21. Wen, X.H., Chen, W.H., 2005, "Real-time Reservoir Model Updating Using Ensemble Kalman Filter", Paper :SPE 92991.
22. http://www.streamsim.com/solutions/streamline-based-history-matching.
23. Vasco, D.W., Yoon, S., Datta-Gupta, A., 1999, "Integrating Dynamic Data into High resolution Reservoir Models Using Streamline-Based Analytic Sensitivity Coefficients", SPE Journal, 4 (1):389-399.

24. Schulze-Riegert, R.W., Axmann, J.K., Haase, O., Rian, D.T., You, Y.L., 2001, "Optimization methods for history matching of complex reservoirs", in SPE Reservoir Simulation Symposium, Houston, Texas, 11-14 February 2001, Paper: SPE 66393.

25. Houtekamer, P.L., Mitchell, H.L., 1998, Data Assimilation Using an Ensemble Kalman Technique, Monthly Weather Review, 126 (6):796-811.

26. Reichle, R.H., Mclaughlin, D.B., Entekhabi, D., 2002, "Hydrologic data assimilation with the ensemble Kalman filter", Monthly Weather review, 130 (1): 103-114.

27. Margulis, S.A., Mclaughlin, D., Entekhabi,D., Dunne,S., 2002, "Land data assimilation and estimation of soil moisture using measurements from the Southern Great Plains 1997 Filed Experiment," Water Resources Research, 38 (12):35.1- 35.18.

28. Evenesen, G., 2003, "The ensemble Kalman filter: Theoritical formulation and practical implementation," Ocean Dynamics, 53: 343-367.

29. Evensen G., 1994, "Sequential Data Assimilation with a nonlinear quasi-geostrophic model using Monte Carlo methods to forecast error statistics", J.Geophysics, 99 (C5): 10.143-10.162.

30. Emerick A., Reynolds A., 2011, "Combining sensitivities and prior information for covariance localization in the ensemble Kalman filter for petroleum reservoir applications", Computational Geosciences, 15 (2):251-269.

31. Houtekamer P.L., Mitchell, H.L., 2001, "A Sequential Ensemble Kalman Filter for Atmospheric Data Assimilation", Monthly Weather Review, 129 (1): 123-137.

32. Anderson, J.L., 2007, "An adaptive covariance inflation error correction algorithm for ensemble filters", Tellus A, 59 (2): 210-224.

33. Hunta B.R., Kostelichb, E.J., Szunyoghc, I., 2006, "Efficient data assimilation for spatiotemporal chaos: A local ensemble transform Kalman filter", Physica D 230 : 112-126.

34. Matheron G., 1968, "Lois stables et loi lognormale", Technical report, Ecole des Mines de Paris, Centre de G´eostatistique, Fontainebleau.

35. Lama, H.M., 2005, "Geostatistic in Reservoir Characterization: From estimation to Simulation methods", Estudios Geology, 61 : 135-145.

36. Journel, A.G, Huijbregts Ch.J., "Mining Geostatistics", Academic Press, 1978.
37. Davis J.C., "Statistics and Data Analysis in Geology", John Wiley & Sons, Inc., 2002.
38. Caers, J., "Modelling Uncertainty in the Earth Sciences", Wiley-Blackwell, John Wiley & Sons, 2011.
39. Deutsch, C.V., "Geostatistical Reservoir Modeling", Applied Geostatistical Series, 2002.
40. Wen, X.H., Chen, W. H., 2006, "Real-time reservoir model updating using ensemble Kalman filter with confirming option", SPE Journal, 11 (4), 431–442.
41. Christie M., Blunt, M., SPE Comparative Solution Project 2001, First Data Set, Available from http://www.spe.org/web/csp//datasets/set01.htmUH .
42. Jafarpour B., McLaughlin D.B., 'History Matching with an Ensemble Kalman Filter and Discrete Cosine Parameterization', SPE Annual Technical Conference, Anaheim, California, USA, 11-14 November 2007, Paper SPE 108761.
43. Jacquard P., Jain C., "Permeability distribution from field pressure data", SPE Journal, 5 (4): 281-294.
44. Nejadi, S., Trivedi, J., Leung, J., 2011. "Improving Characterization and History Matching Using Entropy Weighted Ensemble Kalman Filter for Non-Gaussian Distributions". presented at the SPE Western North American Regional Meeting, Anchorage, Alaska, USA, May 7-11 2011, SPE Paper 144578.
45. Nejadi, S., Trivedi, J., Leung, J., 2012, "Ensemble Kalman Filter Predictor Bias Correction Method for Non-Gaussian Geological Facies Detection". Proceedings of the 2012 IFAC Workshop on Automatic Control in Offshore Oil and Gas Production, Norwegian University of Science and Technology, Trondheim, Norway, May 31 - June 1, 2012.
46. Wang, H.Z., Yao C.Y., "Mapping an uncertainty zone between interpolated types of a categorical variable", Computers and Geosciences, 40 : 146-152.
47. Wang, H., 2008. "Application of Temperature Observation Wells during SAGD Operations in a medium Deep Burial Extra Heavy Oil Reservoir". Paper 2008-118, proceedings of the Canadian International Petroleum Conference/ SPE Gas Technology Symposium Joint Conference, Calgary, Alberta, Canada, 17-19 June 2008.

48. Jafarpour B., McLaughlin D.B. (2009),"Estimating reservoir permeabilities using the ensemble Kalman filter: the importance of the ensemble design", SPE Journal, 14 (2): 374-388.

49. Mallat, S. 1999, "A wavelet tour of signal processing", second edition, San Diego, California, USA: Academic Press.

50. Lu,P., 2001, "Reservoir Parameter Estimation using Wavelet Analysis", Ph.D. dissertation, Stanford University, May 2001.

51. Sahni I., Horne, R.N., 2011, "Generating Multiple History Matched Reservoir Realizations Using Wavelets", SPE Journal, 9 (3): 217-226.

52. Gavalas, G.R., Shah, P.C., Seinfeld, J.H., 1976, "Reservoir history matching by Bayesian estimation", SPE Journal, 16 (6): 337-350.

53. Oliver D.S., 1996, "Multiple Realization of the permeability Field from Well Test Data", SPE Journal, 1 (2): 145-154.

54. Reynolds A.C., He, N., Chu, L., Oliver, D.S., 1996, "Reparameterization Techniques for Generating Reservoir Descriptions Conditioned to Variograms and Well-Test Pressure Data", SPE Journal, 1 (4): 413-426.

55. Sarma, P., Durlofsky, L.J., Aziz., K., 2007, "A New Approach to Automatic History Matching Using Kernal PCA", presented at the SPE Reservoir Simulation Symposium held in Houston, Texas, U.S.A., 26-28 February 2007, Paper SPE 106176.

56. de Marsily, G., Lavedan, G., Boucher, M., Fasanino, G. 1994, "Interpretation of interference tests in a well field using geostatistical techniques to fit the permeability distribution in a reservoir model", Geostatistics for Natural Resources Characterization, Part 2. Dordrecht: Reidel: 831-849.

57. RamaRao BS, LaVenue A.M., de Marsily G., Marietta M.G., 1995, "Pilot point methodology for automated calibration of an ensemble of consitionally simulated transmittivity fileds", Water Resources Research, 31(3): 475-493.

58. La Venue, A.M., Pickens, J.F., 1992, “Application of a coupled adjoint sensitivity and kriging approach to calibrate a groundwater flow model”, Water Resources Research, 28 (6): 1543-1569.

59. Gómez-Hernández, J.J., Sahuquillo, A., Capilla, José, E., 1997, “Stochastic Simulation of Transmissivity Fields Conditional to Both Transmissivity and Pizometric Data”, 1. Theory, Journal of Hydrology, 203 (3): 175-188.

60. Leila Heidari. History-matching of petroleum reservoir models by the ensemble Kalman filter and parameterization methods. Earth Sciences. Ecole Nationale Sup´erieure des Mines de Paris, 2011. English. <NNT : 2011ENMP0006>. <pastel-00581082>

61. Arroyo-Negrete, E.R., 2006, “Continuous Reservoir Model Updating Using Streamline-Assisted Ensemble Kalman Filter”, presented at the 2006 Annual Technical conference Exhibition, Texas, 24-27 September 2006, Paper : SPE 106518.

62. Furrer, R., Bengtsson, T., 2007, “Estimation of High Dimensional Prior and Posterior Covariance Matrices in Kalman Filter Variants”, Journal of Multivariate Analysis, 98 (2): 227-255.

63. Lee, S.-Y., Carle, S.F., Fogg, G.E., 2007, “Geologic heterogeneity and a comparison of two geostatistical models: Sequential Gaussian and transition probability-based geostatistical simulation”, Advances in Water Resources 30(9), 1914-1932.

64. Cressie, N., 1990. The origins of kriging. Mathematical Geology 22(3), 239-252.

65. Chitralekha, S.B., 2010, “Computational Tools for Soft Sensing and State Estimation”, Ph.D. thesis, University of Alberta.

66. Gordon, N. J., Salmond, D. J., Smith, A. F. M., 1993, “Novel approach to nonlinear/non-gaussian Bayesian state estimation”, Radar and Signal Processing, IEE Proceedings F, 140 (2): 107‑113.

67. Doucet, A., Freitas, N.D., Gordon, N.J., 2001, “An Introduction to Sequential Monte Carlo Methods”, New York :Springer.

68. Achilias, D.S., Kiparissides, C., 1992, “Development of a general mathematical framework for modeling diffusion controlled free-radical polymerization reactions”, Macromolecules, 25(14): 3739–3750.

69. Chitralekha, S.B., Prakash, J., Raghavan, H., Gopaluni, R.B., Shah, S.L., 2010, "A comparison of simultaneous state and parameter estimation schemes for a continuous fermentor reactor". Journal of Process Control, 20 (8): 934–943.
70. Doucet, A., Johansen, A.M., 2008, "A Tutorial on Particle Filtering and Smoothing: Fifteen years later".
71. Van Leeuwen, P.J., 2009, "Particle filtering in geophysical systems", Monthly Weather Review, 137 (12):4089—4114.
72. Kitagawa, G., 1998, "Self organizing state–space models", Journal of the American Statistical Association, 93(443): 1203–1215.
73. Andrieu, C., Doucet, A., Tadic, V.B., 2005, "Online parameter estimation in general state-space models", Proceedings of the 44th IEEE Conference on Decision and Control and European Control Conference. Seville, Spain: 332–337.
74. Andrieu, C., Doucet, A., Singh, S.S., Tadic, V.B., 2004, "Particle methods for change detection, system identification, and control", Proceedings of the IEEE 92 (3): 423–438.
75. Higuchi, T., 2001, "Sequential Monte Carlo Methods in Practice". Chap. Self organizing time series model. Springer–Verlag, New York.
76. Liu, J., West, M., 2001, "Sequential Monte Carlo Methods in Practice", Chap. Combined parameter and state estimation in simulation–based filtering. Springer–Verlag, New York.
77. Gustafsson, F., Sch¨on, T.B., 2003, "Particle filters for system identification of statespace models linear in either parameters or states", Proceedings of the 13th IFAC Symposium on System Identification. Rotterdam, The Netherlands: 1287–1292.
78. Ristic, B., Arulampalam, S., Gordon, N., 2004, "Beyond the Kalman Filter: Particle Filters for Tracking Applications", Chap. A tutorial on particle filters. Artech House, Boston.
79. Chen, T., et al., 2005, "Particle filters for state and parameter estimation in batch processes", J. Process Control, 15 (6): 665 – 673.
80. Thomas, B. S., 2006, "Estimation of nonlinear dynamic systems – theory and applications", Ph.D. thesis, Linko¨pings Univ., Linko¨pings, Sweden.

APPENDIX A: Reservoir simulator equations

A.1 Introduction

Reservoir simulators simulate the oil productivity of a reservoir given relevant input parameters by solving a set of governing equations dictating the flow of fluids in a reservoir. Reservoir characterization being a large scale porous media problem, several differential equations such as mass conservation, energy conservation, phase equilibrium equations and well equations are needed for its definition. Today, a number of commercial reservoir simulators like CMG and ECLIPSE have been developed and successfully implemented to model real reservoir fields. In this thesis, CMG has been used as the primary reservoir simulator. This appendix provides a brief summary of the mass and energy conservation equations used in CMG STARS module.

A.2 Conservation Equations

Conservation equations are developed for each component and fluids of interest in the reservoir. Generally, reservoir fluids are comprised of oil, water and gas. While constructing conservation equations, it is important to note that they are based on a particular region of volume V, where the basic laws of conservation of mass and energy are obeyed.

A.2.1 Mass conservation equations

The volume of the region of interest is denoted by V. This region of interest is generally a discretized grid block. This total volume V is composed of five individual volumes:

1. Volume of solid rock matrix (V_r)
2. Volume of solid and adsorbed component (V_s)
3. Volume of water or aqueous phase (V_w)
4. Volume of oil or oleic phase (V_o)
5. Volume of gaseous phase (V_g)

$$V = V_r + V_S + V_w + V_o + V_g \tag{A.1}$$

The subscripts w, o and g is used to refer to water, oil and the gas components respectively.

The total fluid volume V_f and void volume V_v are defined as:

$$V_f = V_w + V_o + V_g \tag{A.2}$$

$$V_v = V - V_r = V_f + V_s \tag{A.3}$$

Porosity of a reservoir is defined as the ratio of void volume to total volume in a reservoir. Void porosity φ_v and fluid porosity φ_f are defined as:

$$\varphi_v = \frac{\mathrm{Vv}}{\mathrm{V}} \tag{A.4}$$

$$\varphi_f = \frac{Vf}{V} = \frac{V_v}{V}\left(1 - \frac{V_s}{V_v}\right) \tag{A.5}$$

Since $\frac{V_s}{V_v}$ gives the ratio of volume occupied by solid and adsorbed components to that of the void volume, which is equal to $\sum \frac{c_{si}}{\rho_{si}}$, equation (A.5) can be modified as:

$$\varphi_f = \varphi_v * \left(1 - \sum \frac{c_{si}}{\rho_{si}}\right) \tag{A.6}$$

The fluid saturations in a reservoir must sum to 1. Hence,

$$S_w + S_o + S_g = 1 \tag{A.7}$$

where

$$S_w = \frac{V_w}{V_f} = \frac{\mathrm{Vw}}{\varphi_f \mathrm{V}}\ , S_o = \frac{V_o}{\varphi_f V} \text{ and } S_g = \frac{V_g}{\varphi_f V} \tag{A.8}$$

Thus, the accumulation term for flowing, solid and adsorbed component can be written as:

$$V\frac{\partial}{\partial t}\left[\varphi_f(\rho_o S_w w_i + \rho_o S_o x_i + \rho_g S_g y_i) + \varphi_v A d_i + \varphi_v c_i\right] \tag{A.9}$$

Between any two regions, flowing components constitute to the flow term as given below:

$$\rho_w v_w w_i + \rho_o v_o x_i + \rho_g v_g y_i + \emptyset\, \rho_w D_{wi} \Delta w_i + \emptyset\, \rho_g D_{gi} \Delta g_i + \emptyset\, \rho_o D_{oi} \Delta o_i \tag{A.10}$$

Flow taking place due to transmissibility between two regions must also be taken into account while developing conservation equations. The volumetric flow rate due to transmissibility for water, oil or gas components is given by:

$$v_j = T\left(\frac{\mathrm{k_{rj}}}{\mu_i \mathrm{r_j}}\right) \Delta\emptyset_j, j = w, o, g \quad \text{(A.11)}$$

T is the transmissibility between two regions, which takes into account factors such as cross sectional area, interface permeability and geometric orientation. $\Delta\emptyset$ refers to the potential difference between the node of the adjacent region and the current region. Inflow and outflow are indicated by the positive and negative values of $\Delta\emptyset$ respectively. Δw_i, Δg_i and Δo_i are the phase concentration differences between the nodes.

One of the important contributors to the flow term in the mass conservation equation is the source or sink terms of the well. The flow term for flowing components corresponding to well source/ sink is written as:

$$\rho_w q_{wk} w_i + \rho_o q_{ok} x_i + \rho_g q_{gk} y_i \quad \text{(A.12)}$$

Solid components are not considered in the above equations since they do not flow.

Another mass conservation term comes from chemical reaction and interfacial mass transfer source/sink terms. This can be written as:

$$V \sum_{k=1}^{n_r} (s'_{ki} - s_{ki}) * r_k \quad \text{(A.13)}$$

s'_{ki} and s_{ki} are the stoichiometric coefficients of component i in reaction k, with s'_{ki} representing product and s'_{ki} representing reactants. r_k refers to the volumetric rate of reaction.

The final source term for mass flow is thermal aquifer source/sink, whose contribution to the flow term is given below:

$$\sum_{k=1}^{n_f} \rho_w \ qaq_{wk}, \quad \text{(A.14)}$$

qaq_{wk} indicates the volumetric water flow rate through a block face k to or from the adjacent aquifer.

Conservation of mass is satisfied if the rate of change of accumulation is equal to the sum of the net rate of inflow from adjacent regions and the net rate of addition from sources and sinks. Considering equations (A.8) to (A.14), the mass conservation equation for the flowing component i can be mathematically written as:

$$V\frac{\partial}{\partial t}\left[\varphi_f(\rho_w S_w w_i + \rho_o S_o x_i + \rho_g S_g y_i) + \varphi_v A d_i\right] = \sum_{k=1}^{n_f}\left[T_w \rho_w w_i \Delta\emptyset_w + T_o \rho_o x_i \Delta\emptyset_o + T_g \rho_g y_i \Delta\emptyset_g\right] + V\sum_{k=1}^{n_r}(s'_{ki} - s_{ki}) * r_k + \sum_{\mathrm{k=i}}^{\mathrm{n_f}}\left[\phi\, \mathrm{D_{wi}}\ \rho_{\mathrm{w}}\, \Delta \mathrm{w_i} + \phi\, \mathrm{D_{oi}}\ \rho_{\mathrm{o}}\, \Delta \mathrm{x_i} + \phi\, \mathrm{D_{gi}}\ \rho_{\mathrm{g}}\, \Delta \mathrm{y_i}\right] + \delta_{iw}\sum_{k=1}^{n_f} \rho_{\mathrm{w}}\ \mathrm{qaq_{wk}} + \rho_w q_{wk} w_i + \rho_o q_{ok} x_i + \rho_g q_{gk} y_i \quad \text{(A.15)}$$

For the solid component, the conservation equation is written as:

$$V\frac{\partial}{\partial t}[\varphi_v c_i = V\sum_{k=1}^{n_r}(s'_{ki} - s_{ki}) * r_k \quad \text{(A.16)}$$

B.2.2 Energy conservation equations

Energy conservation equations can also be derived along similar lines to the mass conservation equations.

$$V\frac{\partial}{\partial t}\left[\varphi_f(\rho_w S_w U_w + \rho_o S_o U_o + \rho_g S_g U_g\big) + \varphi_v c_s U_s + (1-\varphi_v)U_r = \sum_{k=1}^{n_f}\left[T_w \rho_w H_w \Delta\emptyset_w + T_o \rho_o H_o \Delta\emptyset_o + T_g \rho_g H_g \Delta\emptyset_g\right] + \sum_{k=1}^{n_f} K\,\Delta T + V\sum_{k=1}^{n_r} H_{rk}\ r_k + HL_o + HL_v + HL_c + \sum_{k=1}^{n_f}(HA_{CV} + HA_{CD})_k + \rho_w q_{wk} H_w + \rho_o q_{ok} H_o + \rho_g q_{gk} H_g \quad \text{(A.17)}$$

APPENDIX B: Geostatistical algorithms used in SGeMS

B.1 Introduction

Geostatistics is a branch of applied statistics dealing with the determination of spatially related properties. It was developed by George Matheron to estimate the changes in ore grade within a mine. Since its inception, this field has witnessed ever increasing application towards the challenging problem of reservoir characterization. The widespread adoption of this field in reservoir applications is due to its ability to exploit the spatial characteristics of reservoir properties such as porosity, permeability and formation thickness. Many geostatitical simulation packages like SGeMS, GSLIB and VISIM have successfully emerged over the past few decades to assist in reservoir modeling. For the work described in this thesis, SGeMS was chosen as the modeling software for performing geostatistical computations. SGeMS (Stanford Geostatistical Modeling Software) is a 3D visualization and modelling platform used for generating geostatistical models honoring conditioning data and estimating the values of spatially correlated variables. This appendix gives a brief summary of the fundamentals of geostatistics and the algorithms used in SGeMS.

B.2 Variogram analysis

A variogram is a measure of the average correlation of spatially related properties and is described by equation B.1.

$$\gamma(h) = \frac{1}{2}\,\varepsilon[\{Z(u+h) - Z(u)\}^2] \tag{B.1}$$

where h is the lag distance and Z(u) is the value of the spatial property. The variogram is inversely related to the correlation index. The variograms are characterized by unique parameters, the sill, range and nugget, which are shown in figure B.1.

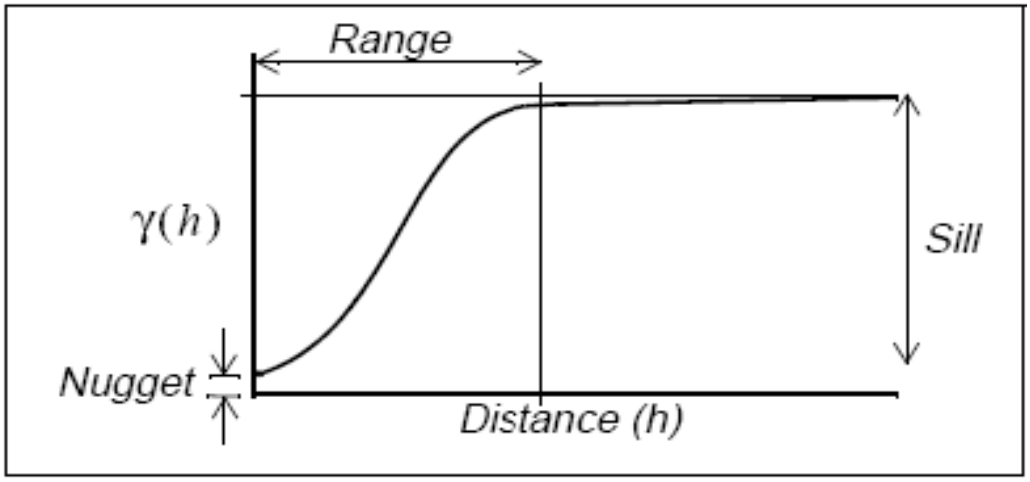

Theoretically, the ideal value of variogram at the origin should be zero. However, in real cases, small values of variogram, called the nugget are observed at zero lag, possibly due of measurement errors. The nugget in a variogram model represents this error. With increasing lag distance, the average autocorrelation between properties separated by h units decrease. The lag distance at which this autocorrelation value reduces to zero is called the range of the variogram. The variogram value at the lag distance corresponding to its range is called the sill.

Since a variogram represents the reservoir soft data information obtained through seismic surveys, it has to be fitted against sound theortical variogram models to facilitate the estimation of reservoir properties. Table B.1 represents the four basic isotropic models used by SGeMS for computing variograms.

Table B.1 Mathematical formulation of isotropic models used in geostatistics

Isotropic Model	Mathematical formulation
Nugget effect model	$\gamma(h) = \begin{cases} 0 & \text{if } \| \text{h} \| = 0 \\ 1 & \text{otherwise} \end{cases}$
Spherical model with actual range a	$\gamma(h) = \begin{cases} \frac{3}{2}\frac{\| \text{h} \|}{a} - \frac{1}{2}\left(\frac{\| \text{h} \|}{a}\right) & \text{if } \| \text{h} \| < a \\ 1 & \text{otherwise} \end{cases}$

Exponential model with practical range *a*	$\gamma(h) = 1 - \exp(\frac{-3 \,\|\| \mathrm{h} \,\|\|}{a})$
Gaussian model with practical range *a*	$\gamma(h) = 1 - \exp(\frac{-3 \,\|\| \mathrm{h} \,\|\|^2}{a^2})$

B.3 Algorithms

Geostatistical simulation packages like SGeMS and GSLIB, use a set of algorithms to generate spatial properties conditioned on the hard and soft data. These algorithms fall into two categories, geostatistical estimation algorithms and geostatistical simulation algorithms. Geostatistical estimation is used for obtaining unbiased estimates of reservoir properties like porosity and permeability with minimum variance by means of interpolation techniques. Geostatistical simulation methods, on the other hand, give multiple equally probable realizations of the property to be estimated. Estimation methods do not yield accurate results compared to the simulation methods because the estimation is based on interpolation, which does not lead to realistic values of the properties due to smoothing. But, simulation techniques honors spatial variability of the property defined by the variogram and allows an assessment of property uncertainty by using several realizations. The algorithms used in SGeMS are given in Table B.2.

Table B.2 Classification of estimation and simulation methods used in geostatistics

Geostatistical estimation methods	Geostatistical simulation methods
Simple Kriging (SK)	Sequential gaussian simulation (SCG)
Ordinary Kriging (OK)	Sequential indicator simulation (SIS)
Kriging with a trend	Direct sequential simulation
Universal kriging (UK)	Sequential gaussian co-simulation
Cokriging	Sequential indicator co-simulation

The most common algorithms used in geostatistical estimation are ordinary kriging and simple kriging and sequential Gaussian simulation is the most common simulation method. These algorithms are explained in detail in the following section.

B.3.1 Kriging:

Kriging is an optimal regression-based interpolation method of estimating spatial property values at unknown locations given a few true values at certain locations by means of assigning weights to the known data points. The data points close to the unknown location are given higher weights and vice-versa. If the data points form a cluster, then the individual data points in the cluster are given lower weights compared to the isolated data points, thereby nullifying the effect of data clustering. In addition to the estimates of the spatial property, kriging also gives an estimate of its variance. The main goal of kriging is to find the best unbiased minimum variance estimate of the properties and its basic form is given by equations B.2 and B.3:

$$Z^*(\boldsymbol{u}) - m(\boldsymbol{u}) = \lambda_\alpha [Z(\boldsymbol{u}_\alpha) - m(\boldsymbol{u}_\alpha)] \tag{B.2}$$

$$\sigma_E^2(\boldsymbol{u}) = Variance[Z^*(\boldsymbol{u}) - Z(\boldsymbol{u})] \tag{B.3}$$

where λ_α represent the weights given to data points, $m(\boldsymbol{u})$ is the mean of the property at location $\boldsymbol{u}$ and $\sigma_E^2(\boldsymbol{u})$ corresponds to the estimated variance.

The weights λ_α are determined such that the estimate variance $\sigma_E^2(\boldsymbol{u})$ is minimized and the constraint $E[Z^*(\boldsymbol{u})] = E[Z(\boldsymbol{u})]$ is obeyed to satisfy the unbiased estimate requirements.

The specific kriging methods to be used depends on the property exhibited by the mean $m(\boldsymbol{u})$. The two most common kriging variants are explained below.

B.3.1.1 Simple kriging (SK)

Simple kriging is performed in certain situations, where the mean component of the property to be estimated ($m(\boldsymbol{u})$) is known and assumed to be constant in the entire estimation region. In this case, the equation (B.2) can be modified for simple kriging estimation as follows:

$$Z_{SK}^*(\boldsymbol{u}) = m + \lambda_\alpha^{SK}(\boldsymbol{u})[Z(\boldsymbol{u}_\alpha) - m] \tag{B.4}$$

Since the mean is constant, i.e., $E[\mathrm{Z}(\boldsymbol{u_\alpha}) - m] = 0$, the above estimate is unbiased. The estimation error can be written as:

$$\mathrm{Z}^*_{\mathrm{SK}}(\mathbf{u}) - \mathrm{Z}(\boldsymbol{u}) = [\mathrm{Z}^*_{\mathrm{SK}}(\mathbf{u}) - \mathrm{m}] - [\mathrm{Z}(\mathbf{u}) - m] = \sum_{\boldsymbol{\alpha=1}}^{\boldsymbol{n(u)}} \lambda_\alpha^{\mathrm{SK}}(\mathbf{u})\ R(\mathbf{u}_{\boldsymbol{\alpha}}) - R(\mathbf{u}) = \mathrm{R}^*_{\mathrm{SK}}(\mathbf{u}) - R(\mathbf{u}) \quad \text{(B.5)}$$

The error variance can then be written as:

$$\sigma_E^2(\boldsymbol{u}) = Variance\{R^*_{SK}(\boldsymbol{u})\} + Variance\{R_{SK}(\boldsymbol{u})\} - 2\ Covariance\{R^*_{SK}(\boldsymbol{u}), R_{SK}(\boldsymbol{u})\} = \sum_{\alpha=1}^{n(u)} \sum_{\beta=1}^{n(u)} \lambda_\alpha^{\mathrm{SK}}(\mathbf{u})\, \lambda_\beta^{\mathrm{SK}}\ C_R\big(\boldsymbol{u_\alpha} - \boldsymbol{u_\beta}\big) + C_R(0) - 2\sum_{\alpha=1}^{n(u)} \lambda_\alpha^{\mathrm{SK}}(\mathbf{u})\ C_R(\boldsymbol{u_\alpha} - \boldsymbol{u}) \quad \text{(B.6)}$$

Since the kriging estimate is a minimum variance estimator, it is necessary to take the derivative of the above equation with respect to each kriging weight and set it to zero. On doing so, we get the following set of equations:

$$\sum_{\beta=1}^{n(u)} \lambda_\beta^{\mathrm{SK}}(\mathbf{u}) C_R\big(\boldsymbol{u_\alpha} - \boldsymbol{u_\beta}\big) = C_R(\boldsymbol{u_\alpha} - \boldsymbol{u})\ \ \alpha = 1, 2, 3, 4, \ldots\ldots\ldots n(u) \quad \text{(B.7)}$$

The covariance functions for *Z(u)* and *R(u)* are equal since the mean is constant for the entire domain. Hence, $C(h) = C_R(h)$. Using this in equation (B.7), we have:

$$\sum_{\beta=1}^{n(u)} \lambda_\beta^{\mathrm{SK}}(\mathbf{u}) C\big(\boldsymbol{u_\alpha} - \boldsymbol{u_\beta}\big) = C(\boldsymbol{u_\alpha} - \boldsymbol{u})\ \ \alpha = 1, 2, 3, 4, \ldots\ldots\ldots n(u) \quad \text{(B.8)}$$

In matrix form, this can be represented as:

$$\boldsymbol{K}\lambda_{SK}(\boldsymbol{u}) = \boldsymbol{k} \quad \text{(B.9)}$$

where $\boldsymbol{K}$ is the covariance matrix between data points and its elements are represented as:

$$\boldsymbol{K_{i,j}} = C(\boldsymbol{u_i} - \boldsymbol{u_j}) \quad \text{(B.10)}$$

$\boldsymbol{k}$ is the vector of covariance matrix of the estimation points and the data points and its elements are represented as:

$$\boldsymbol{k_i} = C(\boldsymbol{u_i} - \boldsymbol{u}) \quad \text{(B.11)}$$

From equation (B.9), the kriging weights can be determined by the following equation:

$$\lambda_{SK}(\boldsymbol{u}) = \boldsymbol{K^{-1}k} \tag{B.12}$$

After obtaining the weights, the simple kriging variance can be estimated by the relation:

$$\sigma^2_{SK}(\boldsymbol{u}) = C(0) - \sum_{\boldsymbol{\alpha=1}}^{\boldsymbol{n(u)}} \lambda_{\alpha}^{\mathrm{SK}}(\mathbf{u})\, C(\boldsymbol{u_\alpha - u}) \tag{B.13}$$

B.3.1.2 Ordinary Kriging (OK)

Ordinary kriging is very similar to simple kriging except that the mean is not assumed constant over the entire estimation region but is assumed instead to be constant in the local neighborhood of the estimation points. In other words, $m(\boldsymbol{u_\alpha})= m(\boldsymbol{u})$, where **u** refers to a location very near to the estimation location $\boldsymbol{u_\alpha}$.

The kriging estimate for ordinary kriging is given by:

$$Z^*(\boldsymbol{u}) = m(\boldsymbol{u}) + \sum_{\boldsymbol{\alpha=1}}^{\boldsymbol{n(u)}} \lambda_{\alpha}(\mathbf{u})\,[Z(\boldsymbol{u_\alpha}) - m(\boldsymbol{u_\alpha})] = \sum_{\boldsymbol{\alpha=1}}^{\boldsymbol{n(u)}} \lambda_{\alpha}(\mathbf{u})\, Z(\boldsymbol{u_\alpha}) + [1 - \sum_{\boldsymbol{\alpha=1}}^{\boldsymbol{n(u)}} \lambda_{\alpha}(\mathbf{u})] m(\boldsymbol{u}) \tag{B.14}$$

The local mean can be computed by making use of the constraint that the sum of the kriging weights is equal to 1, i.e., $\sum_{\boldsymbol{\alpha=1}}^{\boldsymbol{n(u)}} \lambda_{\alpha}^{\mathrm{OK}}(\mathbf{u}) = \mathbf{1}$, leading to the following equation,

$$Z^*_{OK}(\boldsymbol{u}) = \sum_{\boldsymbol{\alpha=1}}^{\boldsymbol{n(u)}} \lambda_{\alpha}^{\mathrm{OK}}(\mathbf{u})\, Z(\boldsymbol{u_\alpha}) \tag{B.15}$$

Lagrange's method of optimization is used to find the minimum error variance estimator as shown below:

$$L = \sigma^2_E(\boldsymbol{u}) + 2\mu_{OK}(\boldsymbol{u})[1 - \sum_{\boldsymbol{\alpha=1}}^{\boldsymbol{n(u)}} \lambda_{\alpha}(\mathbf{u})] \tag{B.16}$$

where L is the Lagrange parameter and the minimization constraint with respect to L is given by

$$\frac{1}{2}\frac{\partial L}{\partial \mu} = 1 - \sum_{\boldsymbol{\alpha=1}}^{\boldsymbol{n(u)}} \lambda_{\alpha}(\mathbf{u}) = 0 \tag{B.17}$$

The kriging weights can be solved using equation B.18.

$$\begin{cases} \sum_{\boldsymbol{\alpha=1}}^{\boldsymbol{n(u)}} \lambda_{\alpha}(\mathbf{u})\; C_R\left(\mathbf{u}_{\boldsymbol{\alpha}} - \mathbf{u}_{\boldsymbol{\beta}}\right) + \mu_{OK}(\mathbf{u}) \\ \qquad\qquad \sum_{\boldsymbol{\beta=1}}^{\boldsymbol{n(u)}} \lambda_{\beta}^{\mathrm{OK}}(\mathbf{u}) \end{cases} \qquad \alpha = 1,2,3,\ldots\ldots,\mathrm{n(u)} \tag{B.18}$$

After obtaining the kriging weights, the ordinary kriging variance can be written as:

$$\sigma_{OK}^2(\boldsymbol{u}) = C(0) - \sum_{\boldsymbol{\alpha}=\mathbf{1}}^{\boldsymbol{n(u)}} \lambda_{\alpha}^{\mathrm{OK}}(\mathbf{u})\ C(\boldsymbol{u_\alpha} - \boldsymbol{u}) - \mu_{OK}(\mathbf{u}) \quad \text{(B.19)}$$

B.3.2 Stochastic simulation:

Stochastic simulation is concerned with the generation of several equiprobable realizations of the reservoir property to be estimated, instead of just estimating the mean and variance of the estimate, as was the case in the estimation algorithms described in the previous section. The generation of

these realizations gives reservoir engineers an invaluable source to realistically quantify the uncertainty involved in the property estimation. Sequential Gaussian simulation, direct sequential simulation and sequential indicator simulation are the most widely used stochastic simulation methods.

The sequential Gaussian simulation (SGS) algorithm is built around the simple kriging estimation technique explained in section **B.3.1.1**. It differs from simple kriging in the manner in which the variable at each grid node is represented. While simple kriging yields an estimate of the mean and variance of the property value at each grid node and hence can be described as following a Gaussian distribution, SGS selects a uniform random number from the probability distribution and then considers a random deviate from this Gaussian distribution. A sequential Gaussian simulation is comprised of five steps. Firstly, a point is chosen at random in the unknown data location. The mean and the variance of this unknown data point is then estimated by using one of the standard kriging procedures. In this work, we have used the ordinary kriging method. In the next step, an unknown data point value is randomly chosen from a normal probability distribution having the mean and variance computed from the previous step. This data point is now considered to be a simulated point and used as conditioning data for estimating the remaining unknown data points. This process is repeated until all the data points are simulated.

In SGS, it is necessary for the data set to strictly follow a normal distribution. If it does not follow a normal distribution, the data set has to be transformed into normal form by using a normal score transformation.